

## Modulation of melanoma-associated immune cells for the optimization of anti-tumoral immunotherapy

Caterina Isabella Iuliano

Vollständiger Abdruck der von der TUM School of Medicine and Health der Technischen Universität München zur Erlangung einer

Doktorin der Naturwissenschaft (Dr. rer. nat.)

genehmigten Dissertation.

Vorsitz: Prof. Dr. Percy A. Knolle

Prüfende der Dissertation:

1. Prof. Dr. Tilo Biedermann
2. Prof. Dr. Dr. h.c. mult. Martin Hrabě de Angelis

Die Dissertation wurde am 11.01.2024 bei der Technischen Universität München eingereicht und durch die TUM School of Medicine and Health am 08.05.2024 angenommen.

*This thesis is dedicated to my Nonno, who was so proud of me and, unfortunately, cannot be here to see me finish this journey.*

## **Acknowledgment**

First, I would like to express my sincere gratitude to my supervisor, Dr. Tilo Biedermann, for allowing me to conduct my Ph.D. in his lab and offering support, guidance, and the possibility to grow professionally and personally. Of course, my gratitude extends to my mentor, Dr. Susanne Kaesler, who supported me throughout the entire journey of this thesis with excellent mentorship and dedication. I am grateful to her for sharing her knowledge and expertise and allowing me to find my way of exploring the scientific world. And, though not attributed to my team, I would like to thank Dr. Miriam Hils, whose moral support and encouragement throughout these years have been highly appreciated and often the motivation needed to achieve great results.

But work is not only working, so I would like to thank my lab “microenvironment”. I want to emphasize my appreciation of the collaborative spirit and support provided by the members of this lab. I have seldom experienced such great team spirit; pushing through long days is much easier when they are filled with laughter, jokes, and good companionship. And special thanks go to Inga Hölge for listening to all my work-unrelated and sometimes work-related stories. And, of course, to the members of my Skat-Stammtisch, these regular card sessions were indispensable in maintaining my sanity.

Lastly, I want to express my deep gratitude to my support system. Thank you to Maren Frey, who never faltered to toast the good and the bad days with one or many delicious Aperol Spritz! To my loving fiancé, René Köster, who was by my side every step of the way and always had my back, for always cheering me on despite my sometimes-lousy mood and his unwavering belief in me. Thanks to my family for supporting me in my endeavors and pushing me to strive for bigger.

## Abstract

Bone marrow-derived mast cells (BMMC) are used as an *in vitro* model to study mast cells (MC) and their role in health and disease. *In vivo*, however, BM-derived hematopoietic stem cells account for only a fraction of MC, the majority of MC *in vivo* are and remain tissue resident. We first established a side-by-side culture with BMMC, fetal skin (FSMC) and fetal liver (FLMC) to identify the best surrogates for mature connective-tissue MC (CTMC). All three MC types showed comparable morphology by histology and MC phenotype by flow cytometry. Heterogeneity was detected in the transcriptome with the most differentially expressed genes in FSMC compared to BMMC being Histidine (*Hdc*) and Tryptase (*Tpsb2*). FLMC showed a reduced surface expression of ST2 and a diminished secretion of type 2 cytokines. Higher granule content, stronger response to FcεRI activation and significantly higher release of histamine from FSMC indicated differences in MC development *in vitro* dependent on the tissue of origin. Thus, tissues of origin imprint MC precursor cells to acquire distinct phenotypes and signatures despite identical culture conditions.

Resistance to immunotherapy in melanoma is linked to an increase of phenotypic heterogeneity of melanoma cells to their response to pro-inflammatory signals from the tumor microenvironment (TME). Within the TME of melanoma, an accumulation of MC has been found, especially in areas of immune regression. To decipher the role of MC plasticity in melanoma progression, we introduced the alarmin IL-33 into the TME of a murine B16 melanoma model and found an accumulation of MC. *In vivo* experiments using the MC-deficient *Mcpt5-cre-RDTA<sup>fl/fl</sup>* mice showed that the combined treatment of implanted tumors with IL-33 and the TLR2/6 agonist Pam2Cys induces tumor control in a MC-dependent manner by recruiting cytotoxic T cells and modulating the TME into hot tumors. We further found that the absence of MC induces lymphatic metastasis in this setting.

Among melanoma immunotherapy are drugs targeting the immune checkpoints, anti-CTLA-4, and anti-PD-1 inhibitors. Cutaneous adverse immune events (cutAE) are common during immunotherapy and are often dose-limiting and can lead to discontinuation of therapy. In a clinical study with a small cohort of patients with melanoma, we found that melanoma patients presented with increased Th17 and Th22 cells in the blood during a cutAE and increased levels of associated cytokines in the plasma.

In conclusion, this work showed that MC play an essential role in tumor control of melanoma and can be targeted for more efficacy. Further, we identified that the *Mcpt5-cre-RDTA<sup>fl/fl</sup>* mice could be used as a novel model for investigating lymphatic metastasis in melanoma.

## Zusammenfassung

Aus Knochenmark generierte Mastzellen (BMMC) werden als In-vitro-Modell verwendet, um Mastzellen (MC) zu untersuchen. Im Körper machen die aus dem Knochenmark stammenden MC nur einen Bruchteil aller MC aus; der Großteil der MC in vivo ist und bleibt gewebsständig. Eine Parallelkultur mit MC aus dem Knochenmark, fetaler Haut (FSMC) und fetaler Leber (FLMC) wurde angelegt, um die besten Surrogate für reife Bindegewebs-MC (CTMC) zu identifizieren. Alle drei MC-Typen zeigten eine vergleichbare Morphologie in der Histologie und einen vergleichbaren MC-Phänotyp in der Durchflusszytometrie. Jedoch wurde eine transkriptionelle Heterogenität festgestellt, wobei die am stärksten unterschiedlich exprimierten Gene in FSMC im Vergleich zu BMMC Histidin und Tryptase waren. FLMC zeigte eine verringerte Oberflächenexpression von ST2 und eine verminderte Sekretion von Typ-2-Zytokinen. Eine höhere Anzahl an Granula, eine stärkere Reaktion auf die FcεRI-Aktivierung und eine deutlich höhere Histamin Freisetzung aus FSMC deuteten auf Unterschiede in der MC-Entwicklung in Abhängigkeit vom Ursprungsgewebe hin. Das Ursprungsgewebe prägt somit MC-Vorläuferzellen, um trotz identischer Kulturbedingungen unterschiedliche Phänotypen zu erzeugen.

Innerhalb des TME des Melanoms wurde eine Anhäufung von MC festgestellt, insbesondere in Bereichen mit Immunregression. Um die Rolle der MC-Plastizität beim Fortschreiten des Melanoms zu entschlüsseln, wurde das Alarmin IL-33 in das TME eines murinen B16-Melanommodells eingeführt, welches zur Anreicherung von MC führte. In-vivo-Experimente mit MC-defizienten *Mcpt5-cre-RDTA<sup>fl/fl</sup>*-Mäusen zeigten, dass die kombinierte Behandlung implantierter Tumoren mit IL-33 und dem TLR2/6-Agonisten Pam2Cys eine MC-abhängige Tumorkontrolle durch die Rekrutierung zytotoxischer T-Zellen induzierte. Zudem wiesen MC-defiziente Mäuse Anzeichen einer lymphatischen Metastasierung auf.

Zur Melanom-Immuntherapie gehören Medikamente, die auf die Immun-Checkpoints abzielen, sowie Anti-CTLA-4- und Anti-PD-1-Inhibitoren. Kutane Nebenwirkungen (cutAE) treten während der Immuntherapie häufig auf, sind oft dosislimitierend und können zum Abbruch der Therapie führen. In einer klinischen Studie stellten wir fest, dass Melanom Patienten während einer cutAE erhöhte Th17- und Th22-Zellen im Blut und erhöhte Spiegel damit verbundener Zytokine im Plasma aufwiesen.

Zusammenfassend zeigte diese Arbeit, dass MC eine wesentliche Rolle bei der Tumorkontrolle von Melanomen spielt und für eine höhere Wirksamkeit gezielt aktiviert werden können. Darüber hinaus haben wir festgestellt, dass die *Mcpt5-cre-RDTA<sup>fl/fl</sup>*-Mäuse als neues Modell zur Untersuchung der Lymphmetastasierung bei Melanomen verwendet werden könnten.

## Table of content

<i>Acknowledgment</i> .....	<i>III</i>
<i>Abstract</i> .....	<i>IV</i>
<i>Zusammenfassung</i> .....	<i>V</i>
<i>Table of content</i> .....	<i>VI</i>
<i>List of Tables</i> .....	<i>VIII</i>
<i>List of Figures</i> .....	<i>IX</i>
<i>List of abbreviations</i> .....	<i>X</i>
<b>1 Introduction</b> .....	<b>1</b>
<b>1.1 Mast cell biology</b> .....	<b>1</b>
1.1.1 Developmental origin of MC.....	1
1.1.2 Morphology and heterogeneity of MC .....	3
<b>1.2 MC activation and granule secretion</b> .....	<b>4</b>
1.2.1 MC activation via IgE-receptor .....	6
1.2.2 MC activation via TLR.....	7
1.2.3 MC activation via IL-33R/ST2.....	9
<b>1.3 MC models for in vivo and in vitro analysis</b> .....	<b>10</b>
<b>1.4 MC in health and disease</b> .....	<b>12</b>
1.4.1 The role of MC in cancer .....	12
1.4.2 Pro-tumorigenic functions of MC .....	13
1.4.3 Anti-tumorigenic functions of MC .....	13
<b>1.5 Cutaneous melanoma</b> .....	<b>14</b>
1.5.1 Characterization of CM .....	14
1.5.2 Metastasis formation in CM .....	15
1.5.3 Therapeutic interventions in CM.....	17
1.5.4 The tumor microenvironment of CM .....	18
1.5.5 Hot vs. cold tumors .....	19
<b>1.6 Aim of this study</b> .....	<b>20</b>
<b>2 Materials and methods</b> .....	<b>21</b>
<b>2.1 Materials</b> .....	<b>21</b>
2.1.1 Laboratory devices .....	21
2.1.2 Chemicals and solutions .....	21
2.1.3 Antibodies .....	22
2.1.4 Primer sequences for qPCR.....	24
2.1.5 Software .....	25
<b>2.2 Methods</b> .....	<b>26</b>
2.2.1 In vitro methods .....	26
2.2.1.1 In vitro generation of MC.....	26
2.2.1.2 Flow Cytometry analysis of MC surface markers .....	26
2.2.1.3 Histologic staining of MC .....	26
2.2.1.4 Transmission electron microscopy .....	27
2.2.1.5 Proliferation, histamine release and hexosaminidase assay .....	27
2.2.1.6 Cytokine measurement .....	28
2.2.1.7 Patch-Clamp analysis .....	28
2.2.1.8 Intracellular calcium measurement.....	29
2.2.1.9 Analysis of gene expression .....	29
2.2.1.10 Bulk RNA sequencing.....	30
2.2.2 In vivo methods .....	30
2.2.2.1 Animals .....	30
2.2.2.2 Murine B16 melanoma model.....	31

2.2.2.4	Preparation of tumors, skin and lymph nodes and flow cytometry .....	31
2.2.2.5	Cytokine measurement of serum .....	31
2.2.2.6	Histology of tumors.....	32
2.2.3	Human study methods.....	32
2.2.3.1	Study design and patient cohort .....	32
2.2.3.2	Plasma analysis and PBMC isolation.....	33
2.2.3.3	Flow cytometry analysis of T cell subtypes .....	33
<b>3</b>	<b><i>Results</i></b> .....	<b>34</b>
<b>3.1</b>	<b>Fetal tissue-derived MC as experimental surrogate for in vitro CTMC.....</b>	<b>34</b>
3.1.1	MC phenotypes following cultures of BM cells and fetal tissue .....	34
3.1.2	MC from different tissues show transcriptional heterogeneity .....	39
3.1.3	Responsiveness of MC types to IgE stimulation .....	41
3.1.4	MC response to endogenous stimuli.....	43
<b>3.2</b>	<b><i>Targeting MC plasticity re-shapes the TME of melanoma.....</i></b>	<b>47</b>
3.2.1	IL-33 mediates tumor control in melanoma and recruits MC to the TME .....	47
3.2.3	IL-33 activated MC are essential for recruiting T-cells to the TME .....	50
3.3	Education of melanoma cells by MC impairs lymphatic metastasis .....	53
3.3.1	The impact of MC secretome on melanoma migration .....	54
3.3.2	Loss of MC results in lymphatic metastasis in a murine melanoma model.....	55
<b>3.4</b>	<b>Distinct shift of T cell subtypes during cutAE in melanoma patients under ICI .....</b>	<b>65</b>
3.4.1	Clinical characteristics of the patient cohort .....	65
3.4.2	Shift towards Th1 cells in PBMC during ICI is not associated with a favorable clinical response....	69
3.4.3	cutAE show a Th17/Th22-related immune profile .....	70
3.4.4	Plasma levels of IL-10 is associated with cutAE and response to ICI.....	72
<b>4.</b>	<b><i>Discussion</i></b> .....	<b>74</b>
<b>4.1</b>	<b>Fetal Tissue-derived MC as experimental surrogate for in vitro CTMC .....</b>	<b>74</b>
4.1.1	Different functionalities of MC types are based on transcriptional heterogeneity .....	75
4.1.2	Limitations of the study.....	77
<b>4.2</b>	<b>ST2/TLR2 activated MC promote anti-tumoral functions in the TME of melanoma.....</b>	<b>78</b>
4.2.1	High levels of IL-33 are associated with better survival in melanoma .....	78
4.2.2	Treatment of B16 melanoma with IL-33/Pam2Cys attenuates tumor progression.....	79
4.2.3	IL-33 stimulated MC recruit T cells and induce hot tumors in a murine melanoma model .....	79
4.2.4	MC as a target for novel combination therapy in melanoma.....	81
4.2.5	Limitations of the study.....	82
<b>4.3</b>	<b>Melanoma education by MC impairs lymphatic metastasis .....</b>	<b>82</b>
4.3.1	Education of melanoma cells by MC .....	83
4.3.2	Chemotactic recruitment of immune cells by MC to the TME .....	84
4.3.3	Outlook.....	86
<b>4.4</b>	<b>Distinct shift of T cell subtypes during cutAE in melanoma patients under ICI .....</b>	<b>87</b>
4.4.1	Cutaneous adverse events show a Th17 phenotype.....	88
4.4.2	Each cutAE presents with a unique cytokine profile.....	89
4.4.3	Serum IL-10 levels as a potential diagnostic marker for cutAE.....	90
4.4.3	Outlook and limitations .....	91
<b>5.</b>	<b><i>Conclusion</i></b> .....	<b>92</b>
	<b><i>List of References</i></b> .....	<b>93</b>

## List of Tables

Table 1: MC proteases among MC subclasses .....	4
Table 2: List of available mouse models to analyze MC.....	11
Table 3: Laboratory devices .....	21
Table 4: Medium and supplements.....	21
Table 5: Buffers and solutions.....	21
Table 6: Chemicals and reagents .....	22
Table 7: Murine antibodies for flow cytometry.....	23
Table 8: human antibodies for flow cytometry.....	24
Table 9: Primers used for qPCR.....	24
Table 10: Total cell yield and maturation time for MC of different tissue origins .....	35
Table 11: Top 50 DEG in primary tumors from MC-deficient mice.....	57
Table 12: Clinical characteristics of melanoma patients included in this study .....	68
Table 13: Summarized data of MC surrogate characteristics .....	76

## List of Figures

Figure 1: New perception of the hematopoietic landscape .....	1
Figure 2: MC arise from three distinct developmental waves .....	2
Figure 3: Surface receptors on MC.....	6
Figure 4: Intracellular signaling pathway of TLR 2/6 and ST2 signaling .....	10
Figure 5: Six-step process of metastasis formation .....	16
Figure 6: Generation and characterization of MC. ....	36
Figure 7: Morphology of MC cultures .....	38
Figure 8: Transcriptomic analysis of MC cultures .....	40
Figure 9: MC response to IgE stimulation.....	42
Figure 10: MC response towards endogenous stimuli .....	44
Figure 11: MC response to IL-33 stimulation .....	46
Figure 12: IL-33 recruits MC to the TME of melanoma .....	48
Figure 13: Synergistic effect of ST2 and TLR2/6 on MC activation.....	50
Figure 14: IL-33 activated MC mediate T-cell inflamed tumors.....	52
Figure 15: ST2 <sup>-/-</sup> MC in the TME abrogates the anti-tumoral effect. ....	53
Figure 16: MC inhibit B16 migration.....	55
Figure 17: Metastasis formation in MC deficient mice. ....	56
Figure 18: Altered chemokine expression in tumor bearing mice .....	59
Figure 19: Altered immune cell composition in tumors of MC-deficient mice.....	61
Figure 20: Depletion of DC and macrophages does not impact metastasis formation .....	62
Figure 21: MC-reconstitution of the skin rescues non-metastasis phenotype.....	64
Figure 22: Study design and Th1/Th2 immune profile of patients .....	67
Figure 23: Shift towards Th1 cells in PBMC during ICI.....	69
Figure 24: cutAE show a Th17/Th22-related immune profile.....	71
Figure 25: IL-10 as prognostic marker. ....	73
Figure 26: Graphical abstract for IL-33-activated MC in melanoma .....	80
Figure 27: Graphical abstract for cutAE study .....	89

## List of abbreviations

AND	anaphylactic degranulation
BMCP	MC/Basophil-progenitor
BMMC	Bone-marrow derived mast cell
BSA	Bovine Serum Albumin
Ca <sup>2+</sup>	calcium
CaCl <sub>2</sub>	calcium chloride
cDC	conventional DC
cDNA	complementary DNA
CLR	C-type lectin-like receptors
ct	cycle threshold
CTLA4	cytotoxic T-lymphocyte-associated protein 4
CTMC	connective-tissue mast cell
cutAE	cutaneous adverse event
DAMP	damage-associated molecular patterns
DC	Dendritic Cell
DMSO	Dimethyl Sulfoxide
DNP-HSA	2,4-Dinitrophenyl hapten conjugated to Human Serum Albumin
EDTA	Ethylenediaminetetraacetic acid
ELISA	enzyme linked immunosorbent assay
EMT	Epithelia-to-mesenchymal transition
FCS	fetal calf serum
FFPE	Formalin Fixed Paraffin Embedded
FLMC	fetal-liver mast cell
FSMC	fetal-skin mast cell
GO	Gene Ontology
ICI	checkpoint immunotherapy
iMC	inflammatory mast cells
irAE	Immune-related adverse events
KEGG	Kyoto Encyclopedia of Genes and Genomes
LPS	lipopolysaccharide
mAB	monoclonal antibody
MAPK	mitogen-activated protein kinase
MC	mast cell
MCAS	MC-activating syndromes
MCP	mast cell progenitor

MDSC	myeloid-derived suppressor cells
MFI	mean fluorescent intensity
MMC	mucosal mast cell
MRGPRX	Mas-related G protein-coupled receptor
NK	natural killer cells
NLR	nucleotide-binding oligomerization domain (NOD)-like receptors
OVA	ovalbumin
PAMP	pathogen-associated molecular patterns
PBMC	peripheral blood mononuclear cell
PBS	phosphate buffered saline
PD1	programmed cell death protein 1
PMC	peritoneal mast cell
PMD	piecemeal degranulation
PMN	premetastatic niche
PRR	pattern recognition receptor
RLR	retinoic acid-inducible gene I receptor
RNA	ribonucleic acid
ROS	reactive oxygen species
RT-PCR	real-time polymerase chain reaction
SCF	stem cell factor
TAMC	tumor-associated MC
TAM	tumor-associated M2-like macrophages
TLR	toll-like receptor
TME	tumor microenvironment
TNF	tumor necrosis factor
Tregs	regulatory T cells
TSLP	thymic stromal lymphopoietin
WHO	World Health Organization

Units:

°C	celsius
μM	micro molar
μm	micro meter
h	hours
kg	kilogram
mg	milligram
min	minutes

# 1 Introduction

## 1.1 Mast cell biology

Paul Ehrlich first described mast cells (MC) in 1877. MC can be characterized as long-lived tissue-resident mononuclear immune cells distributed throughout the body in the mucosal and epithelial tissues. Since then, research has come a long way in defining this cell type's origins, morphology, and function.

### 1.1.1 Developmental origin of MC

MC progenitors (MCP) are the first hematopoietic immune cells to arise in embryonic development. Contrary to the classic tree-like model describing hematopoiesis, single-cell RNA sequencing studies suggest that hematopoietic stem cells and progenitor cells differentiate along trajectories [4]. These studies postulate that the MC developmental route, both murine and in humans, is positioned adjacent to the erythrocyte and basophil trajectories, and a common MC/Basophil-progenitor (BMCP) exists in the bone marrow (BM), with strong expression of the genes *Ms4a2*, *Cpa3*, *Cma1* and *Gzmb* (Figure 1)[5-7].

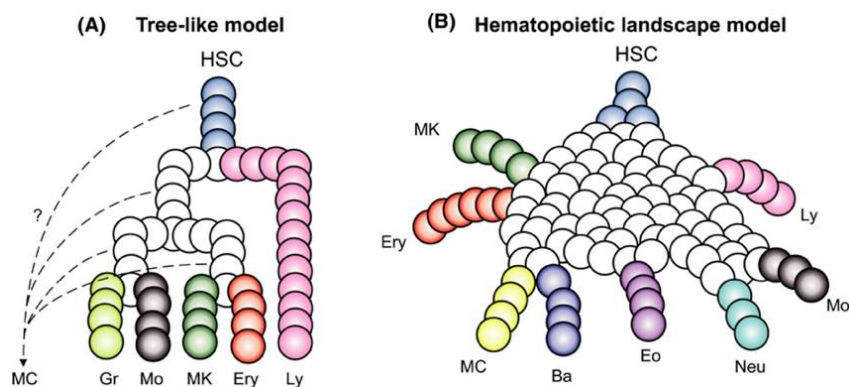


**Figure 1: New perception of the hematopoietic landscape**

(A) Classic tree-like model depicting hematopoiesis as a sequential series of discrete progenitor states, with each branching point defining a more committed lineage progenitor. (B) Hematopoietic landscape model depicting hematopoiesis as a continuum of progenitor cells moving along a continuous landscape of cellular progenitor states culminating in various lineage committed entry pathways. Ba, basophil; Eo, eosinophil; Ery, erythrocyte, Gr, granulocyte, HSC, hematopoietic stem cell; Ly, lymphocyte; MC, mast cell; MK, megakaryocyte; Mo, monocyte, Neu, neutrophil [3].

MC were found to arise from three distinct temporally separate developmental waves. The first wave arises from the yolk sac, where erythroid–myeloid progenitors (EMP) from stage E7.5 (E7) contain committed MC precursors. These can enter the fetus after the initial establishment

of the circulation at around E8.5 and function as a source of the mature MC found in tissues throughout subsequent fetal development. During the second wave, transient definitive hematopoiesis, late EMP from the yolk sac generate other myeloid cells, including neutrophils, basophils, and eosinophils. Many other myeloid lineage cells are produced from hematopoietic stem cells (HSC) in the aorta–gonad–mesonephros (AGM). From there, the progenitors, including MCP, travel to the fetal liver, the primary site of hematopoiesis. These two early MC waves mainly comprise the adult connective-tissue MC (CTMC) and serosal-type MC populations. In the last wave of development at stage E16.5, the definite hematopoiesis, the bone marrow begins to take over as the binding site of hematopoiesis, which persists until after birth and into adulthood. Based on fate mapping experiments using *Cdh5*–CreERT2:Rosa<sup>tdT</sup> mice, it could be shown that early yolk sac-derived MC are replaced in the skin by those arising from definitive hematopoiesis, beginning at E10.5 and continuing throughout life (Figure 2).

In contrast, definitive hematopoiesis-derived MC emerge from the fetal liver. They are maintained in the periphery in adult mice even after the initiation of hematopoiesis in the BM. Of note, postnatally *in vivo*, BM-derived hematopoietic stem cells account for only a fraction of MC in the body and mainly replenish the mucosal MC population, but not CTMC [2].

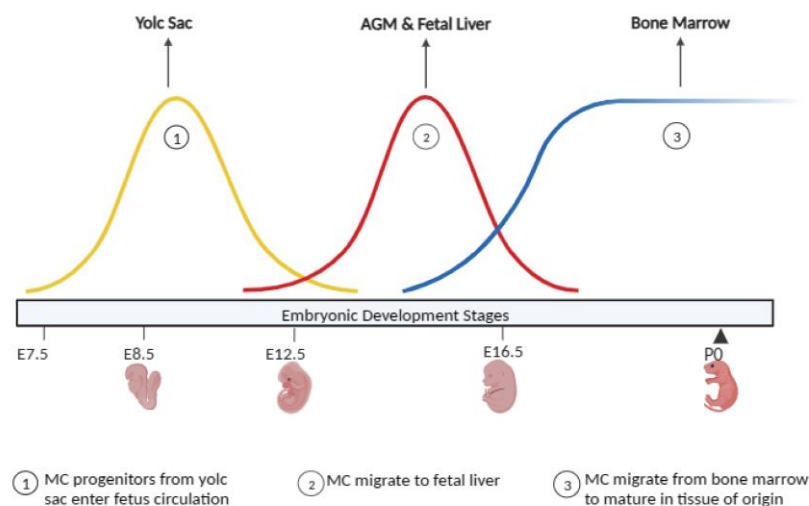


**Figure 2: MC arise from three distinct developmental waves**

MC originate from three distinct developmental waves. The first wave arises from the yolk sac, where EMP from stage E7.5 enter the fetus circulation (in yellow). During the second wave, MC precursors are generated from HSC and migrate to the fetal liver (in red). During the third wave at stage E16.5. The BM begins to take over as the binding site of hematopoiesis, generating MC that persist until adulthood (in blue). Own illustration based on Gentek et al. [1, 2].

Lineage-committed MCP of different origins enter the circulation and home to peripheral tissues, where they undergo maturation and become tissue-resident immune cells. This tissue homing depends on adhesion molecules and chemoattracting gradients, such as specific integrins and chemokine receptors. For example, MCP recruitment from the blood into the lung and the gut depends on the interaction of  $\alpha 4\beta 1$  and  $\alpha 4\beta 7$  integrins with VCAM1, as well as interaction with stromal cell-derived CCL2 and its receptor CXCR2 [8, 9]. Experiments by Weller et al. identified leukotriene B<sub>4</sub> as the chemotactic molecule for MCP migration into the skin [8, 10, 11]. Unlike other immune cells, MCP mature in the target tissue because of the tissue microenvironment and cytokines within this microenvironment such as IL-3, IL-4, IL-9, IL-33 and SCF [12].

### **1.1.2 Morphology and heterogeneity of MC**

MC are mononuclear cells identified by metachromatic staining of their secretory granules. The cytoplasm of MC contains up to 200 granules that store inflammatory mediators such as histamine, heparin, various cytokines, and chemokines [13]. A well-established method for detecting secretory granules is toluidine blue staining, which binds to heparin and stains MC in dark violet compared to the orthochromatic staining of other cell types [14]. Another method to determine MC by histology is Giemsa staining, which stains the cytoplasm of MC dark blue while staining the granules red [15]. To further distinguish between mucosal-like MC (MMC) and CTMC, the combined staining with Alcian blue and Safranin-O can be used to allow simultaneous differentiation between the MC types [16].

In classical perception, MC were divided into two phenotypes, MMC and CTMC, based on their granule content and localization (see Table 1) [17]. MMC develop from agranular MCP generated from BM. These progenitors are home to the intestinal mucosa, where they are further recruited to the intestine and lung during T cell-mediated inflammation [18-20]. Interestingly, T cell-deficient humans and mice lack MMC [21]. In contrast, CTMC are found in most connective tissues and are seeded during embryogenesis by circulating progenitors derived from the fetal liver [22]. Experiments using BM transfers found that tissue MC can be derived from grafted BM cells in irradiated mice. However, donor-derived MC showed poor engraftment in connective tissues, suggesting that the MC compartment in connective tissue is maintained by longevity or self-renewal rather than replacement by BM-derived precursor cells [22].

**Table 1: MC proteases among MC subclasses**

MC subclasses	Granule Proteases		
	Tryptases	Chymases	Peptidases
MMC	/	mMCP-1 mMCP-2	/
CTMC	mMCP-6 mMCP-7	mMCP-4 mMCP-5	CPA-3

Recent advances in single-cell transcriptomics have shown that the heterogeneity of MC goes beyond the standard classification based on proteases. Analysis of transcriptional profiles of MC showed that MC from different tissues are distinct [23]. Comparative analysis revealed considerable tissue-specific gene expression, indicating that MC maturation in peripheral tissue is regulated by stimuli secreted by the microenvironment and neighboring fibroblast [24]. Recently, a new subpopulation, called inducible MMC, has been postulated. These inducible MC arise from BM-derived MCP that express  $\beta 7$ -integrin and are recruited to mucosal tissues in response to T cell-mediated type 2 inflammation. Further, inflammatory MC (iMC) have been postulated, which is a subepithelial population that changes in the microenvironment during inflammation [25] [26]. However, these findings are often based on results from in vitro generated MC or sequencing of bulk MC samples. It has been shown that the heterogeneity of MC goes beyond tissue residence. Comparing the transcriptome of isolated human skin MC with ex vivo cultured MC showed significant differences in the gene expression profile of both groups, suggesting MC undergo de- or trans-differentiation associated with the in vitro culture [27].

## 1.2 MC activation and granule secretion

The process of MC granule biogenesis initiates with the fusion of clathrin-coated vesicles that originate from the trans-Golgi network. Subsequently, progranules are formed by fusing enough vesicles. These progranules undergo extensive vesicle fusion events to mature into granules. During granule maturation, the continuous accumulation of MC mediators and serglycin proteoglycan occurs, as well as the acidification of pro granules resulting from fusion with other immature or mature granules [28].

Mediators are released from MC by three main mechanisms: constitutive exocytosis, piecemeal degranulation (PMD), and anaphylactic degranulation (AND) [29]. Constitutive exocytosis is

a continuous process where secretory vesicles matured in the trans-Golgi cisternae are transported to the cell surface, resulting in the release of soluble cytokines or the transport of proteins to the cell surface. On the other hand, activated MC can release their granules through differential processes such as PMD or AND [30]. PMD is a poorly understood process involving the selective release of granule contents. In contrast AND involves the complete fusion of granules with the plasma membrane and the rapid release of granule mediators or whole granules. PMD is characterized by partially releasing granule contents without full granule fusion events with the plasma membrane. In contrast AND is the rapid release involving granule-granule and granule-membrane fusion [31, 32].

Three distinct types of granules have been identified and categorized in rodents based on their contents and surface markers *in vitro*. Type I granules are characterized by MHC class II,  $\beta$ -hexosaminidase, LAMP-1, LAMP-2, and mannose-6-phosphate receptors on their surface. In contrast, type II granules contain high levels of serotonin and histamine and lower levels of lysosomal enzymes such as cathepsins. Type III granules exhibit high levels of  $\beta$ -hexosaminidase and serotonin but lack lysosomal enzymes and MHC class II. The regulation of granule-granule fusion events may play a role in generating granule diversity and supporting the hypothesis of MC granule biogenesis [33, 34].

Therefore, MC can - dependent on the provided stimuli – differentially secrete their granule-derived mediators and thus distinctly remodel and shape inflammatory milieu. MC can secrete numerous inflammatory mediators that are either pre-formed and stored in their secretory granules or synthesized *de novo* upon MC activation. Amongst these pre-stored mediators are histamine, tryptase, and  $\beta$ FGF. Following activation, MC can *de novo* generate and release a wide variety of either pro-inflammatory or anti-inflammatory cytokines such as IL-1 $\beta$ , IL-6, IL-10, or IL-13, respectively [30]. MC express several stimulatory and inhibitory surface receptors, allowing them to respond to external stimuli by finely tuned immune responses [35]. Among the activating receptors of MC is the high-affinity IgE receptor Fc $\epsilon$ RI, the Mas-related G protein-coupled receptor X2 (MRGPRX2), the alarmin IL-33 receptor ST2/IL33R and pattern recognition receptors (PRR) sensing also danger signals, such as Toll-like receptors (TLR) (Figure 3).

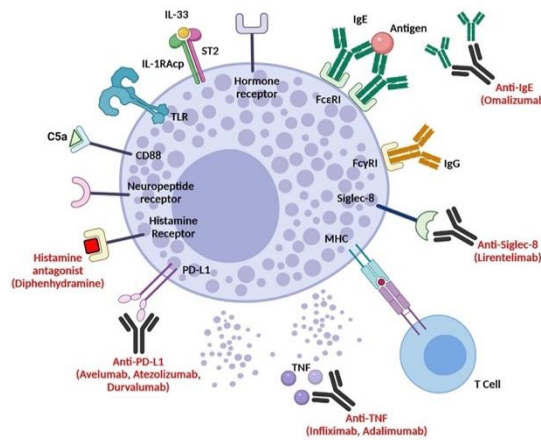


**Figure 3: Surface receptors on MC**

Activating and inhibiting receptors on the cell surface of MC. MC can be activated by antigen-dependent cross-linking of IgE: FcεRI, as well as via the alarmin IL-33 receptor ST2/IL33R and DAMP—image modified from [36].

### 1.2.1 MC activation via IgE-receptor

The most studied mechanism of MC activation is IgE-mediated activation of the Fcε receptor. The Fcε-receptor is constitutively expressed on the surface of MC and is comprised of the IgE-binding α-chain, the membrane-spanning β-chain, and the disulfide-linked homodimer γ-chains [37]. There are two IgE receptors expressed on the cell surface of MC. The low-affinity IgE receptor, FcεRII (or CD23), is a major mediator believed to amplify allergic responses. This receptor is not only present on MC but also on B- and T cells, eosinophils, and monocytes. Additionally, CD23 can form complexes with antigen-bound IgE molecules, enhance antigen presentation, and lead to downstream epitope spreading - a process that results in the production of IgE antibodies to other epitopes on both similar and different antigens, exacerbating allergic disease or further progressing it [32]. Through the CD23 activation, both IL-4 and IL-13 are secreted by MC, promoting a Th2 response. The FcεRI, a high-affinity IgE receptor, amplifies subsequent MC-mediated allergic reactions and is also present on other myeloid lineage cells, including basophils, eosinophils, Langerhans, and dendritic cells (DC). Upon IgE binding to the receptor, FcεRI stabilizes, resulting in heightened levels of surface FcεRI expression on MC [38]. This is evidenced by studies showing that individuals with elevated circulating IgE levels, indicative of allergic disorders, also exhibit increased expression of FcεRI on their immune cells [39]. The enhanced surface expression enables MC to respond to more antigens and induce degranulation at lower antigen concentrations [40].

For a specific allergen to trigger a type 2 allergic response, it typically requires DC to encounter it initially. IL-4 influences the process produced early on by other immune cells, including MC. This cytokine skews naive T cells towards becoming Th2 cells, producing IL-4 and IL-13 to establish a Th2 response in the tissue. In conjunction with co-stimulation, these cytokines cause

B cells to switch to the IgE subclass. The soluble IgE can then enter circulation, binding to surface bound FcεRI on MC in their respective tissue environments. This sensitization process does not cause symptoms in the host. Still, all subsequent encounters with the sensitized allergen will cause an immediate and robust allergic response (type I hypersensitivity). Upon encountering a sensitized allergen, the antigen brings together two FcεRI receptors through interaction with IgE, a process known as cross-linking. This interaction activates the Src family kinases Lyn and Fyn, which subsequently phosphorylate immunoreceptor tyrosine-based activation motifs (ITAM) and activate spleen tyrosine kinase (SYK) upon binding to an ITAM. Additionally, Fyn activates the phosphatidylinositol-3-kinase (PI3K) pathway. Several pathways, including the mitogen-activated protein kinase (MAPK), phospholipase C-gamma (PLC-γ), and PI3K pathways, are also activated during this signaling cascade [32]. This signaling cascade increases cytosolic calcium, causing the MC to degranulate [41]. During MC degranulation, granules containing specific cytokines, phospholipases, chemokines, histamine, and growth factors, including transforming growth factor-beta (TGF-β) and vascular endothelial growth factor, among other products, fuse with the plasma membrane to secrete their contents into the surrounding tissue [37]. This process directly releases prostaglandins (primarily prostaglandin D2) and leukotrienes, which cause typical allergy symptoms such as vasodilation, smooth muscle contraction in the airways, and mucus production [42].

### **1.2.2 MC activation via TLR**

MC are not limited to responding to allergic stimuli only. Under non-allergic conditions, they can be activated and release their granules without involving FcεRI-mediated crosslinking or downstream signaling. These non-IgE-mediated activation mechanisms are less specific [43]. MCs serve as sentinels in host defense, strategically positioned in areas of frequent microbial exposure. They express cell surface receptors that detect and recognize harmful substances and pathogens, utilizing germline-encoded pattern recognition receptors (PRR) to rapidly respond to infections or cellular damage [44]. PRR recognize pathogen-associated molecular patterns (PAMP) or host-derived molecules called damage-associated molecular patterns (DAMP). They belong to four classes: Toll-like receptors (TLR), C-type lectin-like receptors (CLR), retinoic acid-inducible gene I (RIG-I)-like receptors (RLR), and nucleotide-binding oligomerization domain (NOD)-like receptors (NLR). In mice, eight TLR have been identified, with at least TLR2 and TLR4 being involved in innate immunity. In murine MC, TLR1-4 and TLR6-9 have been identified [45]. MC stimulation with TLR agonists produces and releases various cytokines and chemokines without degranulation [46].

TLR2 and TLR4, expressed on the surface of MC, primarily respond to external stimuli. Research indicates that BM-derived MC (BMMC) express a truncated form of TLR2 that lacks an intracellular signaling domain. Most TLRs function as homodimers, except for TLR2, which forms a heterodimer with TLR1 or TLR6 upon ligand binding, activating the adaptor protein MyD88 and initiating an intracellular signaling cascade. Despite the truncated protein, heterodimer formation ensures MC responsiveness to TLR2 activation [47]. Upon engagement with microbial components such as lipopeptides, lipoteichoic acid, or peptidoglycan, TLR2 triggers intracellular signaling pathways that activate NF- $\kappa$ B and MAPK. These pathways culminate in releasing pro-inflammatory cytokines, chemokines, and other mediators from MC.

TLR2 on MC can be activated by a wide range of stimuli, each triggering specific signaling pathways that release distinct cytokines and mediators. TLR2 ligands include microbial ligands, endogenous molecules, and environmental factors. TLR2 can recognize a variety of microbial components, such as lipopeptides, lipoteichoic acid, and peptidoglycans, which are present in bacteria and subsequently induce MC to release the cytokines TNF- $\alpha$ , IL-6, IL-8, and IL-1 $\beta$  [48, 49]. In addition, endogenous molecules such as heat shock proteins (Hsp) and high-mobility group box one protein (HMGB1) can activate TLR2 on MC. These molecules have been shown to induce the release of pro-inflammatory cytokines, including TNF- $\alpha$  and IL-6 [50]. Furthermore, environmental factors such as pollutants, allergens, and toxins can also stimulate TLR2 on MC. Allergens like pollen, dust mites, and specific food components can engage TLR2, leading to MC activation and subsequent release of cytokines. This activation can exacerbate allergic reactions and inflammatory responses [51]. It is also worth noting that TLR2 stimulation has been found to synergize the release of cytokines when used to prime cells for later IgE activation [52].

MC release cytokines upon activation of TLR2, which play critical roles in immune responses. TNF- $\alpha$  induces inflammation and modulates other immune cells, while IL-6 involves inflammation, immune responses, and the acute-phase reaction. IL-8 is a potent chemokine that attracts neutrophils to the site of inflammation, and IL-1 $\beta$  contributes to inflammatory responses and fever [53-56]. Understanding TLR2 activation on mast cells and cytokine release is crucial for understanding immune responses. Targeting TLR2-mediated signaling in MC may offer promise for therapeutic interventions in various inflammatory conditions, allergies, and immune-related disorders by modulating cytokine release and immune responses [57, 58].

### 1.2.3 MC activation via IL-33R/ST2

MC, along with ILC2, Tregs, and endothelial cells, are the immune cells that constitutively express the IL-33R/ST2 receptor, making them highly susceptible to stimulation by the alarmin IL-33 [59]. Furthermore, the observation that IL-33 expression levels were considerably reduced in MC-deficient mice implies that MC play a crucial role in producing IL-33 and are also directly affected by IL-33 stimulation [60]. The receptor for IL-33 (IL-33R, formerly known as ST2) is a member of the IL-1R family. IL-33 is predominantly categorized as an alarmin and is primarily associated with Type 2 immune responses. The primary source of IL-33 are stromal cells, such as fibroblasts, which are located in tissue and release cytokines in response to trauma or other local stressors [61, 62]. Upon ligand binding, the adaptor protein MyD88 is recruited to the Toll/interleukin-1 receptor (TIR) domain, leading to the phosphorylation of IL-1R-associated kinase 1 (IRAK1) and IRAK4, which induces the activation of NF- $\kappa$ B and MAPK, in a p38-dependent manner, implying a role in orchestrating inflammatory diseases [63, 64]. The activation of the MAPK pathway has been shown to accelerate the maturation of CD34<sup>+</sup> MC and enhance the secretion of chemoattracting chemokines such as CXCL8, CCL17, CCL22, and CCL2 [65]. However, the effect of IL-33 on MC is controversially discussed, as acute stimulation shows an Fc $\epsilon$ RI-dependent degranulation and cytokine secretion.

In contrast, prolonged exposure reduces MC activation and a hyporesponsive phenotype [66, 67]. It has further been described that MC can potentiate the functionality of IL-33 by truncating the full-length IL-33 into a more active form through chymases and tryptases [68]. IL-33 allows MC to react to cell damage, but IL-33 also works synergistically with thymic stromal lymphopoietin (TSLP), promoting MC survival, cytokine production, and degranulation [69]. A comparison of the transcriptomic profiles of IgE-activated and IL-33-activated MC has revealed distinct gene expression patterns, suggesting diverse biological functions. While IgE activation is associated with the upregulation of genes involved in oxidative phosphorylation, angiogenesis, and p53 signaling, IL-33 activation displays a gene expression profile similar to that of TNF, STAT3, and IFN- $\gamma$  responses, which are implicated in inflammation [70].

In tissues that are the interface to the external environment, such as the skin, lung, and gastrointestinal tract (GI), a co-existence of high IL-33 expressing epithelial cells and high MC numbers was discovered [71]. IL-33, secreted by surrounding cells, stimulates MC and other immune cells to produce Type 2 cytokines. Specifically, the production of IL-4 and IL-13 by IL-33-activated MC is crucial for establishing a robust Type 2 response in tissues [63]. However,

additional research has revealed that IL-13 is critical in limiting the inflammatory activity associated with IL-33/ST2 by upregulating the expression of an IL-33 decoy receptor, soluble ST2 (sST2) [72].

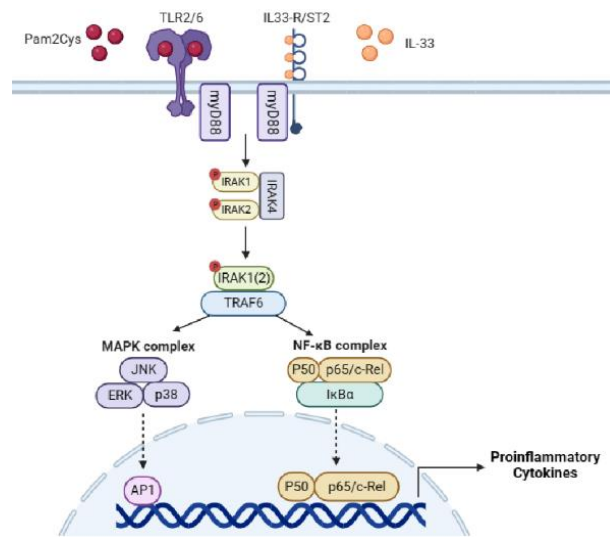


**Figure 4: Intracellular signaling pathway of TLR 2/6 and ST2 signaling**

The signaling Pathway of both IL33R/ST2 and TLR2/6 activation shows that both receptors signal through the myD88 cascade. The recruitment of the adaptor protein myD88 phosphorylates IRAK1 and IRAK4, which induces the activation of the MAPK or NF-κB complex. This leads to the gene translocation of AP-1 or NF-κB, which induces the production of proinflammatory cytokines. Own illustration adapted from Loiarro et al. [73].

### 1.3 MC models for in vivo and in vitro analysis

To study and fully understand MC-specific functions on a cellular level, in vitro experiments are necessary, and appropriate surrogates for humans and mice are required. In vivo models using constitutive or inducible MC-deficient mice are also very important and have helped gather compelling evidence for the relevance of MC in different physiological and pathological processes. Given their evolutionary conservation, many similarities exist between human and mouse MC [74]. However, since MC mature within tissues under the direct influence of the local tissue microenvironment, leading to heterogeneity among MC, it is crucial to define MC surrogates for in vitro studies more closely. The most widely used in vitro model for mouse MC is BMMC. However, BMMC are phenotypically and functionally different from tissue-resident MC populations. Indeed, previous studies indicated that these differences include those associated with the in vivo process of MC maturation and result in alterations, e.g., regarding MC protease expression [75]. Over the past decades, researchers have developed various methods to effectively promote the differentiation and maturation of MC from precursor cells and extract them from tissues [49]. However, the transcriptional analysis of MC originating from

different tissues demonstrated considerably more heterogeneity across tissues than previously assumed [23].

A wide range of mouse models are available to study the role of MC in vivo. Previous research was conducted in mice with a mutation in KIT, for example, the KIT<sup>w-sh</sup> mice, also known as sash-mice. However, it was later realized that these mice also lacked monocytes and showed an aberrant myelopoiesis, leading to an accumulation of myeloid-derived suppressor cells (MDSC) [76]. New mouse models are summarized in Table 2. In this thesis, we worked with the Mcpt5-Cre<sup>R-DTA</sup> model, as it solely affects CTMC, which are relevant for analyzing skin-related diseases. Studying humans is more problematic as no MC deficiency exists in humans, nor do pharmacological tools to deplete MC in humans [77].

**Table 2:** List of available mouse models to analyze MC

MC subclasses	Principle	MC affected
Constitutive:		
Mcpt5-Cre <sup>R-DTA</sup>	Cre expression under the control of the Mcpt5 promoter; Cre-driven expression of DT	CTMC
Cpa3-Cre; ("Cre-Master")	Cre expression under the control of the Cpa3 promoter	CTMC + MMC
Cpa3-Cre; Mcl-1 <sup>fl/fl</sup> ("Hello Kitty")	Mcl-1 deletion under the control of the Cpa3 promoter	CTMC + MMC
Chm-Cre; Mcl-1 <sup>fl/fl</sup>	Mcl-1 deletion under the control of the baboon- $\alpha$ -chymase gene	MMC
Inducible:		
Mas-TRECK	DT receptor expressed under the control of an MC-specific IL-4 enhancer element	CTMC, MMC not determined
Mcpt5-Cre; iDTR	DT receptor expressed under the control of the Mcpt5 promoter	CTMC
Red mast cell and basophil (RMB) mouse	DT receptor and bright red td-Tomato fluorescent protein expressed under the control the $\beta$ chain of Fc $\epsilon$ RI (Ms4a2)	CTMC, MMC not determined

## **1.4 MC in health and disease**

MC are tissue-resident immune cells that play a crucial role in different immune responses [78]. Owing to their location at the host–environment interface, respectively connective and mucosal tissues, MC act as sentinels for invading pathogens [32, 79]. Research on MC over decades focused on the crucial role of MC in allergic diseases such as allergic asthma and delayed type 1 hypersensitivity [80]. More recently, it has become apparent that MC play a crucial role as effector cells in innate immune responses [81]. MC express several stimulatory and inhibitory surface receptors, allowing them to respond to external stimuli and fine-tune immune responses [82]. Among the activating receptors of MC are the high-affinity IgE receptor FcεRI, the Mas-related G protein-coupled receptor X2 (MRGPRX2), the alarmin IL-33 receptor ST2/IL33R and PRR also sensing danger signals, such as TLR [83].

### **1.4.1 The role of MC in cancer**

Recently, the role of MC in cancer biology has gained increasing interest from researchers. However, their role remains multifaceted, as they can either promote or impede tumor progression depending on the context [35]. The microenvironment of cancer is essential for homeostasis and tumorigenesis. Aberrant signaling and a shift in immune cell composition of the microenvironment can allow or even promote tumor growth. Tumor-associated MC (TAMCs) have been identified in several human tumors; however, whether MC elicit pro- or anti-tumor functions seems dependent on the tumor entity [84-87]. Within the same cancer entity, the localization of MC can influence the outcome. In prostate cancer and renal cell carcinoma, intra-tumoral MC negatively regulate angiogenesis and cancer growth, while peritumoral MC support tumor development [88-91]. A potential explanation for the ambiguous function of MC is the microenvironment of cancer and how it shapes MC and vice versa. Aberrant signaling and a shift in immune cell composition of the microenvironment can thus promote tumor growth and proliferation [35].

The tumor microenvironment (TME) is a complex ecosystem surrounding cancer cells, comprising a diverse array of cellular and non-cellular elements that interact intricately within the tumor's vicinity. The TME includes immune cells, fibroblasts, blood vessels, extracellular matrix (ECM), and signaling molecules, significantly influencing tumor behavior and progression. The dynamic nature maintains a delicate balance between promoting or inhibiting tumorigenesis, affecting processes such as immune surveillance, angiogenesis, and therapeutic responses [92, 93].

### **1.4.2 Pro-tumorigenic functions of MC**

Pro-tumorigenic effects of MC have been associated with the development of angiogenesis, inflammation, and tissue homeostasis. In cases of pancreatic cancer, an accumulation of MC within tumor sites was associated with poor prognosis [94]. This was also supported in a corresponding mouse model of Myc-induced beta cell pancreatic cancer, where restraining MC degranulation led to reduced tumor growth and angiogenesis [85]. Also, in bladder cancer, an elevated MC count was linked to high-grade lesions and facilitated cancer metastasis through an ER $\beta$ /CCL2/CCR2 pathway, triggering epithelial-to-mesenchymal transition (EMT) [95]. Furthermore, in thyroid cancer, MC-derived IL-8 sustains EMT and stemness by activating Akt phosphorylation and Slug in tumor cells with the secretion of CXCL1, CXCL10, and histamine by MC also supporting thyroid cancer growth [96]. Moreover, studies in mice demonstrate that both genetic and pharmacological inhibition of MC induces the regression of preneoplastic polyps, underlining the role of MC in colon carcinogenesis [97].

### **1.4.3 Anti-tumorigenic functions of MC**

Data has shown that MC can exhibit an anti-tumorigenic role in cancer. Interestingly, while MC induce the regression of preneoplastic polyps, MC also aid in resolving colon inflammation by promoting mucosal healing through IL-33 degradation [98]. Both IL-6 and CXCL10 secretion of activated MC showed anti-tumor effects in mouse melanoma and lung cancer models [99, 100]. The accumulation of MC also showed improved patient survival in human non-small cell lung cancer patients. Especially TNF- $\alpha$  secreted by MC shows promising anti-tumor effects through its cytotoxic potential [101, 102]. The underlying basis of this thesis is the identification of MC as key anti-tumoral players in melanoma. In a study conducted on 38 melanoma patients who developed immune-related adverse events (irAE) while being treated with anti-CTLA-4 and anti-PD-1 antibodies, a relationship between irAE and the patient's overall response and survival was found. This study uncovered a previously unrecognized mechanism of MC-mediated tumor immune defense. Targeting MC with the microbial adjuvant LPS effectively boosted T cell-mediated tumor cell clearance. This strategy takes advantage of the localization of MC near the tumor, their plasticity regarding their effector functions, and the potentiating antitumor effects generated by the recruitment of effector T cells. The findings also highlight the crucial role of CXCL10 in melanoma immune defense. Kaesler et al. clearly showed that MC are a vital source of CXCL10 that could be harnessed for future therapeutic strategies [99, 103].

## **1.5 Cutaneous melanoma**

Cutaneous melanoma (CM) is a malignant neoplasm that arises from melanocytes, a particular kind of skin cell responsible for melanin production. This pigment lends color to the skin. Upon exposure to sunlight, melanocytes increase melanin production, leading to skin darkening or tanning [104]. The incidence of melanoma has been increasing globally, rendering it a more prevalent form of cancer [105]. Previously, it was regarded as a rare type of cancer, but it has now emerged as one of the top ten most common cancers in the United States and several other countries [106]. In 2019, cancer was the first leading cause of death in people before age 70, according to estimates from the World Health Organization (WHO). The incidence of malignant melanoma is steadily rising, with 5% of all new cancer cases in Germany being melanoma of the skin [107]. Even though melanoma accounts for only 4% of dermatological cancers, it accounts for 80% of deaths in patients with skin cancer [108]. This is due to its high metastatic potential.

### **1.5.1 Characterization of CM**

CM is a form of skin cancer that may occur on any part of the body and is associated with various risk factors, such as skin type I and II on the Fitzpatrick scale, a high number of common, congenital, or atypical nevi, a family history of melanoma, and exposure to UV radiation in early age, and immunosuppression [109, 110]. Specific genomic alterations influence the development and progression of cutaneous melanoma. In melanoma, specific mutated genes are considered drivers of the tumor. Gain-of-function mutations can cause oncogenes to become overactive, leading to uncontrolled tumor growth. In contrast, loss-of-function mutations can result in the inactivation of tumor suppressor genes, promoting unchecked tumor growth [111]. Sequencing analysis of human cancer cells has illuminated the daunting array of mutation combinations that can cause life-threatening malignancies, even when they arise from the same cell of origin. Additionally, a great phenotypic diversity within and between patients was identified [112].

Approximately 10% of all melanomas are hereditary. Individuals with germline CDKN2A tumor suppressor gene mutations have a significantly elevated lifetime risk of developing CM [113]. However, most CM is characterized by several somatic genetic alterations, particularly within genes related to the RAS/RAF/MEK/ERK and PI3K/AKT signaling cascades [114, 115]. The MAPK pathway is often disrupted in CM, with 90% of cases exhibiting abnormal activation. This dysregulation can be caused by mutations in the BRAF gene, which are present

in 37-60% of cases. The BRAF gene encodes a protein kinase with three regulatory domains and one catalytic. The latter is involved in the phosphorylation of MEK, and mutations such as V600E result in a constitutively active kinase. Recognizing these mutations is essential for treatment and prognosis, as BRAF V600-mutated melanomas can be treated with BRAF/MEK inhibitors, with higher response rates observed in V600E-mutated cases compared to V600K-mutated patients [116]. The second most common cause of abnormal MAPK pathway signaling in CM is activating mutations in the NRAS gene, which occur in 15-30% of melanomas. These mutations cause persistent aberrant signaling through both the MAPK and PI3K pathways. NRAS and BRAF mutations are generally considered mutually exclusive, although co-mutations have been observed rarely. Melanomas with NRAS and NRAS-BRAF co-mutations have a less favorable prognosis than those with BRAF mutations, as no target therapies are currently available for NRAS mutations [117]. Neurofibromin 1 (NF1) is a gene that suppresses tumor growth and is mutated in approximately 10-15% of CM, making it the third most prevalent genetic mutation in this type of cancer. The NF1 protein regulates the RAS family of proteins, reducing downstream signaling. As a result, LOF mutations in NF1 cause increased signaling through the MAPK and PI3K pathways [118].

Integrative clinical genomics showed that the most predominant genes were somatically changed in metastasis. The PTEN gene, a tumor suppressor, is frequently disrupted during vertical growth. PTEN alterations tend to be mutually exclusive with NRAS mutations but often co-occur with BRAF mutations [119]. Mutations in the TERT promoter provide a proliferative advantage to melanoma cells and are prevalent in advanced stages of the disease, associated with a less favorable prognosis [120]. Due to this high mutational load, melanoma is a highly heterogeneous cancer type.

### **1.5.2 Metastasis formation in CM**

The Clark model is a five-step model describing melanoma formation from melanocytes. In the first stage, structurally normal melanocyte proliferation occurs, which initiates aberrant growth in step two. During the radial-growth phase, these melanocytes then proliferate intraepidermally. During the vertical growth phase, the malignant cells cross the basement membrane, invading local tissue. Invasion is facilitated by the transition of cancer cells from an epithelial- to a mesenchymal phenotype, allowing the dissemination from the local tissue [121]. In melanoma, a mutation in MITF and  $\beta$ -catenin results in the dysregulation of melanocyte differentiation through the constitutive activation of the canonical WNT pathway, resulting in the dermal invasion of melanoma cells [122]. At the same time, tumor cells undergo immune escape at the

primary tumor site. They secrete stimulating factors and extracellular vesicles responsible for forming a microenvironment required for the survival and manifestation of metastasizing tumor cells at a distant location, known as the premetastatic niche (PMN) [123, 124].

The abnormal melanocytes dissociate from the primary tumor and migrate to other skin areas and distant organs to form metastasis [125]. Metastasis formation is one of the eight hallmarks of cancer, and metastasis is represented in figure 5 [126, 127]. The intravasation process in tumor progression involves the movement of cancer cells from the primary tumor site into nearby blood or lymphatic vessels. Several mechanisms facilitate intravasation, including VEGF, which induces vascular leakiness, EGFR, and metalloproteases [128, 129]. Our explanation of how extravasation is happening involves neutrophils. In this concept, extravasation of circulating tumor cells occurs through the interaction with neutrophils, partly mediated by the chemokine IL-8. Neutrophils are attracted to the melanoma cells by a chemokine gradient of IL-8, tethering the two cells together through the interaction of ICAM-1 on the melanoma cell and  $\beta_2$  Integrins on the neutrophils [130].

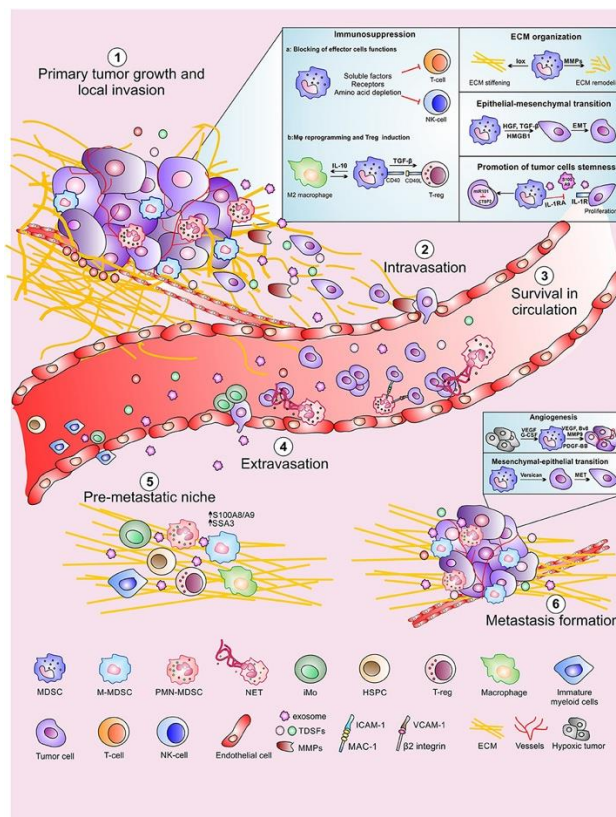


**Figure 5: Six-step process of metastasis formation**

Primary tumor cells undergo EMT transition and invade the bloodstream or lymphatic vessels through intravasation, facilitated by integrins. The tumor cells circulate until they interact with neutrophils, leading to the arrest of movement and extravasation from the vessel. At the distant site, the primary tumor had already established a pre-metastatic niche that comprises the perfect colonization ground for metastasis growth. Illustration taken from Trovato et al. [131].

### 1.5.3 Therapeutic interventions in CM

Based on the tumor thickness (T stage), lymph node involvement (N stage), and presence of metastasis (M stage), adequate therapy is chosen [132]. The first line of treatment in melanoma patients is surgical excision of the malignant cells with a sufficient safety distance. Further therapy can then be divided into targeted and checkpoint immunotherapy (ICI) in the progressive stages of the disease.

Since 2010, the development of ICI and targeted therapies has revolutionized the treatment of melanoma, especially for patients with unresectable melanoma or distant metastasis. These therapies include systemic immunotherapy treatments, either as monotherapy against programmed cell death protein 1 (PD-1; nivolumab or pembrolizumab) or in combination against cytotoxic T-lymphocyte-associated protein 4 (CTLA-4; ipilimumab) as well as BRAF inhibitors in combination with MEK inhibitors (trametinib) and intralesional immunotherapy involving a modified oncolytic herpes virus (T-VEC) [133]. Additional progress has been achieved in ICI, as these therapies can be administered both post-operatively (adjuvant therapy) or pre-operatively (neoadjuvant therapy) in the early stages of cancer development [134, 135]. There is constant development and advancement in the field (clinicaltrials.gov).

Immune checkpoints are receptors expressed on immune cells and tumor cells that regulate immune homeostasis and T-cell function. The two clinically relevant checkpoints are CTLA-4 and PD-1 [136]. PD-1 is expressed on T cells and interacts with its ligand PD-L1 on tumor cells, resulting in T cell exhaustion by abrogating its effector functions. CTLA-4, a member of the CD28 family, interacts with the ligand CD80, which is expressed on DC. As CTLA-4 has a higher affinity to CD80 than CD28, it limits T-cell activation during priming. In metastatic melanoma, the combination of anti-PD-1 and anti-CTLA-4 antibodies increases the response rate of patients to 59% compared to 43% for anti-PD1 monotherapy and 20% for anti-CTLA-4 monotherapy, respectively [137]. Nonetheless, long-term treatment responses are still limited to some patients, and complete remissions are rare due to therapy resistance. Therefore, there is a need for new therapeutic options for melanoma, such as theragnostic modalities [138].

Unfortunately, more than half of the patients encountered severe adverse effects when receiving ICI. irAE encompass autoimmune conditions that can impact any organ within the body. The most common irAE affect the skin (33% of patients), thyroid (20% of patients), gut (10-20% of patients), liver (5-10% of patients), and lungs (1-5% of patients) [139]. These irAE can occur at any time during treatment and are characterized by variability in onset time, severity, and underlying biological mechanisms. The highest incidence typically occurs within the initial three months of treatment [140].

#### 1.5.4 The tumor microenvironment of CM

In CM, the TME is known to play a critical role in the development and progression of this aggressive cancer. The TME is molded and educated by cancer cells to support the advancement of cancer hallmarks, adapt to intrinsic or extrinsic stressors, stimuli, and treatments, and ultimately aid the survival and migration of these cells within an organism. TME can be classified into six specialized microenvironments: hypoxic niche, immune microenvironment, metabolism microenvironment, acidic niche, innervated niche, and mechanical microenvironment [141].

The hypoxic niche refers to an environment with oxygen levels lower than the normal physiological range. The reduced oxygen availability influences the metabolism by activating the hypoxia-inducible factor (HIF) pathway and upregulating VEGF transcription. This pathway helps cells adapt to low oxygen levels by regulating the expression of genes involved in processes like angiogenesis (formation of new blood vessels), glycolysis (a form of cellular energy production), and cell survival. Tumor cells must adapt their metabolism to meet the increased energy demands accompanying their progression. One of the most observed metabolic adaptations in cancer is the enhancement of aerobic glycolysis, also known as the Warburg effect. This significantly increases glucose consumption and lactate secretion in most tumors [142, 143]. Dysregulated or reversed pH has become a commonly recognized feature of cancer. Elevated intracellular pH promotes cancer-cell survival, proliferation, migration, invasion, and glycolysis, inhibiting apoptosis [144]. The acidic niche increases oxidative phosphorylation, epithelial-mesenchymal transition, and invasiveness of melanoma cells [145]. Cancer or stromal cells' innervation relies on the release of neurotransmitters or neuropeptides, such as dopamine, catecholamine, and acetylcholine. Nerve innervation in TME affects immune-cell recruitment and activation, cancer proliferation, metastasis, and response to immunotherapy [146].

The immune microenvironment entails both pro-tumoral and anti-tumoral immune cells. Anti-tumoral immune cells play a critical role in the defense against melanoma. Cytotoxic T cells and natural killer cells (NK cells) are essential to an immune response against cancer cells. In the TME, DC take up tumor-associated antigens. The tumor-associated antigens are taken up by the DC and cross-presented via the MHC molecules on the surface of the cells [147]. DC can be categorized into two groups: conventional type 1 DC (cDC1), which present antigens via MHC-I and initiate activation of cytotoxic CD8<sup>+</sup> T cells, and conventional type 2 DC (cDC2), which present antigens via MHC-II and activate CD4<sup>+</sup> T<sub>helper</sub> cells [148, 149]. NK cells are also an essential part of tumor immune surveillance. They sense stress-associated molecules and damaged cells, forming an immunological synapse, triggering NK cells to degranulate and

release the cytokines IFN $\gamma$ , perforin, and granzyme and thereby promote NK cell-mediated cytotoxicity of the tumor cells [150, 151]. In melanoma, circulating NK cells expressing high levels of the activating receptor NKG2D have been shown to lyse melanoma cells isolated from metastatic lymph nodes efficiently [152]. Furthermore, NK cells have been shown to increase CD8<sup>+</sup> T cell infiltration into the TME thereby increasing the anti-tumoral effects of cytotoxic CD8<sup>+</sup> T cells [153, 154].

On the other hand, pro-tumoral immune cells can limit the effectiveness of the immune response against melanoma by suppressing the activation and function of anti-tumoral immune cells, allowing the tumor to grow. Among the most prominent pro-tumoral cells in the TME are regulatory T cells (Tregs), tumor-associated M2-like macrophages (TAM), and MDSC [155]. Tregs play a crucial role in maintaining tissue homeostasis. However, in the TME, Tregs play a critical role in establishing an immunosuppressive microenvironment. Tumor cells recruit Tregs to the TME mediated by the chemokines CCR8 and CCR4, where they release immunosuppressive cytokines IL-10 and TGF- $\beta$ , which inhibit both antigen-presenting and effector T cells [156, 157]. Based on local hypoxia and a chemokine gradient of CCL2, macrophages are recruited to the TME [158].

TAM have a profound effect on supporting angiogenesis and tumor invasion. Through the production of IL-6, TAM have reportedly been associated with promoting the development of tumors by affecting epithelial-to-mesenchymal transition (EMT) [159, 160]. Another relevant cell type that inhibits immune responses mediated by T cells, B cells, and NK cells are MDSC, which mediate an immunosuppressive environment by secreting reactive oxygen species (ROS), prostaglandin E<sub>2</sub>, and nitric oxide [161]. They also play an essential role in metastasis formation, where they enhance the engraftment of circulating tumor cells by inhibiting killing by immune cells and promoting their extravasation into the tissues [162]. Other suppressive lymphocyte subsets, including IL-10-producing regulatory B cells, have been reported to promote tumor progression and metastasis [163].

### **1.5.5 Hot vs. cold tumors**

The immune cell composition of the TME is responsible for the prognostic outcome. One concept is to classify tumors according to the immune cell infiltration. Based on this, solid tumors can be classified into four groups: hot, cold, excluded, and immunosuppressed. The distinction between hot, cold, and excluded tumors is based on cytotoxic CD8<sup>+</sup> T cells [164]. Hot tumors, also known as immune-inflamed tumors, are defined by infiltration of cytotoxic CD8<sup>+</sup> T cells, increased levels of IFN- $\gamma$  and PD-L1, and a high tumor mutational burden [165]. The environment shows high levels of pro-inflammatory cytokines, and hot tumors respond more efficiently

to immunotherapy. Immunosuppressed tumors show low infiltration of T cells, as well as high levels of immunosuppressive cytokines such as IL-10. While excluded tumors show the presence of CD8<sup>+</sup> T-cells in the marginal areas, they lack T-cell infiltration but have increased immunosuppressive cells and a dense stromal vasculature. On the other hand, cold tumors are characterized by the complete absence of T cells, both infiltrating and at tumor borders, and low MHC levels [166].

## **1.6 Aim of this study**

Recent investigations have found a prominent role of MC associated with cancer. However, whether an accumulation of MC in the TME is pro- or anti-tumorigenic is controversially discussed. This study aimed to analyze MC as an appropriate surrogate for the analysis in disease, as well as to decipher the influence that MC have on melanoma formation and progression.

The specific aims of this thesis are:

1. Determine appropriate in vitro MC surrogates, that best resemble CTMC (Publication 1).
2. Investigate the role of MC in the TME of melanoma through stimulation with endogenous factors (Manuscript 2).
3. Identify immunological mechanisms underlying cutaneous adverse events in patients with melanoma undergoing ICI (Manuscript 3).

## 2 Materials and methods

### 2.1 Materials

#### 2.1.1 Laboratory devices

**Table 3:** Laboratory devices

Device	Supplier	Function
GeneTouch	Bioer	PCR cycler machine
FACS Aria Fusion	BD Biosciences	Cell sorter
Cytoflex LX	Beckman Coulter	Flow cytometer
NanoDrop On <sup>ec</sup>	Thermo Fisher Scientific	DNA/RNA quantification
QuantStudio 3 Real-Time PCR	Thermo Fisher Scientific	Quantitative PCR
BZ-X800 Series	Keyence	Fluorescence microscope
DeNovix CellDrop BF	Biozym	Cell counter
TissueLyser LT	Qiagen	Tissue homogenizer
Azure c600	Biozym	Western Blot imager
Epoch	BioTek	Plate reader

#### 2.1.2 Chemicals and solutions

**Table 4:** Medium and supplements

Media/Supplements	Vendor
DMEM	GIBCO
RPMI medium 1640	GIBCO
Heat-inactivated fetal calf serum (FCS)	HiMedia Laboratories Ld.
L-Glutamine 200 mM	Gibco
Sodium Pyruvate 100mM	Gibco
Penicillin/Streptomycin	Gibco
IL-3	Own culture
SCF	Own culture

**Table 5:** Buffers and solutions

Name	Component	Usage
10x ACK Lysis Buffer	0.15 M Ammonium chloride	Erythrocyte lysis
	0.01 M Potassium bicarbonate	
	0.1 mM Di-sodium EDTA	
	pH 7.4	
FACS Buffer	1x DPBS	Flow cytometry
	2% heat-inactivated FCS	

Tyrodes Buffer	135 mM NaCl 5 mM KCl 5.6 mM D-glucose 1.8 mM CaCl <sub>2</sub> 1 mM MgCl <sub>2</sub> 0.5 mg/mL BSA 20 mM HEPES pH 7.4	β-hexosaminidase assay
Coating Buffer	0.1M sodium carbonate, pH 9.5	ELISA
Blocking Buffer (BD)	10% FCS in PBS w/o Ca <sup>2+</sup> Mg <sup>2+</sup>	ELISA
Blocking Buffer (R&D)	1% BSA in PBS w/o Ca <sup>2+</sup> Mg <sup>2+</sup>	ELISA
Washing Buffer	1x PBS, 0.05% Tween-20 pH 7.2	ELISA
TMB stock solution	100 mM TMB in 50% EtOH, 50% DMSO	ELISA
Substrate Solution	1 mM TMB, 0.05 % H <sub>2</sub> O <sub>2</sub> in citrate buffer	ELISA
Stop Solution	2N H <sub>2</sub> SO <sub>4</sub>	ELISA

**Table 6:** Chemicals and reagents

Chemical	Supplier
β-Mercaptoethanol	Sigma-Aldrich, Taufkirchen, Germany
Bovine Serum Albumin (BSA)	Sigma-Aldrich, Taufkirchen, Germany
Dimethyl Sulfoxide (DMSO)	Sigma-Aldrich, Taufkirchen, Germany
Ethanol	Fisher Scientific, Schwerte, Germany
Methanol	Carl Roth, Karlsruhe, Germany
Acetone	Carl Roth, Karlsruhe, Germany
CaCl <sub>2</sub>	Carl Roth, Karlsruhe, Germany
Ionomycin	Sigma-Aldrich, Taufkirchen, Germany
Phorbol-12-myristat-13-acetat	Sigma-Aldrich, Taufkirchen, Germany
Tris hydrochloride	Carl Roth, Karlsruhe, Germany
Trypan blue solution	Sigma-Aldrich, Taufkirchen, Germany
Trypsin-EDTA (0.05%), phenol red	GibcoBRL, Karlsruhe, Germany
Collagenase type I	Sigma-Aldrich, Taufkirchen, Germany
Formaldehyde solution 3.6-3.7%	Sigma-Aldrich, Taufkirchen, Germany
Triton-X100	Sigma-Aldrich, Taufkirchen, Germany
Tween-20 Detergent	Sigma-Aldrich, Taufkirchen, Germany
DNase I	Sigma-Aldrich, Taufkirchen, Germany

### 2.1.3 Antibodies

All the following antibodies are directed against murine antigens (Table 7) or human (Table 8) and titrated for optimal staining intensity.

**Table 7: Murine antibodies for flow cytometry**

Surface Marker	Fluorophore	Clone	Supplier
CD16/32 (Fc-Block)	/	2.4G2	Biolegend
Live/Dead	Aqua (BV510)	/	Invitrogen
Live/Dead	IR	/	Thermo Fisher
Anti-CD45.2	APC-Cy7	104	Biolegend
Anti-CD8a	PE	53-6.7	Biolegend
Anti-CD11b	PE-Cy7	M1/70	Biolegend
Anti-CD11c	PerCP-Cy5.5	N418	Biolegend
Anti-CD103	BUV395	2E7	Biolegend
Anti-MHCII	BV421	M5/114.15.2	Biolegend
Anti-XCR1	APC	ZET	Biolegend
Anti-CD370 (Clec9a)	PerCP	9A11	eBioscience
Anti-CD172 (Sirp1 $\alpha$ )	PE	P84	Biolegend
Anti-B220	APC	RA3-6B2	Biolegend
Anti-F4/80	PE	BM8	Biolegend
Anti-CD206	BV605	C068C2	Biolegend
Anti-CD86	BV650	GL-1	Biolegend
Anti-Gr1	APC	RB6-8C5	Biolegend
Anti-Ly-6G	FITC	1A8	Biolegend
Anti-Ly-6C	BV711	HK1.4	Biolegend
Anti-CD3	BV605	145-2C11	Biolegend
Anti-NK1.1	FITC	PK136	Biolegend
Anti-NK1.1	BV711	PK136	Biolegend
Anti-CD49a	APC	HMa1	Biolegend
Anti-CD49b	PE-Cy7	DX5	Biolegend
Anti-CD49b	BV711	HMa2 (RUO)	BD
Anti-CD19	BUV	1D3	BD
Anti-ST2	PE	DIH4	Biolegend
Anti-Sca1	PerCP-Cy5.5	D7	Biolegend
Anti-CD4	BV421	GK1.5	Biolegend
Anti-CD8	PE/Dazzle	53-6,7	Biolegend
Anti-CD44	PerCP-Cy5.5	IM7	Biolegend
Anti-CD62L	FITC	MEL-14	Biolegend
Anti-CD25	PE	PC61	BD

**Table 8:** human antibodies for flow cytometry

Surface Marker	Fluorophore	Clone	Supplier
CD16/32 (Fc-Block)	/	/	Miltenyi
7-AAD	PerCP	/	Biolegend
Anti-CD3	FITC	3.9	Biolegend
Anti-CD4	PB	Okt 04	Biolegend
Anti-CD8	PerCP-Cy5.5	SK1	Biolegend
Anti- $\alpha\beta$ TCR	APC	IP26	Biolegend
Anti- $\gamma\delta$ TCR	PE-Cy7	11F2	BD
Anti-CD86	PE	BU63	Biolegend
Anti-CD69	BV510	FN50	Biolegend
Anti-CLA	PerCP-Cy5.5	HECA-452	Biolegend
Anti-CCR5	PE	2D7/CCR5	BD
Anti-CXCR3	APC	G025H7	Biolegend
Anti-CCR8	PE	L263G8	Biolegend
Anti-CCR3	APC	5.e8	Biolegend
Anti-CCR4	APC	L291H4	Biolegend
Anti-CCR6	PE	G034E3	Biolegend
Anti-CCR10	PE	6588-5	Biolegend

#### 2.1.4 Primer sequences for qPCR

**Table 9:** Primers used for qPCR

Gene	Sequence Forward (5'- 3')	Sequence Reverse (5'- 3')
CXCL10	GGATGGCTGTCCTAGCTCTG	ATAACCCCTTGGGAAGATGG
CXCL11	AGTAACGGCTGCGACAAAGT	GCATGTTCCAAGACAGCAGA
CXCL9	TTTTCTCTTGGGCATCAT	GCATCGTGCATTCCTTATCA
TNF- $\alpha$	TTG AGA TCC ATG CCG TTG	CTG TAG CCC ACG TCG TAG
Perforin	AAGGTAGCCAATTTTGCAGC	GGTTTTTGTACCAGGCGAAA
IFN- $\gamma$	CTCTGAGACAATGAACGCTAC	TCTTCCACATCTATGCCACTT
GrzmB	GATCGGGAGTGTGAGTCCTAC	GAAAGCACGTGGAGGTGAAC
CXCR3	GCCAAGCCATGTACCTTGAG	GGAGAGGTGCTGTTTTCCAG
CXCR4	TAGGATCTTCTGCCACCAT	TGACCAGGATCACCAATCCA
Melan-A	TGCTCTGCTTATCGGCTGCT	GCTTCTCATAGGCAGGCGGA
CD3	TCCCAACCCAGACTATGAGC	GCGATGTCTCTCCTATCTGTCA
ST2	GTGATAGTCTTAAAAGTGTCTGG	TCAAAAGTGTTTCAGGTCTAAGCA
IL13	CGTTGCACAGGGGAGTCT	CCTCTGACCCTTAAGGAGCTTAT
E-cadherin	TACAACGCTGCCATCGCCTA	TTGGTCGTGGGGTCTGTGAC
N-cadherin	CTTCCCCGAGGCGCTCTAC	GCTCCTCAGTCAGGGTTGGC

Vimentin	GGCCAAGCAGGAGTCAAACG	TTCACGAAGGTGACGAGCCA
Claudin1	GACTGTGGATGTCCTGCGTT	TCATGCCAATGGTGGACACA
Claudin 4	CCCGCCAGCAACTATGTGTA	TGTCCCCAGCAAGCAGTTAG
Occludin	CCTCTTTCCTTAGGCGACAGC	AAATGTCCAGGCTCCCAAGA
ZO-1	AGAGACAAGATGTCCGCCAG	TCACTGTGTGCTGTTCCCAT
MITF-H	AGGAGGACTAAGTGGTCTGCG	CCCTGGTTGCTGTAGAGGTCG
Mcpt1	GGAAAACCTGGAGAGAAAGAACCTAC	GACAGCTGGGACAGAATGGGG
Mcpt2	ATTCATTGCCTAGTTCCTCTGAC	AGGATGAGAACAGGCTGGGAT
Mcpt4	GACAGAATCCACACAGCAGAAG	CCTCCAGAGTCTCCCTTGTATG
Mcpt5	GGCAGAACAAACGTGAATGAGCC	AAGAACCTTCTGGAAGCTCAGGG
Mcpt6	GCTCCTCTCTTTGAACCGGATC	GGTGGGAGAGGCTCGTCATTA
Mcpt7	GGCTGGGGTAACATCGACAAT	CAAGTAATAGGTGACCCGGGTGTA
Mcpt9	TTCCAAGTTCAATGACATCGTATTAC	GATACTTTTTTTCCTCCAGTTCCG
Cpa3	ACACAGGATCGAATGTGGAG	TAATGCAGGACTTCATGAGC
TLR1	ACTATGCTGGTGCTGGCTGT	CCAGGGCAGGTCAAAGTAGA
TLR2	GGGGCTTCACTTCTCTGCTT	AGCATCCTCTGAGATTTGACG
TLR3	GCTCAGAAAGGCCTGGAAAT	GCCCTTAAAAGCAACAACACTCTG
TLR4	GGAATCTGATCATGGCACTG	CTGATCCATGCATTGGTAGGT
TLR5	GCTACCCAGGTGGCAAGAG	GCACAGAAAGCATGAAGCTG
TLR6	CTCACCAGAGGTCCAACCTT	CGAGCACTTCCAGGTTGTTT
TLR7	AAACTCAGCTGTGACAGAATGG	TCTTGGATCTTCCAATTTTGC
TLR9	GAATCCTCCATCTCCCAACA	CCAGAGTCTCAGCCAGCACT
β-actin	CTAAGGCCAACCGTGAAAAG	ACCAGAGGCATACAGGGACA

### 2.1.5 Software

**Table 10:** Software

Software	Supplier
FlowJo (v10.0)	FlowJo, LLC, Ashland, USA
GraphPad Prism 9	GraphPad Software, San Diego USA
Microsoft Office 2019	Microsoft Corporation, Redmond, USA
R-Studio	R Core Team, world wide
BioRender	BioRender, Toronto, Canada

## **2.2 Methods**

### **2.2.1 In vitro methods**

#### **2.2.1.1 In vitro generation of MC**

Generation of BMBC: BM cells were prepared from femur and tibia of 6- to 8-week-old C57BL/6N and cultured in RPMI1640 medium (Biochrom, Berlin, Germany) with 20% FCS (CH 30160.03 Hyclone Perbio, ), 1% X63Ag8-653mIL-3-conditioned medium corresponding to 10ng IL-3/ml, 1% CHO-murine stem cell factor conditioned media corresponding to 50ng mSCF/ml), 50 U/mL penicillin/streptomycin (Biochrom, Berlin, Germany) and 20  $\mu$ M  $\beta$ -mercaptoethanol (Merck, Darmstadt, Germany), for 21 days at 37°C and 5% CO<sub>2</sub>. Conditioned media were obtained from cell culture supernatants of the above-mentioned cell lines. Concentration estimation of IL-3 and SCF was performed using proliferation assays with FDCP-1 cells (IL-3 dependent) and TF-1 (SCF-dependent).

Generation of fetal skin- and fetal liver MC: fetuses were retrieved from C57Bl/6N mice 16-days post gestation. Back skin was prepared from the fetus, digested in 0.25 % Trypsin-EDTA solution (Gibco Thermo Fisher Scientific, Munich, Germany), and passed through cell strainers (Cambrex, New Jersey, USA). The livers were removed from fetuses and single cell suspension were prepared. Erythrocytes were lysed with ACK lysis buffer (BioWhittaker, Lonza, Swiss) and cell suspension cultured for 21 days in complete mast-cell medium as described before. All cultured media were tested regularly for mycoplasma and no contamination has been detected.

#### **2.2.1.2 Flow Cytometry analysis of MC surface markers**

The surface expression of Fc $\epsilon$ RI, c-kit (CD117), ST2 and  $\beta$ -Integrin was analyzed by flow cytometry. Briefly,  $1 \times 10^6$  MC were incubated with an antiCD16/CD32 monoclonal antibody (mAb) (32: Biologend, San Diego, CA, USA) for Fc receptor blocking. The following antibodies were used for analysis: anti-CD45.2-APC-Cy7, anti-Fc $\epsilon$ RI-FITC (Biologend, San Diego, CA, USA), anti-CD117-APC (Biologend, San Diego, CA, USA), anti-ST2-PE (Biologend, San Diego, CA, USA), anti- $\beta$ 7-PE (Biologend, San Diego, CA, USA).

#### **2.2.1.3 Histologic staining of MC**

$1 \times 10^4$  cells MC were cytocentrifuged onto a glass slide and air-dried. For Alcian Blue staining, slides were stained with 1.0% alcian blue (Sigma-Aldrich/Merck, Darmstadt, Germany) at pH

2.5 in 1% acetic acid, followed by staining for 15 min with 0.1% safranin O (Sigma-Aldrich/Merck, Darmstadt, Germany). For toluidine staining, slides were stained with 1% toluidine (Sigma-Aldrich/Merck, Darmstadt, Germany) in EtOH for 30 min. For Giemsa staining slides were stained in 5% Giemsa (Sigma-Aldrich/Merck, Darmstadt, Germany) for 20 min. Slides were examined under a light microscope (DM3000, Leica Biosystems; Nußloch, Germany).

#### **2.2.1.4 Transmission electron microscopy**

Cells were fixed with Karnovsky's fixative for 24h at 4°C. Post-fixation was based on 1.0% osmium tetroxide containing 1.5% K-ferrocyanide in 0.1M cacodylate buffer for 2 h. After following standard methods, blocks were embedded in glycidic ether and cut using an ultramicrotome (Ultracut, Reichert, Vienna, Austria). Ultra-thin sections (30 nm) were mounted on copper grids and analyzed using a Zeiss LIBRA 120 transmission electron microscope (Carl Zeiss, Oberkochen, Germany) operating at 120 kV.

#### **2.2.1.5 Proliferation, histamine release and hexosaminidase assay**

For proliferation experiments, MC were cultured with 0.25  $\mu\text{Ci}$  of [ $^3\text{H}$ ]Thymidine (Amersham, GE Healthcare, Freiburg, Germany) for 14h. The cells were harvested using a FilterMate Harvester (PerkinElmer LAS, Rodgau, Germany) and incorporation analyzed in a MicrobetaTriLux Luminescence Counter (PerkinElmer LAS, Rodgau, Germany). Incorporated radioactivity is expressed as counts per minute. For IgE sensitization,  $1 \times 10^5$  cells were pre-incubated with 1  $\mu\text{g}/\text{ml}$  anti DNP IgE (Sigma-Aldrich/Merck, Darmstadt, Germany) over night at 37°C. For cross-binding and activation of the receptor, the cells were then stimulated with 40ng/ml DNP-HSA (Sigma-Aldrich/Merck, Darmstadt, Germany) for 30 minutes. Control stimulation was performed with phorbol-12-Myristat-13-Acetate (PMA) (Sigma, Taufkirchen, Germany) and Ionomycin (Sigma-Aldrich/Merck, Darmstadt, Germany) or 0.1% TritoxX100 (Sigma-Aldrich/Merck, Darmstadt, Germany) for complete lysis. Histamine release was analyzed using histamine ELISA (LSBio, Seattle, USA). For  $\beta$ -hexosaminidase release, 50  $\mu\text{l}$  of supernatant were incubated with 50  $\mu\text{l}$  of p-nitrophenyl-N-acetyl- $\beta$ -D-glucosaminide (Sigma-Aldrich/Merck, Darmstadt, Germany) for 2 hours at 37°C. Reaction was stopped with Tris-HCl buffer (Sigma-Aldrich/Merck, Darmstadt, Germany) and colorimetric measured at 405 nm using an ELISA Reader Multiskan EX (Thermo Fisher Scientific, Munich, Germany).

### 2.2.1.6 Cytokine measurement

$1 \times 10^6$  MC were cultured in 24-well plate and stimulated with either 100 ng/ml Pam2Cys (EMC microcollections, Tübingen, Germany), 10 ng/ml LPS from *S. minnesota* (Alexis, Lausen, Swiss), 0.5  $\mu$ M CpG OD 1668 (Eurofins MWC Operon, Ebersberg, Germany), Poly:IC (invivoGen, Toulouse, France), 10 ng/ml Imiquimod (invivoGen, Toulouse, France), 10  $\mu$ g/ml MDP (Nod2 agonist) (invivoGen, Toulouse, France), 5  $\mu$ g/ml Hsp70 (TLR4 agonist), 250 ng/ml Malp2 (TLR2/6 agonist) (Enzo Life Sciences Lausen, Austria), 5  $\mu$ g/ml dsDNA (TLR9 agonist) (invivoGen, Toulouse, France), 10  $\mu$ g/ml C48/80 (Mxgprb2 agonist) (Sigma-Aldrich/Merck, Darmstadt, Germany), 10 ng/ml IL-33 (Peprotech, Hamburg, Germany), 60 ng/ml Ionomycin (Sigma-Aldrich, Darmstadt, Germany), 84 ng/ml PMA (Sigma-Aldrich/Merck, Darmstadt, Germany) or with 1  $\mu$ g/ml IgE + 40 ng/ml IgE-DNP (Sigma-Aldrich/Merck, Darmstadt, Germany) for 24h. Supernatants were quantified by enzyme-linked immunosorbent assay for IL-10 (R&D Systems, Minneapolis, MN, USA, detection limit 15.6–1000 pg/mL), IL-6 (R&D Systems, Minneapolis, MN, USA, detection limit 15.6–1000 pg/mL), TNF- $\alpha$  (R&D Systems, detection limit 10.9–700 pg/mL), LegendPlex Mouse Inflammation panel (BioLegend, San Diego, CA, USA) and LegendPlex Mouse Th Cytokine panel (Biolegend, San Diego, CA, USA).

### 2.2.1.7 Patch-Clamp analysis

Patch-clamp experiments have been performed at room temperature in voltage-clamp, fast whole-cell mode. MC were continuously superfused by a flow system inserted into the dish. The bath was grounded via a bridge filled with NaCl Ringer solution. Borosilicate glass pipettes (2- to 4-megaohm (Mohm) tip resistance; GC 150 TF-10; Clark Medical Instruments) manufactured by a microprocessor-driven DMZ puller (Zeitz) were used in combination with a MS314 electrical micromanipulator (MW; Märzhäuser). The currents were recorded by an EPC-9 amplifier (HEKA) using Pulse software (HEKA) and an ITC-16 Interface (Instrutech). Whole-cell currents were determined as 10 successive 200-ms square pulses from a  $-35$  mV holding potential to potentials between  $-115$  mV and  $+65$  mV. The currents were recorded with an acquisition frequency of 10 and 3 kHz low-pass filtered. Where indicated, DNP-HSA (50 ng/ml), endothelin-1 (100 nM), the channel blocker TRAM-34 (300 nM; Sigma-Aldrich), and/or the  $\text{Ca}^{2+}$  ionophore ionomycin (1  $\mu$ M; Sigma-Aldrich) were added to the bath solution. The offset potentials between both electrodes were zeroed before sealing. The original whole-cell current traces are depicted without further filtering and currents of the individual voltage

square pulses are superimposed. The applied voltages refer to the cytoplasmic face of the membrane with respect to the extracellular space. The inward currents, defined as flow of positive charge from the extracellular to the cytoplasmic membrane face, are negative currents and are depicted as downward deflections of the original current traces.

### 2.2.1.8 Intracellular calcium measurement

Intracellular  $\text{Ca}^{2+}$  measurements were performed using fura-2AM. Briefly, MC were loaded with fura-2AM (2  $\mu\text{M}$ ; Molecular Probes) for 20 min at 37°C. The cells were continuously superfused to remove leaked-out extracellular fura-2. Fluorescence measurements were conducted with an inverted phase-contrast microscope (Axiovert 100; Zeiss). Cells were excited alternatively at 340 and 380 nm and the light was deflected by a dichroic mirror into either the objective (Fluar  $\times 40/1.30$  oil; Zeiss) or a camera (Proxitronic) mounted on the microscope. Emitted fluorescence intensity was recorded at 510 nm and data acquisition was performed by using Metafluor computer software (Universal Imaging). The regions of interest were determined as circuits closely surrounding individual cells to determine the fluorescence intensity in single cells. After a control period to wash the cells and remove any non-gathered dye, intracellular  $\text{Ca}^{2+}$  was measured before and following addition of DNP-HSA (40 ng/ml) to IgE-sensitized MC, in the absence or presence of extracellular  $\text{Ca}^{2+}$ . As a measure of the increase of cytosolic  $\text{Ca}^{2+}$ , the slope and peak of the changes in the 340/380-nm ratio were calculated for each experiment. To reach nominally  $\text{Ca}^{2+}$ -free conditions, experiments were performed using  $\text{Ca}^{2+}$ -free Ringer solution. For intracellular calibration purposes, 10  $\mu\text{M}$  ionomycin was applied at the end of each experiment.

### 2.2.1.9 Analysis of gene expression

Total RNA was extracted from MC or tumors using the PeqGold Total RNA Kit (PeqLab, VWR). DNA was digested with the DNase I Kit according to the manufacturer's protocol (Invitrogen) and RNA was reverse transcribed to cDNA using an iScript cDNA Synthesis Kit (BioRad) according to the manufacturer's instructions. Quantitative real-time PCR was carried out on a QuantStudio 3 machine (Thermo Fisher Scientific). Ct values were normalized to the housekeeping gene  $\beta$ -actin. Where indicated, fold change was calculated using the delta-delta method:

$$\Delta ct(\text{sample}) = ct_{\text{gene of interest}} - ct_{\text{housekeeper}} \quad (1)$$

$$\Delta\Delta ct = \Delta ct_{\text{experimental sample}} - \Delta ct_{\text{control sample}} \quad (2)$$

$$\text{fold change} = 2^{-\Delta\Delta ct} \quad (3)$$

Primers used for qPCR analysis are listed in Table 9.

### **2.2.1.10 Bulk RNA sequencing**

Total RNA was isolated from either tumors, naïve MC or MC stimulated with 10ng IL-33, 20ng Pam2Cys or a combination of both with the PeqGold Total RNA Isolation Kit (VWR, Ismaning, Germany). Quality and integrity of total RNA was controlled using NanoDrop 2000. Agilent Technologies 2100 Bioanalyzer (Agilent Technologies). For library preparation of bulk 30-sequencing of poly(A)-RNA barcoded cDNA of each sample was generated with a Maxima RT polymerase (Thermo Fisher) using oligo-dT primer containing barcodes, unique molecular identifiers (UMIs) and an adaptor. 5' ends of the cDNAs were extended by a template switch oligo (TSO) and full-length cDNA was amplified with primers binding to the TSO-site and the adaptor. NEB UltraII FS kit was used to fragment cDNA. After end repair and A-tailing a TruSeq adapter was ligated and 3'-endfragments were finally amplified using primers with Illumina P5 and P7 overhangs. The library was sequenced on a NextSeq 500 (Illumina).

High-throughput gene expression data was carried out using the R environment for statistical computing. Briefly, genes were normalized and a principal component analysis was performed. Differential gene expression was performed using DeSeq2 and gene ontology analysis performed using GSEA and enrichR. Additional gene set analysis was performed using the Degust webtool.

## **2.2.2 In vivo methods**

### **2.2.2.1 Animals**

C57BL/6N mice were purchased from Charles River for all experiments. Mcpt5-cre- R-DTA<sup>fl/fl</sup> mice were given by A. Roers (Institute for Immunology, Technical University Dresden, Dresden, Germany). Batf3<sup>-/-</sup> knockout mice were kindly donated by J. Böttcher (Technical University Munich, Munich, Germany). ST2<sup>-/-</sup> mice were given by A. Pinschewer (Zurich, Swiss). For all experiments, female mice between the age of 8-12 were used. Animal studies were kept under specific pathogen-free conditions in accordance with the guidelines of the Federation of European Laboratory Science Association. All experiments were authorized by the regional council of Upper Bavaria under the registration TVA\_02-18\_52.

### **2.2.2.2 Murine B16 melanoma model**

*Melanoma model:* Mice were injected with  $7.5 \times 10^4$  B16-OVA cells into the hind flanks. In the first experiment, tumors were treated with peritumoral injections of 500 ng IL-33 or PBS either from d1-d7 or d9-d15. In the following experiments, tumors were treated with peritumoral injections of 500 ng IL-33, 4  $\mu$ g Pam2Cys, the combination of both IL33/Pam2Cys or PBS as control on d9-15. Tumor size was measured with a caliper every second day starting one week after cell inoculation. Mice were sacrificed with isoflurane and cervical dislocation on day 16.

For reconstitution experiments, back skin of mice was intradermally injected with  $1 \times 10^6$  BMDC 6 weeks before B16-OVA melanoma injection [167].

*Macrophage depletion:* For macrophage depletion, C57BL/6N mice were injected intravenously with clodronate liposomes or control liposomes. One day prior to B16 inoculation, mice were injected with 5 mg/kg clodronate liposomes for macrophage depletion. For maintenance of the depletion, 1.25 mg/kg clodronate were injected once a week on day 4, day 9 and day 14 post B16 injection [168].

### **2.2.2.4 Preparation of tumors, skin and lymph nodes and flow cytometry**

Melanoma samples were explanted from mouse skin, dissected with scissors, and digested with 1 mg/ml collagenase I (Serva), 100mM CaCl<sub>2</sub> and 50 mM DNase for 30 minutes at 37°C. Single cell suspension of the tissue was achieved by homogenizing through a 100  $\mu$ m nylon mesh strainer and subsequently through a 70  $\mu$ m nylon mesh strainer and washed 3 times with FACS buffer. Draining lymph nodes were mashed through a 70  $\mu$ m nylon mesh strainer and washed 3 times with FACS buffer.

For flow cytometry analysis, cells were plated into a round-bottom plate and incubated with an antiCD16/CD32 mAb (32: Biolegend) for Fc receptor blocking. Antibodies used for analysis are listed in Table 7. Flow cytometry data were acquired using a FACSCanto II (BD Biosciences) or Cytoflex LX (Beckman Coulter) and analyzed with FlowJo software (Tree Star, BD Biosciences).

### **2.2.2.5 Cytokine measurement of serum**

Mice were drained of blood through cardiac puncture and blood collected in 1.5 ml Eppendorf tubes containing Heparin. After centrifugation, serum was collected and stored at -20°C for

further analysis. Mouse serum was analyzed using a bead-based ELISA. Cytokines were measured using the LegendPlex Mouse Inflammation panel (BioLegend #740150) and LegendPlex Mouse Th Cytokine panel (Biolegend #741043).

#### **2.2.2.6 Histology of tumors**

Histological sections from paraffin-embedded tissues were stained with hematoxylin and eosin (H&E). For MC detection, tissue slides were stained with Giemsa. For fluorescent staining, tumors were embedded in cryo-solution and frozen at -80°C. Histological sections were made using a cryotome. Tissue slides were fixed using a 1:1 aceton:methanol solution for 10 min, washed using TBS and avidin (1:1000) added for 30 min. Slides were washed again and DAPI (1:500) added for 2 min. Images were processed with a Keyence BZ-X800 fluorescent microscope. Full-mount images were taken at 20x magnification.

### **2.2.3 Human study methods**

#### **2.2.3.1 Study design and patient cohort**

A total of 30 patients suffering from stage III/IV malignant melanoma were enrolled in this exploratory prospective non-interventional study. Included patients were naïve for ICI therapies, but previous treatments with targeted therapies (BRAF/MEK inhibition), interferon alpha and radiotherapy followed by disease progression were allowed. In addition, one patient also received 3 chemotherapy cycles with dacarbazine 15 months prior to study inclusion. The study protocol was approved by the Ethics committee at the Technical University of Munich (reference number: 2023-611-S-SB)

According to the clinical setting and after consulting an interdisciplinary tumor board, the patients were treated either with PD-1 monotherapy (in an adjuvant or therapeutic setting) or ipilimumab/nivolumab combination therapy. Blood samples were taken at three different time points: Blood samples were collected before initiation of checkpoint immunotherapy (ICI), hereof referred to as “*naïve*”, to determine baseline levels of immune cells in the peripheral blood as well as cytokine levels in the serum. After initiation of ICI, patients were clinically supervised with regular checkups and a follow-up blood draw was performed six-months under ICI treatment, referred to as “*6mo ICI*”. If within the monitoring time, cutAEs occurred, another blood draw was performed to determine changes in the immune status during an acute phase of cutaneous adverse event, named “*cutAE*”. After informed written consent was obtained, skin

biopsies were taken from eight out of 13 cutAE to confirm the final diagnosis of the subtype of cutAE (Figure 21A).

Routine follow-up was carried out according to current guidelines, including radiological assessment via PET/CT scan every 3 months (or earlier in case of clinical evidence for disease progression). After 6 months (or earlier in case of progressive disease leading to therapy modification or disease associated death) response to therapy response was categorized as responder or non-responder (using RECIST criteria). Patients with no evidence of disease in adjuvant setting and patients with complete response and partial response in therapeutic setting were classified as responder whereas patients with progressive disease were defined as non-responder.

### **2.2.3.2 Plasma analysis and PBMC isolation**

Blood samples were collected in EDTA tubes and centrifuged without break for plasma collection. Cytokine content in the plasma of patients was analyzed using a multiplex Th cytokine ELISA (Biolegend #741027). The remaining serum was stored at -20°C. The remaining blood was diluted 1:4 with 1xPBS and layered over Ficoll. After centrifugation for 15 min at 1000 rpm without break, the interface containing the mononuclear cells (PBMC) was isolated and washed twice with RPMI 1640. PBMC were counted and stored at -80°C in cryo-preservation medium containing FCS and 10% DMSO.

### **2.2.3.3 Flow cytometry analysis of T cell subtypes**

To determine different cell populations by flow cytometry, a multicolor staining of PBMC was performed. For this,  $2 \times 10^5$  cells per staining were plated into a round-bottom plate and incubated with an anti-CD16/CD32 mAb (Miltenyi) for Fc receptor blocking. The following antibodies were used for analysis of the immune cell composition: Antibodies used for analysis are listed in Table 8. Flow cytometry data were acquired using a FACSCanto II (BD Biosciences) or Cytoflex LX (Beckman Coulter) and analyzed with FlowJo software (Tree Star, BD Biosciences).

### **3 Results**

This thesis aims to elicit the role of MC as orchestrators of anti-tumoral immunity in the TME of melanoma. In this context, three projects were performed. The first project deals with MC of different tissue origins to determine the optimal in vitro surrogate for CTMC. Next, using the murine B16 melanoma model, the role of MC in the TME was analyzed, both in an activated form and under steady-state conditions. And lastly, a pilot study investigating irAE in melanoma patients undergoing ICI was performed.

#### **3.1 Fetal tissue-derived MC as experimental surrogate for in vitro CTMC**

In vivo models using constitutive or inducible MC-deficient mice are essential in investigating the involvement and relevance of MC in different physiological and pathological processes. However, to study MC functions on a cellular level, in vitro models are necessary. The most used in vitro model for MC research is based on BMMC. However, as explained in Chapter 1.1, BM-derived HSC account for only a fraction of MC. BMMC is a helpful model for MC studies and is frequently used; however, BMMC phenotypically and functionally differ from tissue-resident MC populations [23, 169]. Due to the increasing evidence of MC heterogeneity and tissue specificity, it is crucial to address this issue in experimental setups to define an appropriate MC surrogate for in vitro studies. A side-by-side culture comparing the commonly used BMMC with MC derived from either fetal skin (FSMC) or fetal liver (FLMC) was established, and comparative studies to identify the best surrogates for mature CTMC were performed. Parts of this chapter were previously published in Iuliano et al., 2022. [169]

##### **3.1.1 MC phenotypes following cultures of BM cells and fetal tissue**

Cells were isolated from the BM of adult C57BL/6N mice and the liver and skin of C57BL/6N day 16 embryos. The isolated precursor cells were cultured in a medium supplemented with 20% FCS, 10 ng/ml IL-3, and 50 ng/ml SCF (here forth referred to as complete MC medium), which are crucial components required for the maturation of MC. The SCF receptor c-kit (CD117), is one of the most critical receptors on mature MC, as a reduction in c-kit signaling leads to MC deficiency [170]. Depriving the precursor BM cells of either SCF or IL-3 showed an impaired maturation, as only BM cells cultured in complete MC medium could generate CD117<sup>+</sup>FcεRI<sup>+</sup> cells (Figure 6A). Adding SCF to the medium is crucial for both the maturation and maintenance of matured MC. After four weeks of development in the complete medium, mature MC were starved in a medium lacking either SCF, IL-3, or both, and MC were later

analyzed by flow cytometry. As early as 24 hours after being deprived of SCF, MC showed a downregulation of the c-kit receptor expression on the surface, indicating that SCF is crucial for maintaining MC in vitro (Figure 6B).

Each week, the degree of maturation for cells from each tissue origin was analyzed by flow cytometry. A vital marker mediating the migration of fetal MC precursors to the designated developing organ is the homing receptor integrin  $\beta 7$ , which is downregulated once the precursors are fully committed [170, 171]. Over five weeks of culture, the surface expression of integrin  $\beta 7$  was downregulated in BMMC, FSMC, and FLMC, respectively, indicating maturation from precursors to mature MC in cell cultures from all three tissues (Figure 6C). Cells were classified as fully matured, with >90% viable cells being CD45.2<sup>+</sup>CD117<sup>+</sup>Fc $\epsilon$ RI<sup>+</sup> positive (Figure 6D). Both BMMC and FSMC were fully developed after four weeks of culture, while FLMC require a longer cultivation time to reach the same degree of maturation. The yield and maturation time for each MC type is summarized in Table 10.

**Table 10:** Total cell yield and maturation time for MC of different tissue origins

Cell Type	Culture time (in weeks)	Yield
BMMC	4-6	1x10 <sup>8</sup> /tibia
FLMC	6-10	5x10 <sup>7</sup> /embryo
FMSC	4-6	1x10 <sup>7</sup> /embryo

The reduced yield of MC generated from fetal skin is due to the reduced proliferation capacity of these cells. Both FLMC and FSMC showed significantly lower levels of radioactive <sup>3</sup>H thymidine, indicating fewer new strands of chromosomal DNA were incorporated during cell division (Figure 6E). The reduced proliferative capacity of fetal-derived MC indicates a higher degree of maturation than the high proliferating and relatively immature BMMC.

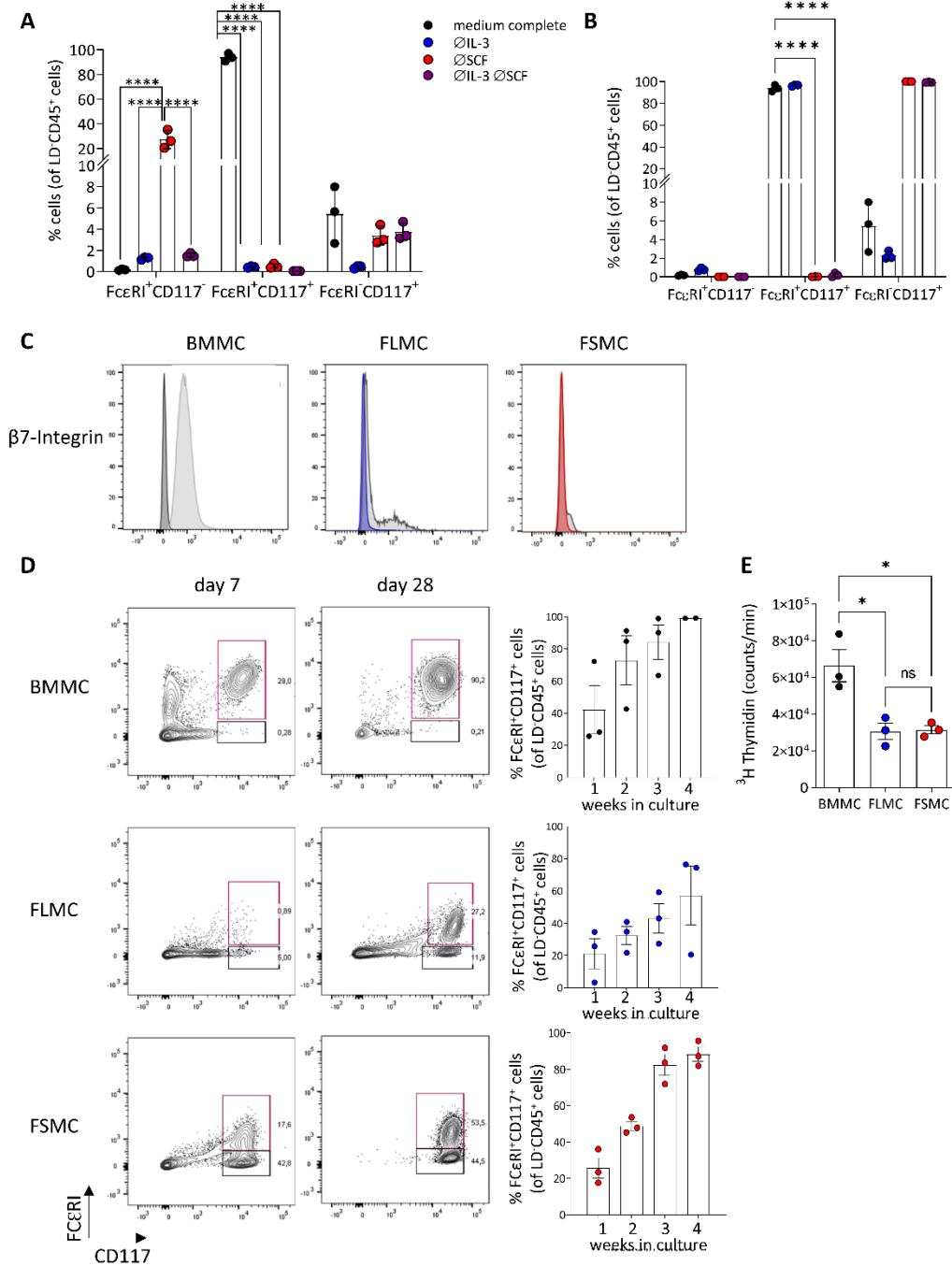


**Figure 6: Generation and characterization of MC.**

(A) Precursor BM cells were isolated and cultured in complete MC medium (black), medium without IL-3 (blue), medium without SCF (red), and medium without IL-3 and SCF (purple). Flow cytometry analysis was performed after four weeks for the MC markers FcεRI and c-kit (CD117) (n=3, mean with SEM, 2way ANOVA, \*\*\*\*p<0.001). (B) Mature MC were cultured in complete MC medium (black) or deprived of IL-3 (blue), SCF (red), or IL-3 and SCF (purple) for one week. Flow cytometry analysis was performed for the MC markers FcεRI and c-kit (CD117) (n=3, mean with SEM, 2way ANOVA, \*\*\*\*p<0.001). (C) Temporal dynamics of β7 integrin for BMMC, FLMC, and FSMC. The light grey histogram represents the expression level at week 1, while the black (BMMC), blue (FLMC), and red (FSMC) histogram represents week 5. (D) Mature MC were classified as living CD45.2<sup>+</sup>FcεRI<sup>+</sup>CD117<sup>+</sup> cells. Bar graphs represent quantification of maturation from day 14 until day 35 of culture (n=3, mean with SEM). (E) The proliferation of MC is based on the incorporation of <sup>3</sup>H-thymidine. The proliferation rate was determined as counts/min (n=3, mean with SEM, Turkey's multiple comparison test \* p<0.05). Flow cytometry analysis also showed a difference in granularity with FSMC showing

the highest granularity (Figure 7A), which is further supported by transmission electron microscopy. Electron microscopy revealed more granules in FSMC, which were also larger and more uniform (representative pictures in Figure 7B). Cross-section analysis of the cells allowed for quantification of the number of granules per section, showing a mean quantity of granules in BMMC of 5 granules/cell, 9 granules/cell in FLMC and 19 granules/cell in FSMC. This demonstrated that BMMC and FLMC have lower numbers of granules per cell, while FSMC exhibited the highest granule density, with 74% more granules per cell (Figure 7C). To confirm this with another method, immunohistochemical staining was performed to visualize the secretory granules of MC. MC were applied on microscopy slides by cytopsin and stained with toluidine blue. Toluidine blue staining is a well-established method for detecting MC by staining the secretory granules resulting in a dark violet coloration specific to MC. The binding of toluidine blue to heparin, which is more abundant in mature connective tissue MC, correlates with the differentiation toward mature MC. BMMC, FSMC, and FLMC were all stained positive for heparin with toluidine blue. Giemsa staining, another method used to identify MC, which involves staining the cytoplasm of MC with a dark blue color while the granules are stained red, confirmed the higher granularity of FSMC compared to BMMC. Metachromatic staining can differentiate between MMC and CTMC by combined staining with Alcian blue and Safranin-O, as described in Chapter 1.2. The granules in FSMC exhibited a more intense red coloration than those in BMMC indicating a higher heparin content, indicative of CTMC (Figure 7D). Based on the phenotypic analysis, cells derived from all three tissues, BM, fetal liver, and fetal skin, respectively, give rise to a mature MC population. However, histological staining and morphological properties indicate that FSMC resemble tissue-derived mature MC more closely, whereas BMMC represent a MC population that is least developed.

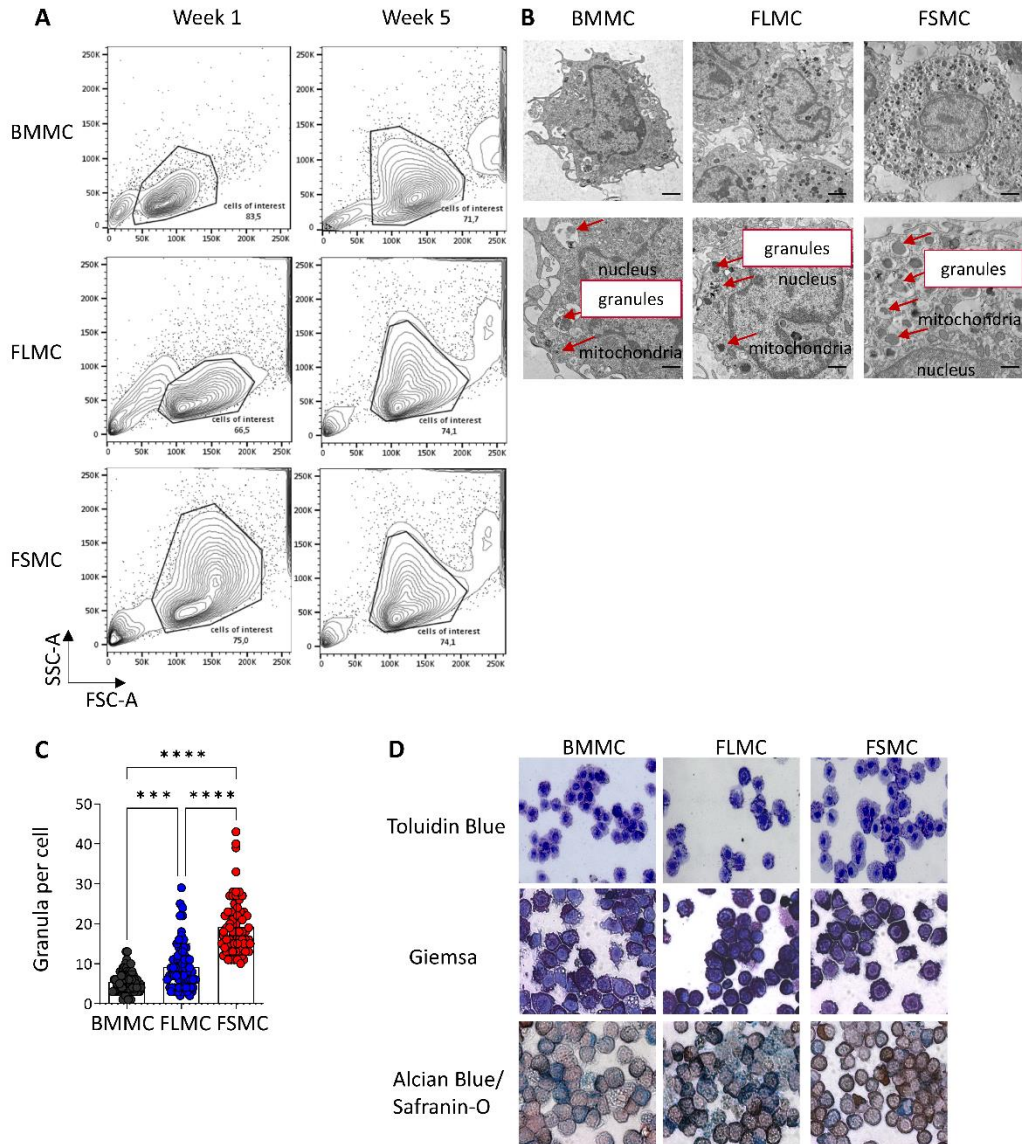


**Figure 7: Morphology of MC cultures**

(A) Forward scatter and side scatter represent the size and granularity of cells. (B) Structural analysis of MC was conducted by electron microscopy. Representative images with red arrows indicating areas with granules (scalebar 1  $\mu$ M) and (C) quantification of EM images as granules per cell (n=70, mean with SEM, ordinary one-way ANOVA, \*\*\*p<0.005; \*\*\*\*p<0.0001). (D) Semithin sections were stained with Toluidine Blue (top panel, 100 $\times$  magnification), Giemsa (middle panel, 40 $\times$  magnification), and Alcian Blue/Safranin O (bottom panel, 40 $\times$  magnification).

### 3.1.2 MC from different tissues show transcriptional heterogeneity

Mature MC were generated from BM, fetal skin, and fetal liver, with FSMC phenotypically and morphologically showing the highest degree of maturation and similarity to CTMC. Transcriptional profiling was conducted to investigate further which MC culture resembles mature CTMC. RNA was isolated from unstimulated cells to represent the transcriptional status at steady state. Historically, human MC were characterized based on the expression profile of MC-specific proteases, such as chymase, tryptase, and carboxypeptidase A. Accordingly, qPCR analysis of all three mature MC types revealed the expression of the CTMC-associated serine protease 5 (Mcpt5), the  $\beta$ -chymase Mcpt4, as well as two different tryptases, namely Mcpt6 and Mcpt7, as well as carboxypeptidase Cpa3. On the other hand, the two types of  $\beta$  chymases, Mcpt1 and Mcpt2, which are predominantly expressed by MMC, were not detected in any of the MC types (Figure 8A). Based on the qPCR data of MC proteases, all MC types can be classified as CTMC and show no major variance in the transcriptome regarding the proteases mentioned. However, the results of the principal component analysis showed that the three MC populations formed distinct clusters, confirming that the observed differences in phenotype, morphology, and behavior, as observed in our previous experiments, were associated with differences detectable in the transcriptome (Figure 8B). Notably, MC derived from fetal skin, depicted in red, exhibited the most distinct population compared to the other MC types.

Dwyer et al. analyzed the heterogeneity of MC on a transcriptional level. They revealed three distinct CTMC subsets with varying capacities for in situ proliferation in the absence of tissue inflammation [26]. Based on this data, the expression of the MC-specific gene signature defined by Dwyer et al. was extrapolated and the expression of this gene was analyzed in fetal-derived MC by normalizing to BMMC. The expression level of genes in fetal-derived MC was normalized against the expression level of BMMC to determine similarities and differences between the generated cells since the reference MC signature defined by Dwyer et al. was also constructed based on mRNA expression in BMMC. Although all three MC types were defined as CTMC according to surface markers, a distinct heterogeneity between the MC types can be seen on a transcriptional level (Figure 8C). Notably, FSMC showed higher expression levels of mas-related G protein-coupled receptor (*Mrgpr*)*b2* and *Mrgpr**b1* (Figure 8D, E). Upregulation of genes related to Mas-related G protein-coupled receptor-X2 (MRGPRX2) is highly interesting, as this novel receptor is thought to activate MC through induction of  $\text{Ca}^{2+}$  mobilization also leading to degranulation. In addition, activation via *Mrgprx2* results in the generation of

cytokines and chemokines via MAPK and NF- $\kappa$ B pathways and is therefore implicated in contributing to the pathogenesis of pseudo-allergic drug reactions, pain, itching, and inflammatory diseases [172]. While Mcpt2 was not detectable in the qPCR analysis, using the more sensitive method of bulk RNA sequencing revealed a downregulation for both fetal-derived MC compared to BMCC (Figure 8D). Visualizing the top 20 differentially expressed genes within BMCC, FLCC, and FSCL as a heatmap further revealed that fetal-derived MC show a strong upregulation of the mRNA of *Tpsb2*, the gene encoding for beta-II tryptase and *Hdc*, which catalyzes the biosynthesis of histamine to histidine (Figure 8F).

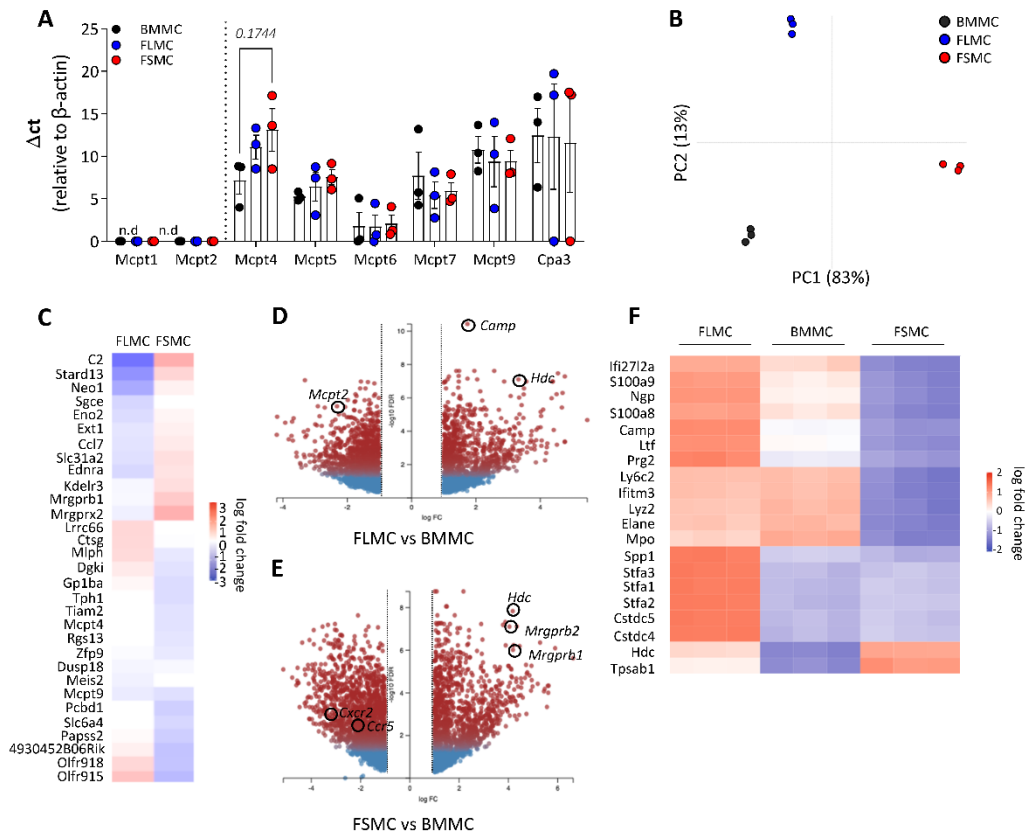


**Figure 8: Transcriptomic analysis of MC cultures**

(A) MC protease mRNA expression was analyzed by qPCR.  $\Delta ct$  values relative to housekeeping gene  $\beta$ -actin ( $n = 3$ , mean with SEM, 2way ANOVA). (B) Bulk RNA sequencing of BMCC (black), FLCC (blue) and FSCL (red) was performed. Principal component analysis showed variance among the MC types ( $n = 3$ ). (C) Differential expression of mRNA associated with the MC signature by Dywer et al. [18]. mRNA expression of FLCC and FSCL normalized against BMCC. Upregulated genes are shown in red and downregulated mRNA of genes in blue. ( $n = 3$ ,  $FDR \leq 0.01$ ,  $abslogFc > 2$ ). (D, E) Volcano plot of differentially expressed genes between the groups (D) FLCC vs. BMCC and (E) FSCL vs. BMCC analyzed with the web tool Degust ( $n = 3$ ,  $FDR \leq 0.01$ ,  $abslogFc > 1$ ). (F) Heatmap showing the top 20 DEG between BMCC, FLCC, and FSCL. Upregulated genes are shown in red and downregulated genes in blue ( $n = 3$ ).

### 3.1.3 Responsiveness of MC types to IgE stimulation

RNA sequencing analysis disclosed a transcriptional difference between the MC types, showing altered expressions of *Camp*, which is associated with calcium-binding and IP3 signaling. This signaling pathway is essential for MC function in allergic reactions. IgE-mediated coupling of the high-affinity IgE receptor FcεRI elicits the activation of the PI3K/Akt and MAPK signaling pathway, resulting in the influx of cytosolic calcium and cellular degranulation. In the unstimulated state, transcriptional differences in genes involved in FcεRI signaling were detected. Differential gene expression of FSMC normalized to BMMC showed a significant upregulation of genes *Pik3cb*, *Pik3r5*, *Mapk13*, and *Vav3*, which are associated with the PI3K/Akt pathway. Interestingly, the genes *Fcer1a* and *Ms4a2*, the β-unit of the FcεRI receptor, showed an upregulation in FLMC normalized to BMMC, suggesting that FLMC reacts stronger towards IgE stimulation (Figure 9A).

To determine whether this apparent difference on a transcriptional level of *Camp*, *Fcer1a*, and *Ms4a2* has a functional implication on the activation potential of MC, changes in calcium levels following crosslinking of the IgE-receptor were analyzed. For this, MC were loaded with 2 μM fura-2AM for 20 min at 37°C and intracellular Ca<sup>2+</sup> was measured before and following the addition of DNP-HSA (50 ng/ml) to IgE-sensitized MC in the absence or presence of extracellular Ca<sup>2+</sup>. All three MC types showed unequivocal FcεRI-mediated Ca<sup>2+</sup> influx and a comparable down-time back to base levels after antigen addition (Figure 9B). Patch-clamp analysis further supported this, which showed equivalent sustained activation of the potassium channel SK4 in FSMC compared to BMMC, which is essential for IgE-dependent MC degranulation. (Figure 9C).

Activation of MC via cross-linking of the FcεRI receptor results in anaphylactic degranulation of MC and the immediate release of stored mediators. All three MC types were forced to degranulate, either IgE-mediated or by adding PMA/ionomycin. The supernatants of stimulated MC were collected and the concentration of released histamine was determined by ELISA. Upon IgE-mediated degranulation, significantly higher levels of histamine were detected in the supernatant of FSMC, with nearly 200 ng/ml, which is a 10-fold higher concentration than in BMMC. (Figure 9D). Another method to evaluate the degree of degranulation is to measure the β-hexosaminidase activity. Fetus-derived MC show a higher release of β-hexosaminidase than BMMC, which correlated with the higher granularity (Figure 9E). Taken together, the transcriptional differences in the expression of genes related to FcεRI- and Ca<sup>2+</sup> signaling between bone-marrow-derived and fetal-derived MC have no functional implication on the activation potential of MC via IgE. However, amongst the top 20 differentially expressed genes, FSMC

showed a 4-fold upregulation in the genes *Tpsb2* and *Hdc* compared to BMMC. This alteration on a transcriptional level is in line with the stronger production and, thereby release of histamine from fetal-derived MC amongst activation through IgE.

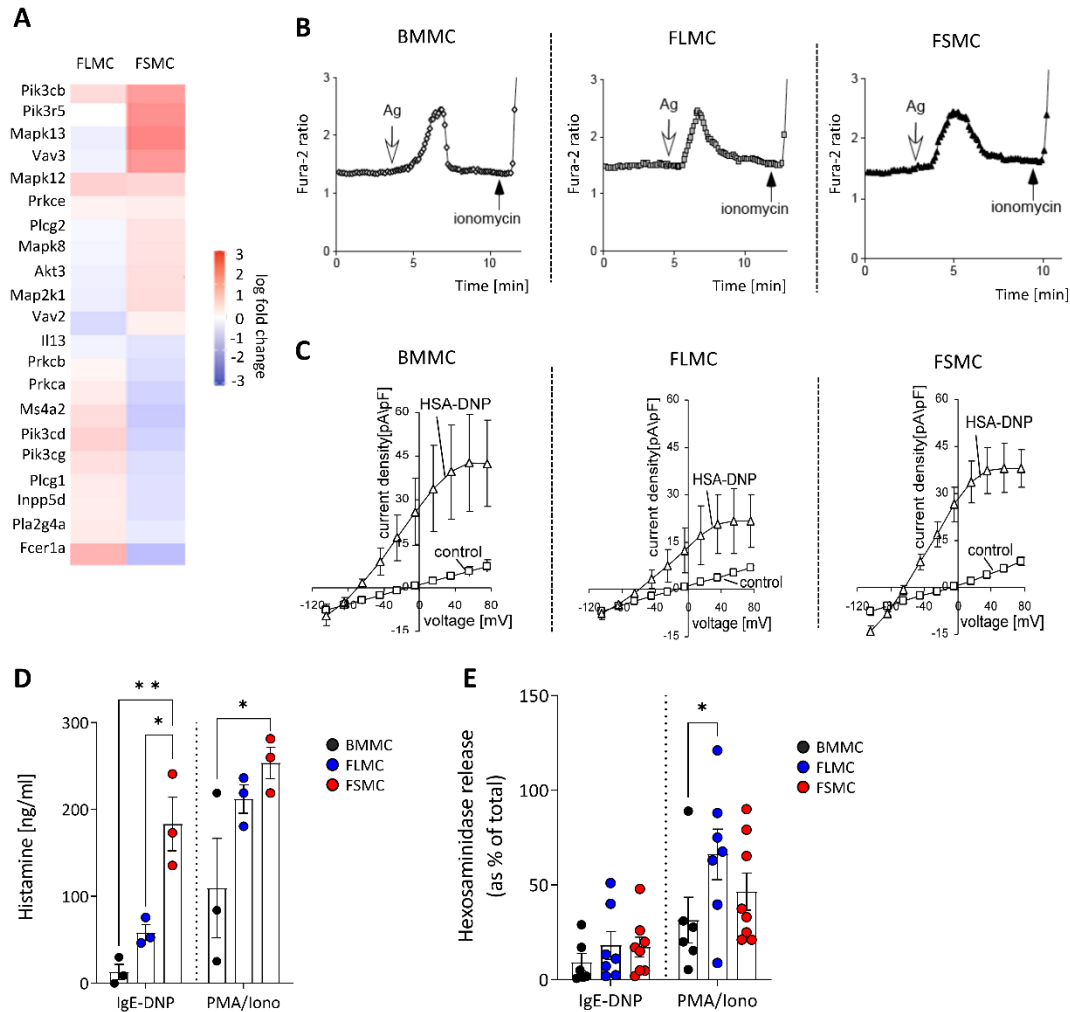


**Figure 9: MC response to IgE stimulation**

(A) Heatmap of differentially expressed mRNA of genes involved in FcεRI signaling in fetal-derived MC relative to BMMC (FDR > 1, abs logFC > 1.5×). (B) MC were incubated overnight with IgE-DNP. Before stimulation, cells were loaded with fluorescent Fura-2. DNP-HSA triggered calcium influx. (C) Comparable sustained activation of the K-channel SK4 as shown by patch clamp analysis. (D) Histamine levels detected in supernatant from BMMC (black), FLMC (blue), and FSMC (red) after PMA/ionomycin or IgE-DNP stimulation for 24 h using an enzyme-linked immunosorbent assay (n = 3, mean with SEM, 2way ANOVA, \*p<0.05; \*\*p<0.001). (E) BMMC (black), FLMC (blue), and FSMC (red) were stimulated with PMA/ionomycin or IgE-DNP for 30 min. Hexosaminidase release was calculated as percent of total cell lysis via Triton-X100. (n = 6-8, mean with SEM, 2way ANOVA, \*p<0.05).

### 3.1.4 MC response to endogenous stimuli

MC are preferentially located at the host–environment interface, which enables them to fulfill their function as sentinels for invading pathogens and inflammation. Apart from IgE-mediated activation of MC, other stimulation pathways have been investigated that induce MC activation, degranulation, and cytokine release in an IgE-independent manner. Host immune responses undergo two phases: rapid and nonspecific elimination of the pathogen involving immune cells of the innate immune system and a slower specific response inducing immunologic memory involving cells of the adaptive immune system. However, recent studies have shown that after infection, cells belonging to the innate immune system undergo epigenetic changes, which result in increased release of inflammatory cytokines upon secondary encounter with the pathogen [173]. It is hypothesized that MC also undergo this trained immunity [174]. DAMP, specifically TLR and NLR, mediate this response toward pathogens. Another endogenous danger signal is the alarmin IL-33, which can interact with MC via the ST2 receptor.

MC are known to express a variety of TLR allowing for their function as innate sentinels. To determine whether there are differences in TLR expression between the MC types, qPCR was performed on unstimulated MC. In steady state, no differences in gene expression, relative to housekeeping gene  $\beta$ -actin, were determined for TLR3, TLR6, TLR7, and TLR9 between the three MC types. However, the toll-like receptors 1, 2, and 4 showed a trend to be expressed at higher quantities in FLMC as low ct-value correlate inversely with the amount of mRNA (Figure 10A). This difference in gene expression of TLR suggests a variance in responsiveness between the three MC types following stimulation with TLR agonist. To verify this, BMMC, FLMC, and FSMC were stimulated with TLR-agonists to stimulate the cells in the next step. MC were stimulated with 100  $\mu$ g/ml Pam2Cys (TLR2/6 agonist), 100  $\mu$ g/ml Pam3Cys (TLR1/2 agonist), 50  $\mu$ g/ml poly: IC (TLR3 agonist), 10  $\mu$ g/ml LPS (TLR4 agonist), 25  $\mu$ g/ml Imiquimod (TLR7 agonist), 0.5  $\mu$ M CpG OD 1668 (TLR9 agonist) or PMA/ionomycin as internal control for MC functionality for 24h. Concentrations of IL-6 and TNF- $\alpha$  were detected in the supernatant. FLMC showed the most substantial release and hence production of IL-6 upon stimulation with TLR-agonists directed against TLR1, TLR2, and TLR4, with concentrations detected >5000 pg/ml. At the same time, FSMC did not react or at least did not release any IL-6 (Figure 10B). Especially the stimulation with Pam3Cys and LPS showed a significant difference in IL-6 release between FLMC and FSMC. Accordingly, the lowest TNF- $\alpha$  concentration was also detected in the supernatant of stimulated FSMC, with a highly significant difference in TNF- $\alpha$  release between BMMC and FSMC following stimulation with LPS (Figure

10C). Signaling of TLR4, the receptor for lipopolysaccharides (LPS) of Gram-negative bacteria, has been thoroughly investigated in MC and leads to NF $\kappa$ -B-dependent production of pro-inflammatory cytokines [81, 99]. The concentrations of a broad spectrum of inflammatory cytokines were analyzed in the supernatant of LPS-stimulated BMMC, FLMC, and FSMC. The heatmap revealed a broad secretion of pro-inflammatory and cutaneous associated cytokines from LPS-stimulated BMMC, such as high levels of MCP-1, IL-27, IL-1 $\beta$ , IL-10, and GM-CSF. Considerably fewer cytokines were detected in the supernatant of LPS-stimulated FLMC and FSMC (Figure 10D). A comparable picture can be seen when stimulating the MC types with the NLR-agonist MDP (Figure 10E).

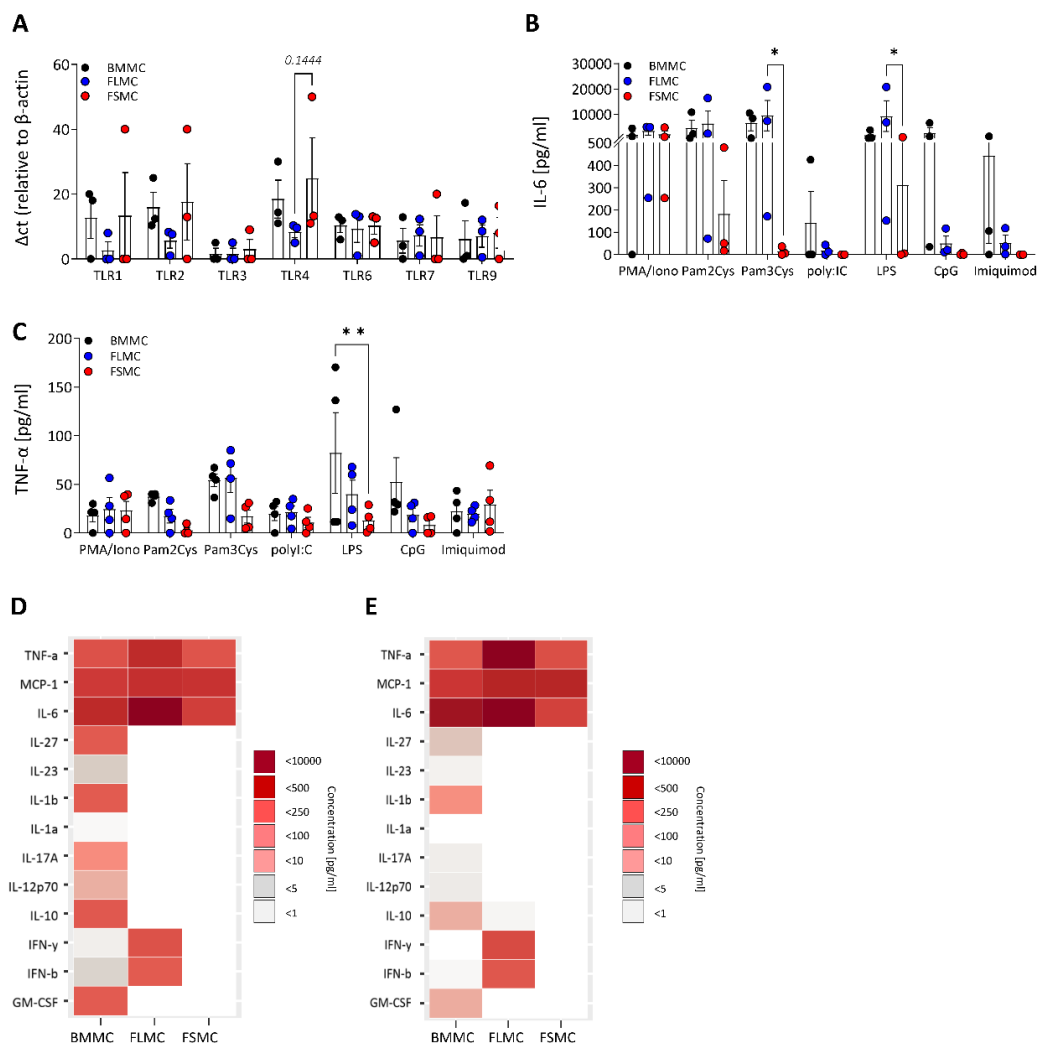


**Figure 10: MC response towards endogenous stimuli**

(A) TLR mRNA expression levels of MC were analyzed by qPCR.  $\Delta$ ct values are shown relative to housekeeping gene  $\beta$ -actin (n = 3, mean with SEM, 2way ANOVA). (B, C) MC were stimulated with various TLR-agonists for 24 h. The concentration of secreted (B) IL-6 and (C) TNF- $\alpha$  was measured in the supernatant via enzyme-linked immunosorbent assay (n = 3, mean with SEM, 2way ANOVA \*p<0.05, \*\*p<0.01). (D, E) MC were stimulated with (D) 10  $\mu$ g/ml LPS or (E) 10  $\mu$ g/ml MDP for 24 h. Cytokines in the supernatant were analyzed using a bead-based multiplex immunoassay. Heatmap representation of median concentrations given in pg/mL. The color gradient is depicted from 0–10000 pg/mL.

Alarmins are naturally occurring, continuously produced proteins or peptides that function as immune activators and chemoattractant. They are produced in response to cell injury, degranulation, or death, or in response to immune stimulation. Alarmins act as intercellular signals to promote immune defense by binding to chemotactic and pattern recognition receptors to recruit immune cells in the body [175]. One prominent alarmin in the skin is IL-33, which belongs to the IL-1 family. MC as well as ILC2 and Tregs, are immune cells that constitutively express the IL-33 receptor ST2 [59]. As expected, MC generated from BM and fetal tissue express ST2 on the cell surface. Surprisingly, FLMC showed a reduced median fluorescent intensity (MFI) for ST2 suggesting a lower receptor expression on the surface (Figure 11A, B). To test the functional relevance of the differential surface expression of the ST2 receptor, MC were stimulated with 10 ng/ml IL-33 and the supernatants were collected as well as RNA prepared from stimulated cells. In line with the reduced MFI of ST2, FLMC showed a substantial reduction in *Il13* expression, a typical MC-derived type 2 immune cytokine (Figure 11C). This confirms result from others who showed IL-33-dependent upregulation of *Il13* expression in skin MC [176]. Both BMMC and FSMC, which showed the highest surface expression of ST2, showed solid response to ST2-dependent activation by secreting high concentrations of type 2 immune cytokines such as IL-4, IL-9, IL-13 but also of IL-17, amongst others (Figure 11D). Thus, the tissue of origin imprints MC precursor cells so that these cells, despite identical in vitro culture conditions and consecutive equal MC marker surface expression of CD117 and FcεRI, acquire distinct phenotypes and signatures. Moreover, FSMC are less responsive to TLR activation and stimulation with IL-33 concerning cytokine production compared to FLMC and BMMC, indicating a more mature and less monocytic-like functionality of FSMC.

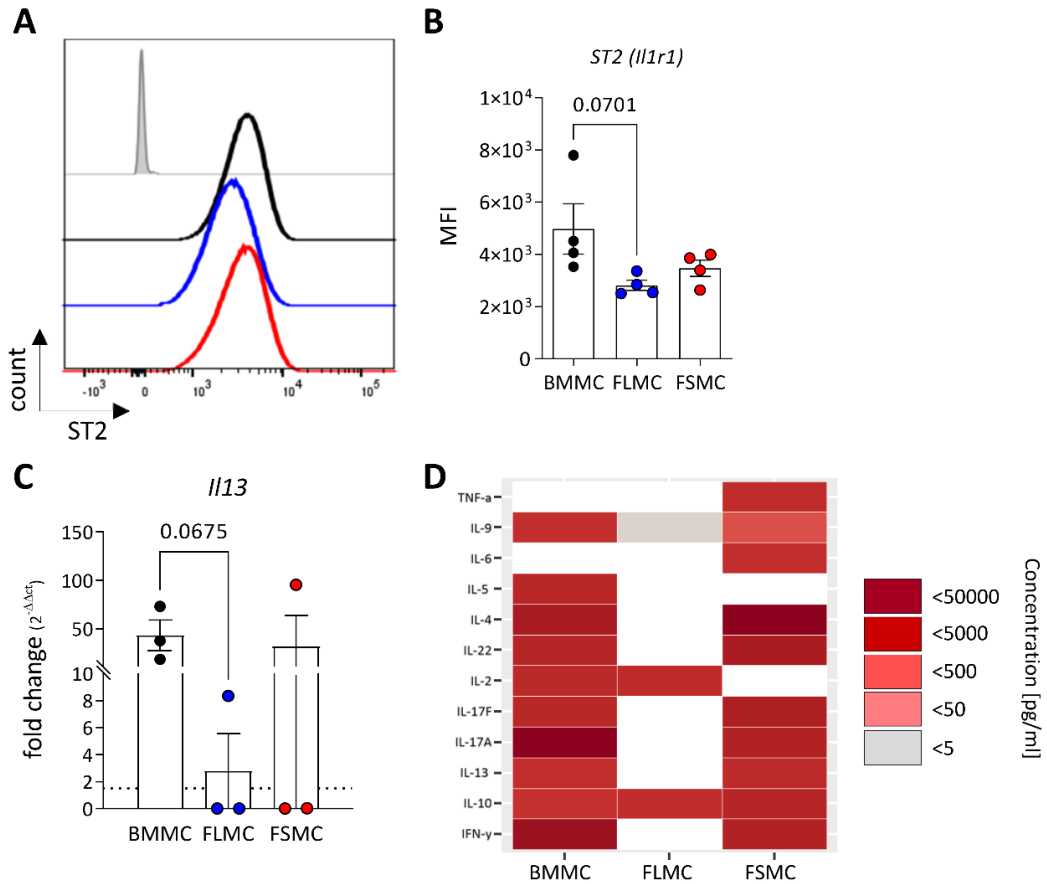


**Figure 11: MC response to IL-33 stimulation**

(A) Representative histogram of ST2 surface expression on BMMC (black), FLMC (blue), and FSMC (red). (B) Surface expression quantified as MFI (n = 4, mean with SEM, 2way ANOVA). (C) MC were stimulated with 10 ng/mL IL-33 for 1 h and RNA was isolated. mRNA expression of IL-13 was analyzed by qPCR. Fold change determined as  $2^{-\Delta\Delta Ct}$  (n = 3, mean with SEM, ordinary one-way ANOVA). (D) MC were stimulated with 10 ng/mL IL-33 for 24 h, and the concentration of secreted type 2 cytokines was measured in the supernatant via beads-based multiplex immunoassay. Heatmap representation of median concentrations given in pg/mL. The color gradient is depicted from 0–50000 pg/mL.

## 3.2 Targeting MC plasticity re-shapes the TME of melanoma

MC are primarily known for their role in allergic reactions due to their IgE signaling and histamine release. In recent research conducted by this group, an accumulation of MC in the TME of melanoma was detected. This accumulation was particularly seen in regions displaying immune regression. Our recent work substantiated that tumor-resident MC, stimulated by LPS, elicit proficient anti-tumoral immune reactions against melanoma [99]. Considering the functional plasticity exhibited by MC and their ability to secrete diverse bioactive mediators, the effects of factors of the TME of melanoma were analyzed to elucidate their role in orchestrating melanoma defense.

### 3.2.1 IL-33 mediates tumor control in melanoma and recruits MC to the TME

IL-33 is an alarmin that is, amongst others, released upon tissue damage [177]. In the TME, the primary sources of IL-33 were described to be endothelial cells, fibroblasts, epithelial cells, and tumor cells themselves [178]. Using the GEPIA web server, a web-based tool which allows for gene expression analysis based on TCGA and GTEx data, showed that high levels of IL-33, determined either through single-cell RNA sequencing or by copy numbers as determined by SNP arrays (CNAs), are significantly better for the overall survival of patients (Figure 12A, B) [179]. We evaluated the antitumor effects of IL-33 in a mouse model of melanoma. C57BL/6N mice were injected intradermally with  $7.5 \times 10^4$  B16.F1 cells in the hind flanks. The transplanted melanomas received 0.5  $\mu\text{g}$  IL-33 injections peri-tumorally either at the time of melanoma implantation (t0, seeding stage, 'S'-stage) or after tumors reached a mean diameter of about 3 mm (d9, manifestation stage, 'M'-stage) (Figure 12C). Early treatment of tumors with IL-33 showed no effect on tumor progression, while later treatment showed a significant anti-tumoral effect, with a substantial reduction in tumor volume and weight compared to control (Figure 12D, E). Since a difference in tumor progression was only identified between 'M'-stage tumors and control tumors, the local immune infiltrate in the two groups was determined by flow cytometry. Evaluation of the tumor growth of 'M'-stage tumors revealed that not all tumors that received IL-33 responded with tumor control. Closer analysis of the tumors by flow cytometry showed that IL-33 treated tumors could be classified based on the infiltration of T cells (Figure 12F). Based on a cut-off of  $1 \times 10^3$  T cells per gram tumor, IL-33 treated tumors were classified as "hot" or "cold" tumors. In contrast to cold tumors, hot tumors were significantly smaller than PBS-treated controls (Figure 12G). Giemsa staining of FFPE-fixed 'M'-stage tumors showed a considerable accumulation of MC in the dermal layer (Figure 12H-I,

indicated by arrows), that were significantly increased in IL-33 treated melanoma (Figure 12J). This accumulation around the tumor was confirmed by a MC-specific avidin stain (Figure 12K).

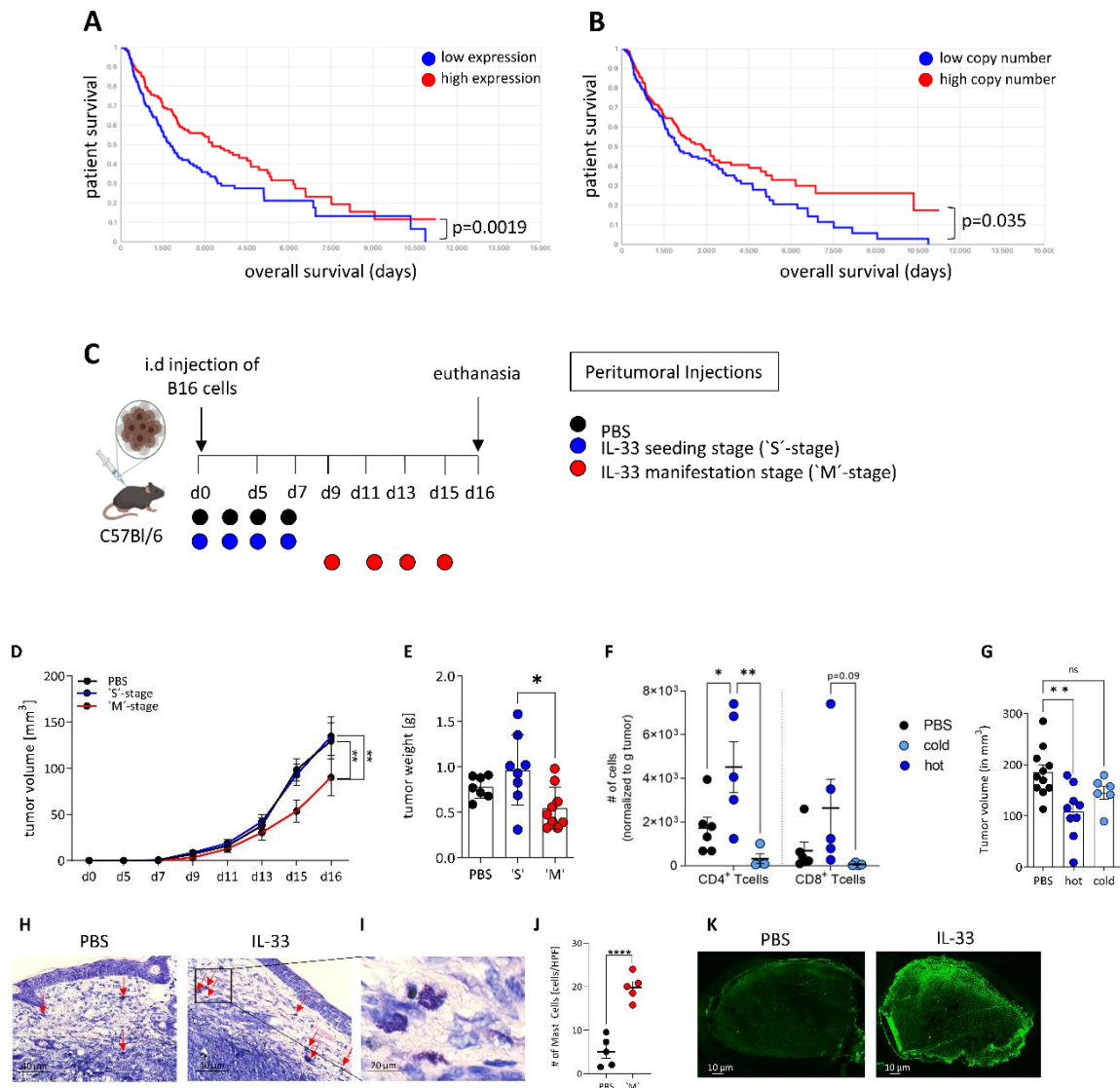


**Figure 12: IL-33 recruits MC to the TME of melanoma**

(A) TCGA analysis of CM revealed better overall survival in patients with high RNA expression levels of IL-33 and (B) high copy numbers of IL-33. (C) Schematic outline of the B16 melanoma mouse model depicting peritumoral administration of PBS (black) and 500 ng IL-33 every other day before tumor manifestation (seeding stage, 'S'-stage; blue) and 500 ng IL-33 every other day after tumor manifestation (manifestation stage, 'M'-stage; red). (D) Tumor volume in mm<sup>3</sup> over time (n=18-20 from two independent experiments, mean with SEM, 2-way ANOVA, \*\*p>0.01) and (E) tumor weight in gram measured on day 16 (n=6-9, mean with SEM, one-way ANOVA, \*p<0.05). (F) Tumors were stratified into hot (dark blue) and cold (light blue) tumors based on the number of T cells (n=4-5 of two independent experiments, mean with SEM, 2way ANOVA, \*p<0.05; \*\*p<0.001). (G) Tumor volume in mm<sup>3</sup> based on hot/cold stratification (n=6-11, mean with SEM, one-way ANOVA, \*\*p<0.01). (H) Giemsa staining of FFP-fixed B16 tumors stained. Red arrows indicate MC, scale bar represents 40µm. (I) Enlargement of Giemsa staining (scale bar represents 20µm). (J) Quantification of MC from Giemsa stain (n=5, mean with SEM, student t-test, \*\*\*\*p<0.001). (K) Avidin staining of cryo-conserved B16 tumors.

### 3.2.2 IL-33 activated MC secrete immune-recruiting chemokines

An accumulation of MC in the TME upon IL-33 treatment was found, indicating a role for IL-33 and MC mediated control of tumor progression. Usually, IL-33 is located in the nucleus and can be released, amongst others, upon damage or death of the cell. The biological activity of the full-length protein can be either increased or abolished when modified by proteases. Interestingly, MC proteases were shown to cleave full-length IL-33 into two more mature forms with significantly enhanced activity [68]. Since we saw an accumulation of MC following IL-33 injections, we closer investigated effects of IL-33 on MC in vitro. Therefore, in vitro generated BMMC were stimulated with 10 ng/ml IL-33, for 1 hour and bulk RNA sequencing was performed. Volcano plot and heatmap of differential gene expression (DGE) showed an upregulation of genes upon IL-33 signaling, such as *Nfkb* and *Cd69*, indicating activation of MC, as well as *Cfs2*, *Il13* and *Ccl1*, involved in the recruitment of immune cells (Figure 13A, B). Enrichment of *Il13* upon IL-33 stimulation in MC was already shown in our previous publication [169]. Gene ontology analysis of gene sets involved in molecular functions (MF) and biological processes (BP) supported this by showing an upregulation of genes associated with cytokine activity and adaptive immune responses (Figure 13C). Based on the localization of MC and the broad repertoire of receptors on their cell surface, it can be assumed that MC respond upon recognition of a wide variety of PAMP and endogenous DAMP in the TME of melanoma. To verify this, BMMC were stimulated with 100 ng/ml Pam2Cys (TLR2/6 agonist), 10 µg/ml MDP (Nod2 agonist), 5 µg/ml Hsp70 (TLR4 agonist), 250 ng/ml Malp2 (TLR2/6 agonist), 5 µg/ml dsDNA (TLR9 agonist), 10 µg/ml C48/80 (Mxgprb2 agonist), or with 1µg/ml IgE + 40 ng/ml IgE-DNP either alone or in combination with 10 ng/ml IL-33 for 24 hours. The supernatant of stimulated cells revealed a broad spectrum of secreted cytokines involved in immune cell recruitment, such as IL-6, CCL2, CCL3 and CCL4. As expected, the stimulation of entire spectrum of analyzed chemokines (Figure 13D). Especially the combination of IL-33 stimulation together with the TLR2/6 agonist Pam2Cys significantly increased concentration levels of the chemokine CCL, as well as increased levels of CCL2 and CCL4 in the supernatant (Figure 13E). This synergistic effect depends on IL-33, as stimulation of *ST2*<sup>-/-</sup> MC with both Pam2Cys and IL-33 only exhibits the CCL3 levels of the single stimulation (Figure 13F).

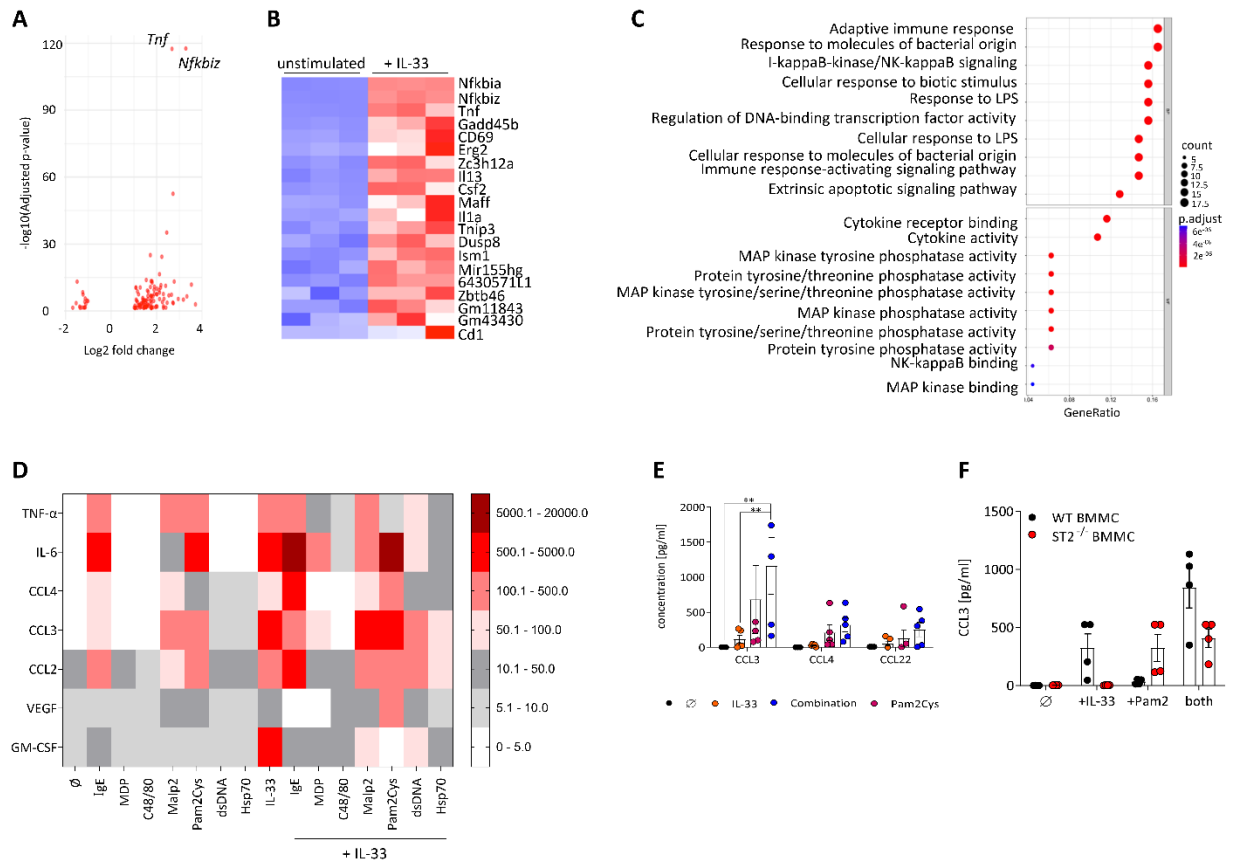


**Figure 13: Synergistic effect of ST2 and TLR2/6 on MC activation**

(A) Volcano plot showing DGE analysis of bulk RNA seq from IL-33 stimulated BMMC compared to unstimulated BMMC. (B) Heatmap of top 20 DGE. Color gradient shows upregulated (red) and downregulated genes (blue). (C) Gene ontology analysis of DGE was performed. Top differentially expressed gene sets in molecular function (MF) and biological processes (BP). (D) BMMC were stimulated with IgE/DNP-HSA or various DAMP, either alone or in combination with 10 ng/ml IL-33 for 24h. Cytokines in the supernatant were analyzed using a beads-based multiplex immunoassay. Heatmap representation of median concentrations given in pg/ml. (E) BMMC were stimulated with 10 ng/ml IL-33, 20 ng/ml Pam2Cys or the combination for 24h. Supernatant was analyzed using ELISA. Concentration of cytokines CCL3, CCL4 and CCL22 in pg/ml (n=6, mean with SEM, 2-way ANOVA with \*\*p>0.01). (F) Wildtype BMMC and ST2<sup>-/-</sup> BMMC were stimulated with 10ng IL-33, 20ng Pam2Cys or the combination of both for 24h. Supernatant was analyzed using ELISA (n=3, mean with SEM, 2-way ANOVA, \*\*\*p>0.005).

### 3.2.3 IL-33 activated MC are essential for recruiting T-cells to the TME

To determine whether the activation of MC through stimulation with both Pam2Cys and IL-33 can demonstrate functional relevance in vivo, *Mcpt5cre<sup>-</sup>-RDTA<sup>fl/fl</sup>* mice were injected intradermally with low-metastasizing B16.F1 cells in the hind flanks and tumors were treated either with peri-tumoral injections of PBS, IL-33 (0.5  $\mu\text{g/ml}$  in 25  $\mu\text{l}$ ), Pam2Cys (4  $\mu\text{g/ml}$  in 25  $\mu\text{l}$ ) or the latter two after tumors reached a mean diameter of 3 mm<sup>3</sup> (day 9) (Figure 14A). Indeed,

treating tumors with the combination of both IL-33 and Pam2Cys showed a significant reduction of tumor progression compared to the single administrations (Figure 14B). The same experimental setup was performed in *Mcpt5cre<sup>+</sup>-RDTA<sup>fl/fl</sup>* mice lacking CTMC. In the absence of MC, only the double treatment showed a slight reduction in tumor growth; MC therefore are essential for an effective anti-tumoral response in this setting (Figure 14C, D). Analyzing local immune infiltration in tumors from MC-competent and MC-deficient mice showed MC-dependent recruitment of T cells, especially cytotoxic T cells ( $CD8^+$ ) and the effector memory subtype ( $CD8^+CD44^+CD62L^-$ ) to the tumors. T-cell composition in MC-deficient mice resembled cold tumors, with a significantly diminished infiltration of tumor-infiltrating lymphocytes (Figure 14E, F). In addition, treatment of tumors with IL-33/Pam2Cys in MC-competent mice showed significant recruitment of NK cells ( $NK1.1^+CD49b^+$ ) to the tumors (Figure 14G). The cytotoxic functions of  $CD8^+$  T cells and NK cells are mediated by cytokines IFN- $\gamma$ , TNF- $\alpha$ , Granzyme B, and Perforin, which were all upregulated in tumors from MC-competent mice (Figure 14H). Also, increased fold change in genes *CXCL9*, *CXCL10*, and *CXCL11* were detected in tumors from MC-competent mice. These are chemokines known to be produced by MC to recruit T cells (Figure 14I). No substantial changes in T cells or NK cells were detectable in tumor-draining lymph nodes (Figure 14J, K).

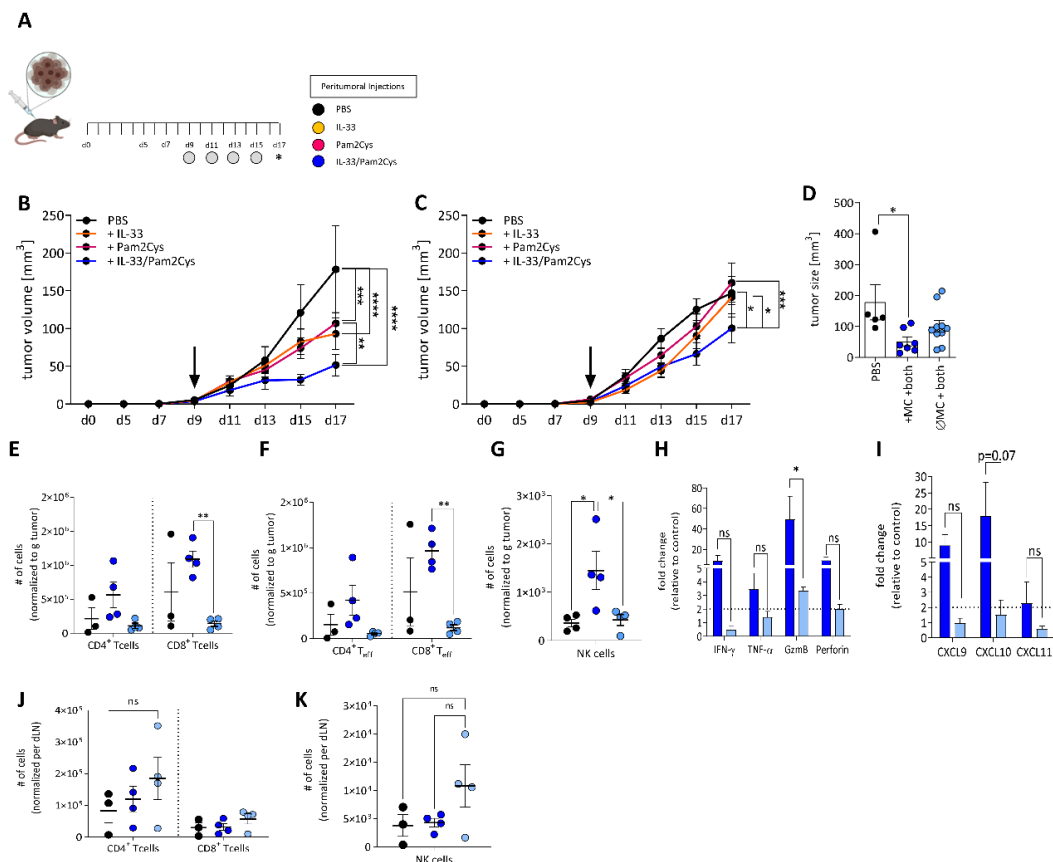


**Figure 14: IL-33 activated MC mediate T-cell inflamed tumors**

(A) Schematic outline of B16 melanoma mouse model. Peritumoral administration of PBS (black), 500ng IL-33 (orange), 4  $\mu$ g Pam2Cys (pink) or the combination of IL-33/Pam2Cys (blue). (B) Tumor development in MC-competent *Mcpt5-cre<sup>-</sup>-RDTA<sup>fl/fl</sup>* mice shown as tumor volume in mm<sup>3</sup> over time (n=5-8, mean with SEM, 2-way ANOVA, \*\*p>0.01; \*\*\*p>0.005; \*\*\*\*p>0.001). (C) Tumor development in MC-deficient *Mcpt5-cre<sup>+</sup>-RDTA<sup>fl/fl</sup>* mice shown as tumor volume in mm<sup>3</sup> over time (n=8-10, mean with SEM, 2-way ANOVA, \*p>0.05; \*\*\*p>0.005). (D) Comparison of tumor volume in mm<sup>3</sup> at day 17 post B16 inoculation between PBS treated tumors (black) and IL-33/Pam2Cs treated tumors in MC-competent (+MC, dark blue) and MC-deficient ( $\emptyset$ MC, light blue) mice. (n=5-8, mean with SEM, one-way ANOVA, \*p>0.05). (E-G) Flow cytometry analysis of cellular tumor composition from control tumors (black), MC-competent mice treated with IL33/Pam2Cys (+MC, dark blue) and MC-deficient mice treated with IL33/Pam2Cys ( $\emptyset$ MC, light blue) shows (E) CD3<sup>+</sup>CD4<sup>+</sup> and CD3<sup>+</sup>CD8<sup>+</sup> T cells (F) CD8<sup>+</sup>CD44<sup>+</sup>CD62L<sup>-</sup> and CD4<sup>+</sup>CD44<sup>+</sup>CD62L<sup>-</sup> effector memory T cells and (G) CD3<sup>+</sup>NK1.1<sup>+</sup>CD49b<sup>+</sup> NK cells (n=3-4, mean with SEM, 2-way ANOVA, \*p>0.05; \*\*p>0.01). All cells were pre-gated on living CD45.2<sup>+</sup> cells and normalized to gram tumor. (H) qPCR analysis of IL33/Pam2Cys treated B16 tumors from MC-competent (+MC, dark blue) and MC-deficient ( $\emptyset$ MC, light blue) mice. Fold change expression of IFN- $\gamma$ , TNF- $\alpha$ , Granzyme B and Perforin, as well as (I) CXCL9, CXCL10 and CXCL11 (n=3-4, mean with SEM, 2-way ANOVA, \*p>0.05). (J) Flow cytometry analysis of dLN for CD3<sup>+</sup>CD4<sup>+</sup> and CD3<sup>+</sup>CD8<sup>+</sup> T cells and (K) CD3<sup>+</sup>NK1.1<sup>+</sup>CD49b<sup>+</sup> NK cells (n=3-4, mean with SEM, 2-way ANOVA). Cells were pre-gated on living CD45.2<sup>+</sup> cells and normalized per dLN.

These data demonstrate that MC are important for mediating an anti-melanoma effect upon activation by IL-33/Pam2. To prove this, the back skin of MC-deficient mice was reconstituted with *ST2<sup>-/-</sup>* BMDC six weeks before melanoma cell inoculation. Tumors were treated according to the scheme outlined in Figure 15A. The loss of the IL-33 receptor on the cell surface of MC abolished the anti-tumoral effect of the treatment, with only a partial reduction in tumor size measurable, attributed to the single impact of Pam2Cys on tumor control (Figure 15B, C). Also, the formation of hot tumors was abolished through the loss of ST2 on MC, as only the MC-competent tumors showed infiltration of cytotoxic T cells (CD8<sup>+</sup>) as well as the effector memory subtype. Tumors from reconstituted mice showed equivalent T cells and NK cell numbers to control tumors treated with PBS (Figure 15D, E).

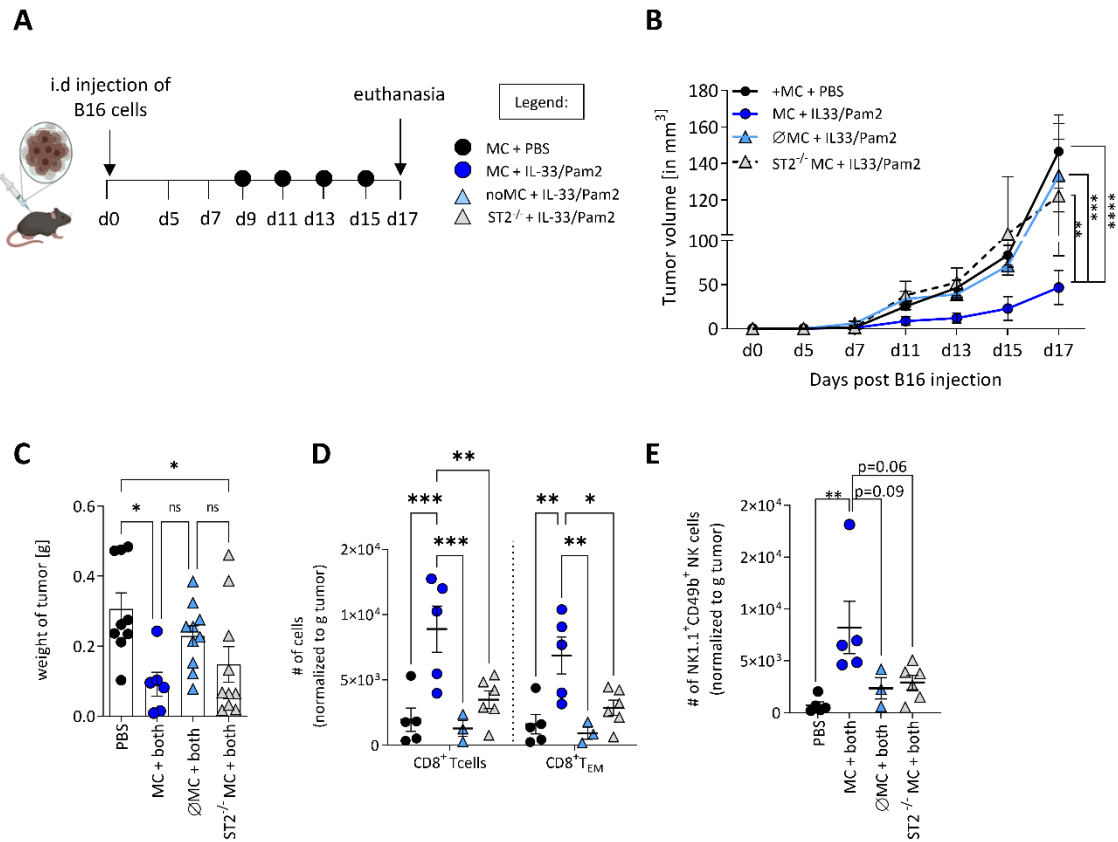


**Figure 15: ST2<sup>-/-</sup> MC in the TME abrogates the anti-tumoral effect.**

(A) Schematic outline of B16 melanoma mouse model. Peritumoral treatment of tumors with PBS in *Mcpt5-cre<sup>-</sup>-RDTA<sup>fl/fl</sup>* (black) and IL-33/Pam2 treatment of tumors in *Mcpt5-cre<sup>-</sup>-RDTA<sup>fl/fl</sup>* (dark blue), *Mcpt5-cre<sup>+</sup>-RDTA<sup>fl/fl</sup>* (light blue) and *Mcpt5-cre<sup>-</sup>-RDTA<sup>fl/fl</sup>* reconstituted with ST2<sup>-/-</sup> MC (grey). (B) Tumor development shown as tumor volume in mm<sup>3</sup> over time (n=6-10, mean with SEM, 2-way ANOVA, \*\*p>0.01; \*\*\*p>0.005; \*\*\*\*p>0.001) (C) Tumor weight on day 17 post B16 inoculation (n=6-10, mean with SEM, one-way ANOVA, \*p>0.05). (D) Flow cytometry analysis of CD3<sup>+</sup>CD8<sup>+</sup> T cells, CD8<sup>+</sup>CD44<sup>+</sup>CD62L<sup>-</sup> effector memory T cells and (E) CD3<sup>-</sup>NK1.1<sup>+</sup>CD49b<sup>+</sup> NK cells (n=3-4, mean with SEM, 2-way ANOVA, \*p>0.05; \*\*p>0.01; \*\*\*p>0.005). All cells were pre-gated on living CD45.2<sup>+</sup> cells and normalized to gram tumor.

### 3.3 Education of melanoma cells by MC impairs lymphatic metastasis

The data in Chapter 3.2 demonstrated that MC, when activated by PAMP, can elicit anti-tumoral functions and recruit T cells and NK cells to the TME. In a next step, the impact of MC on melanoma without the addition of an external stimuli was investigated.

### 3.3.1 The impact of MC secretome on melanoma migration

Cell invasion is one of the hallmarks of cancer, and understanding the mechanisms involved in tumor cell invasion may allow to interfere with tumor progression [180]. MC pre-store bioactive material in intracellular secretory vesicles. This content includes histamine, various proteases, cytokines, chemokines and growth factors [181]. To analyze the impact of MC on B16 melanoma cells, both invasion and migration experiments were conducted using supernatant of unstimulated MC and supernatant of sonicated MC. In a scratch assay using the live-cell analysis function of Incucyte<sup>®</sup>, the addition of MC supernatants showed a decreased relative scratch closure of B16 cells indicating that the supernatant released by MC inhibits the migration of B16 melanoma cells, independent of any external stimuli (Figure 16A, B). Further, a trans-well experiment showed that an effector-to-target ratio (E:T MC:B16 cells) of 1:100 is sufficient to significantly reduce migration of B16 cells through pores of an insert (Figure 16C, E).

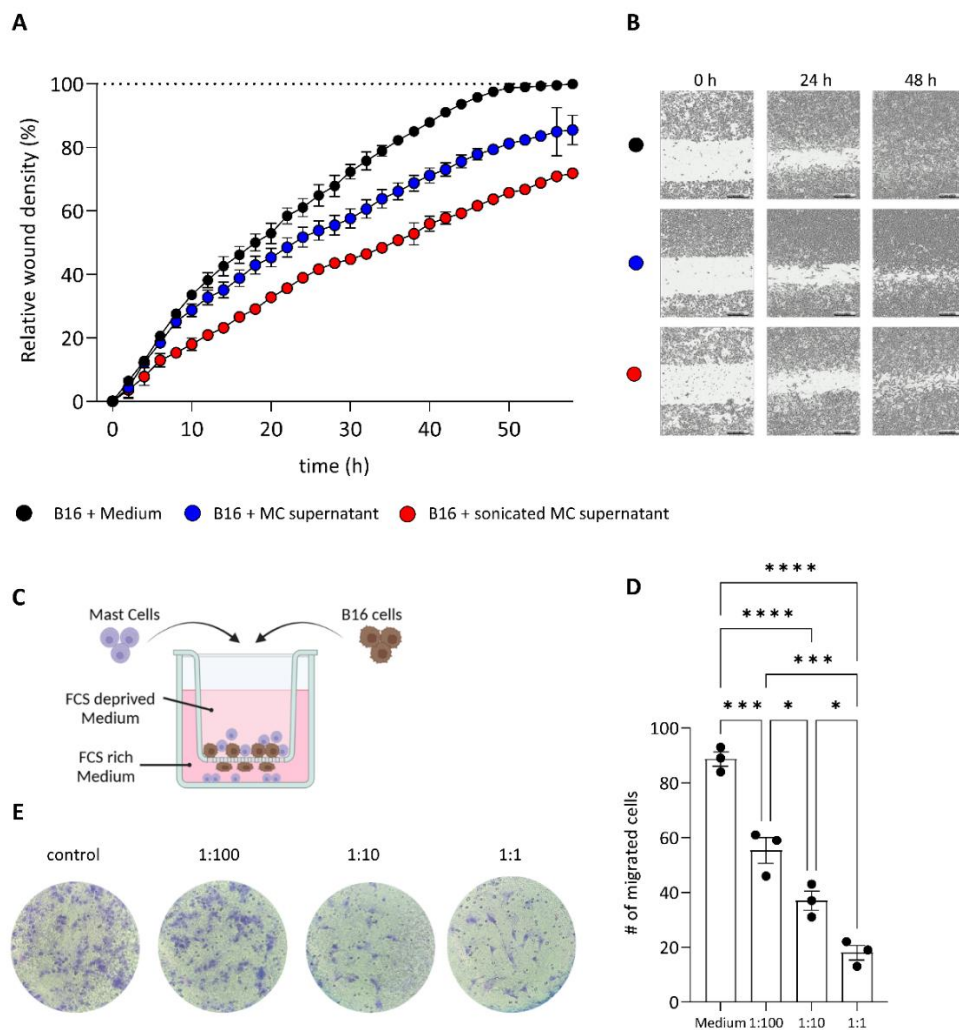


### Figure 16: MC inhibit B16 migration

(A) B16 cells were seeded in an Incucyte<sup>®</sup> plate and a scratch assay was performed. B16 cells were incubated either with control medium (black), supernatant of unstimulated BMMC (blue) or supernatant of sonicated unstimulated BMMC (red). Scratch closure was monitored over 60h in an Incucyte incubator. Migration potential represented as relative wound closure (n=3, mean with SD) and (B) representative images of scratch at the beginning (0h), after 24h and after 48h. (C) Schematic representation of transwell migration assay using an FCS gradient. (D) B16 cells were incubated with medium alone or with MC at an E:T ratio of 1:100, 1:10 or 1:1 for 24h. Migrated cells at the bottom of an 8  $\mu$ m insert were detected with crystal violet and counted under a microscope (n=3, mean with SEM, 2way ANOVA, \*p<0.05; \*\*\*p<0.005; \*\*\*\*p<0.001). (E) Representative images of cell inserts stained with crystal violet.

### 3.3.2 Loss of MC results in lymphatic metastasis in a murine melanoma model

To determine whether MC impact melanoma proliferation and migration in vivo, low metastasizing B16-F1 cells were intradermally implanted into the hind flanks of Mcpt5-cre<sup>-</sup>-RDTA<sup>fl/fl</sup> (MC-competent) and Mcpt5-cre<sup>+</sup>-RDTA<sup>fl/fl</sup> (MC-deficient) mice. Tumors were left untreated as no external stimuli was added to the TME (Figure 17A). The absence of MC increases tumor burden and significantly larger tumors were measurable in MC-deficient mice already after 14 days post inoculation (Figure 17B, C). Interestingly, after euthanasia of the mice, pigmented cell clusters were detected in the tumor-draining lymph nodes (dLN) and along lymphatic vessels indicating melanoma metastases (Figure 17D). Metastases were visible almost exclusively in mice lacking MC (Figure 17E). Histological analysis proved that these cell clusters were indeed melanoma metastases that migrated from the primary tumor. H&E staining showed formation of melanocytic nests (Figure 17F). Furthermore, melanoma cells used in this experiment express ovalbumin (B16-OVA). By performing qPCR from primary tumors, metastasis and control samples, we detected OVA only in the primary tumor and in samples from dLN metastasis, but neither in axial lymph nodes nor in skin from untreated mice. In addition to OVA, also Melan-A, a melanocyte marker, was detectable in samples from dLN metastasis, indicating that melanoma cells have invaded the tissue and that the pigmented cells in the dLN originated from the primary tumor in MC-deficient mice. In conclusion, both histology and qPCR support the fact that the melanoma cells detected were derived from the transplanted melanoma and can therefore be classified as metastases (Figure 17G).

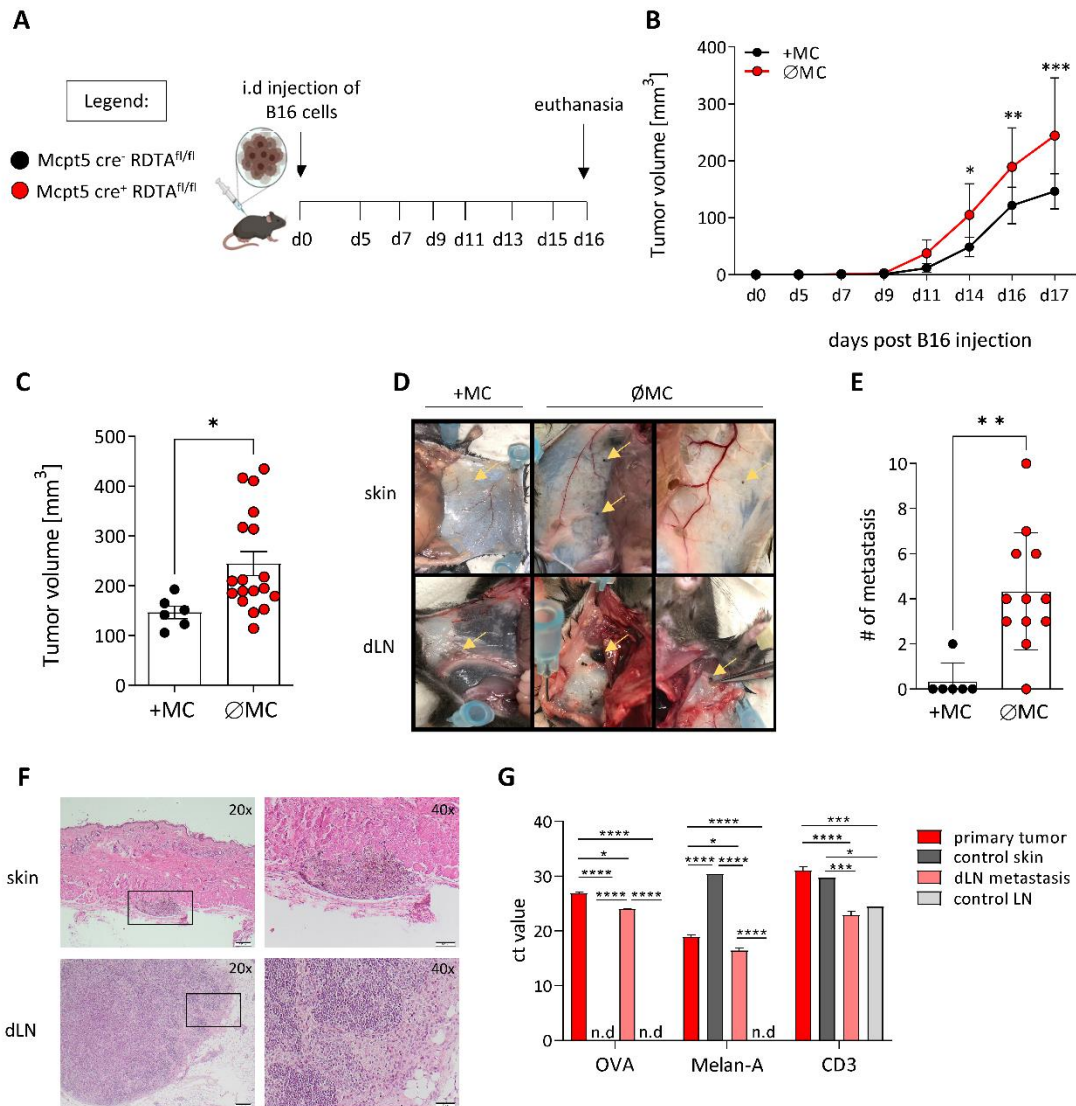


**Figure 17: Metastasis formation in MC deficient mice.**

(A) Schematic representation of experimental set up. *Mcpt5*-cre<sup>-</sup>-*RDTA*<sup>fl/fl</sup> (+MC, black) and *Mcpt5*-cre<sup>+</sup>-*RDTA*<sup>fl/fl</sup> (ØMC, red) mice were injected intradermally with B16-OVA cells in the hind flanks. (B) Tumor development shown over 16 days (n=6-18, mean with SEM, 2way ANOVA, \*\*p<0.01). (C) Endpoint comparison of tumor volume in mm<sup>3</sup> at day 16 between MC-competent (+MC, black) and MC-deficient (ØMC, red) (n=6-18, mean with SEM, ordinary one-way ANOVA, \*p<0.05). (D) Representative photography's of metastases in skin and dLN in MC-competent (+MC) and MC-deficient (ØMC) mice. (E) Quantification of visible metastasis (dLN and skin combined) in MC-competent (+MC, black) and MC-deficient (ØMC, red) mice (n=6-12, mean with SEM, unpaired students t-test, \*\*p<0.01). (F) Representative images of H&E staining of FFPE-embedded tissues. (G) qPCR analysis of primary tumor (red), dLN metastasis (pink), control skin (dark grey) and control LN (light grey) for the genes *OVA*, *Melan-A* and *CD3*. Ct values relative to housekeeping gene  $\beta$ -actin (n=2-3, mean with SEM, 2way ANOVA, \*p<0.05, \*\*\*p<0.005, \*\*\*\*p<0.0001).

Bulk RNA sequencing of primary tumors from MC-competent and MC-deficient mice was performed and differential gene expression analyzed. The top 50 expressed genes in tumors from MC-deficient mice compared to MC-competent mice are depicted in Figure 18C and a detailed list of all genes can be found in Table 11.

**Table 11:** Top 50 DEG in primary tumors from MC-deficient mice

Gene Name	Log2 Fold Change	Wald test p value
Gypa	12,48	2,10E+00
Hbb-bt	1.750,15	6,82E+00
Apol11b	15,88	1,33E+01
Alas2	122,87	7,50E+01
Hba-a1	1.651,09	1,12E+01
Hba-a2	1.215,53	1,52E+01
Hbb-bs	4.989,48	2,63E+01
Bpgm	138,23	2,45E+01
Rps24-ps3	37,16	2,51E+02
Gm6030	25,06	1,65E+02
Rps24	2.551,77	2,23E-03
Rpl30	151,27	5,51E+01
Psmb10	308,80	3,43E+02
Bst2	510,14	1,38E+02
Ifitm3	1.004,28	8,82E+00
Psme1	269,24	2,58E+01
Ifi35	157,15	7,29E+01
Nmi	164,91	7,29E+01
Isg15	221,33	9,58E+01
Dtx3l	56,08	2,09E+02
B2m	3.569,14	7,64E-02
Ifit1	143,31	4,64E+00
Stat1	248,90	1,42E+00
Xaf1	59,74	1,49E+02
Parp12	80,62	1,76E+01
Psme2	150,15	5,19E+01
Usp18	110,42	9,66E+00
Sp100	120,61	2,48E+02
Cmpk2	53,20	5,57E+01
Irf7	135,80	1,62E+02
Phf11d	60,01	2,49E+02
Ccl2	77,42	3,82E+00
Rtp4	135,24	1,08E+00
Mndal	69,34	1,35E+01
Irgm1	274,01	1,89E-01
Ifit3b	59,28	5,89E+00
Ccl7	90,60	2,08E+00
H2-T22	128,27	1,49E+00
Casp12	48,81	2,54E+01
Apol9a	107,56	3,55E+00
Ifi203	52,67	1,20E+00
Kcnj13	49,05	1,03E+00
Tap2	92,49	5,39E+00
Oasl2	45,72	7,83E+00
Ifit3	302,89	1,08E-04
Cxcl9	61,66	9,95E+01
Nlrc5	25,24	1,44E+02
Apol9b	100,16	6,61E-01
Irf1	125,62	2,48E-01
Irgm2	73,22	1,52E-01

Gene ontology analysis of bulk RNA sequencing showed that tumors from MC-deficient mice express an upregulation of genes associated with the molecular function pathway of GPTase activity and GTP binding. There are many GPTases which are known to be highly activated in cancers and are associated with cancer migration and metastasis [182, 183]. Bulk RNA sequencing analysis further revealed that tumors from MC-deficient mice showed a downregulation of genes such as *CCL2*, *CCL7*, *Irf*. *CCL2* and *CCL7* are both known to be chemoattractants for monocytes and DC [184, 185]. Furthermore, *Bst2*, an autologous melanoma antigen, known to be implicated in HLA-restricted recognition of melanoma cells by tumor infiltrating lymphocytes was downregulated in tumors from MC-deficient mice (Figure 18B) [186, 187]. Serum samples of MC-competent and MC-deficient mice were analyzed using a bead-based multiplex immunoassay that combines flow cytometry and ELISA. It showed a slight increase in chemokines involved in the recruitment of Th2 cells and IL-10-producing Tregs such as MIP-1 $\beta$  and MDC (CCL22) in MC-deficient mice. Tumor-bearing mice deficient in MC had significantly higher levels of CXCL5 in the serum (Figure 18C). CXCL5 is a known chemoattractant for neutrophils and was found to promote lymph metastases [188]. Indeed, primary tumors of MC-deficient mice showed an increased infiltration of CD11b<sup>+</sup>Gr1<sup>+</sup> neutrophils (Figure 18D). Several chemokines and chemokine receptors have been identified to facilitate lymph node metastasis [189-191].

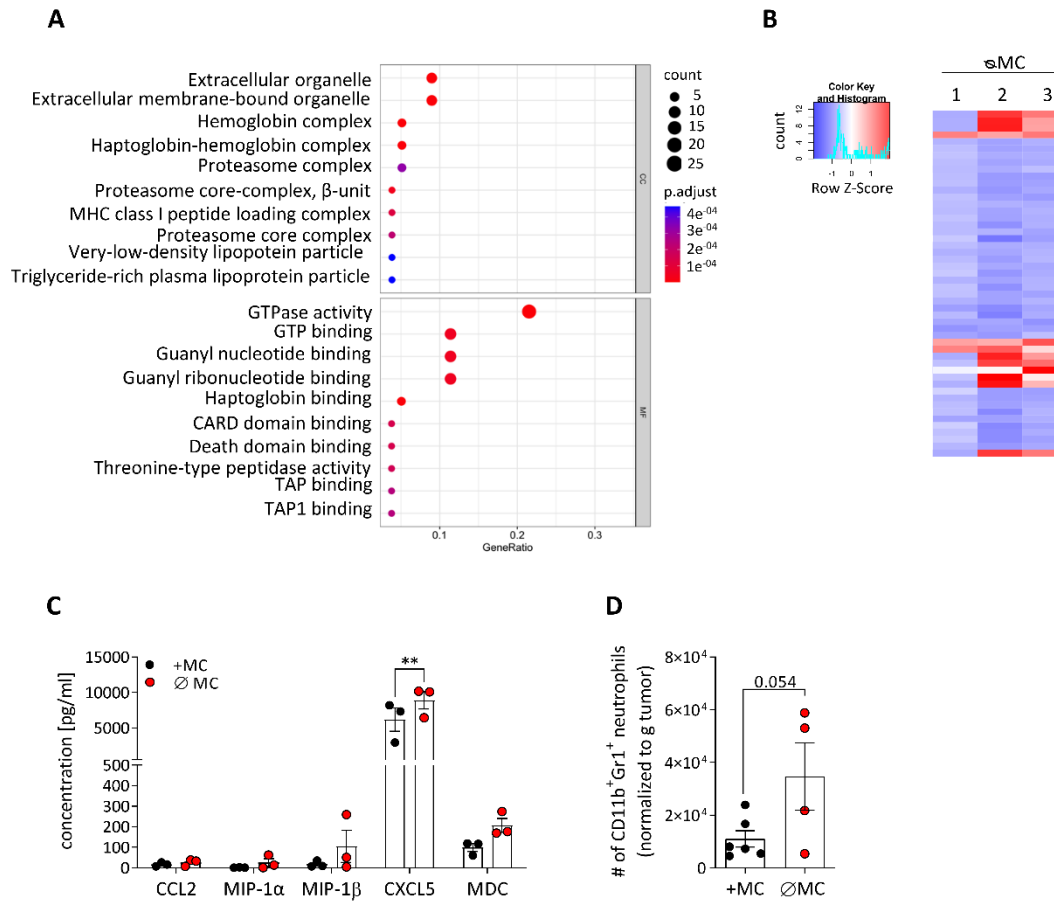


**Figure 18: Altered chemokine expression in tumor bearing mice**

(A) Gene ontology analysis of DEG from tumors from MC-deficient mice was performed. Top differentially expressed gene sets in cellular components (CC) and molecular function (MF). (B) Heatmap of top 50 differentially expressed genes in tumors from MC-deficient mice. Color gradient shows upregulated (red) and downregulated genes (blue). (C) Serum of MC-competent (+MC, black) and MC-deficient ( $\emptyset$ MC, red) mice was analyzed by ELISA. Significant differences in CXCL5 in MC-deficient ( $\emptyset$ MC, red) and (D) flow cytometry analysis of CD45.2<sup>+</sup>CD11b<sup>+</sup>Gr1<sup>+</sup> neutrophils normalized to gram tumor (n=4-6, mean with SEM, unpaired students t-test).

### 3.3.2.1 Loss of MC from the TME shows reduced recruitment of myeloid cells

Analysis of the TME by flow cytometry showed changes in the immune cell composition of lymphocytes between primary tumors from MC-competent and MC-deficient mice (Figure 17A). This data supports the findings from Chapter 3.2, which showed that MC were crucial for the recruitment of T cells (Figure 19B). Interestingly, however, in the absence of external stimuli to the TME, a significant decrease in the accumulation of CD11c<sup>+</sup> DC (Figure 19C, D) was found. Supportive of newest insights, tumors from MC-deficient mice showed a reduction in anti-tumoral cDC1 and a strong reduction in CD11b<sup>+</sup> cDC2 (Figure 19D) [192]. We also found a significant reduction in F4/80<sup>+</sup> macrophages in tumors of MC-deficient mice (Figure 19 E, F). Of note, no significant differences in CD206<sup>+</sup> M2-like or CD86<sup>+</sup> M1-like macrophages

were found between the groups suggesting that further markers are required to determine which sub-class of macrophages is indeed affected by the absence of MC (Figure 19F). Analysis of dLN showed a reduction in XCR1<sup>+</sup> cDC1s in MC-deficient mice (Figure 19G). Contrary to the common hypothesis, dLN from MC-deficient mice showed increased numbers of CD4<sup>+</sup> T cells (Figure 19H). This indicates an impaired trafficking of T cells and, thus a possible retention of T cells in the dLN. In conclusion, the absence of MC showed a shift in the immune composition in intradermal B16 tumors indicating that MC play an essential role in the development and recruitment of immune cells and, thus, in the progression of melanoma.

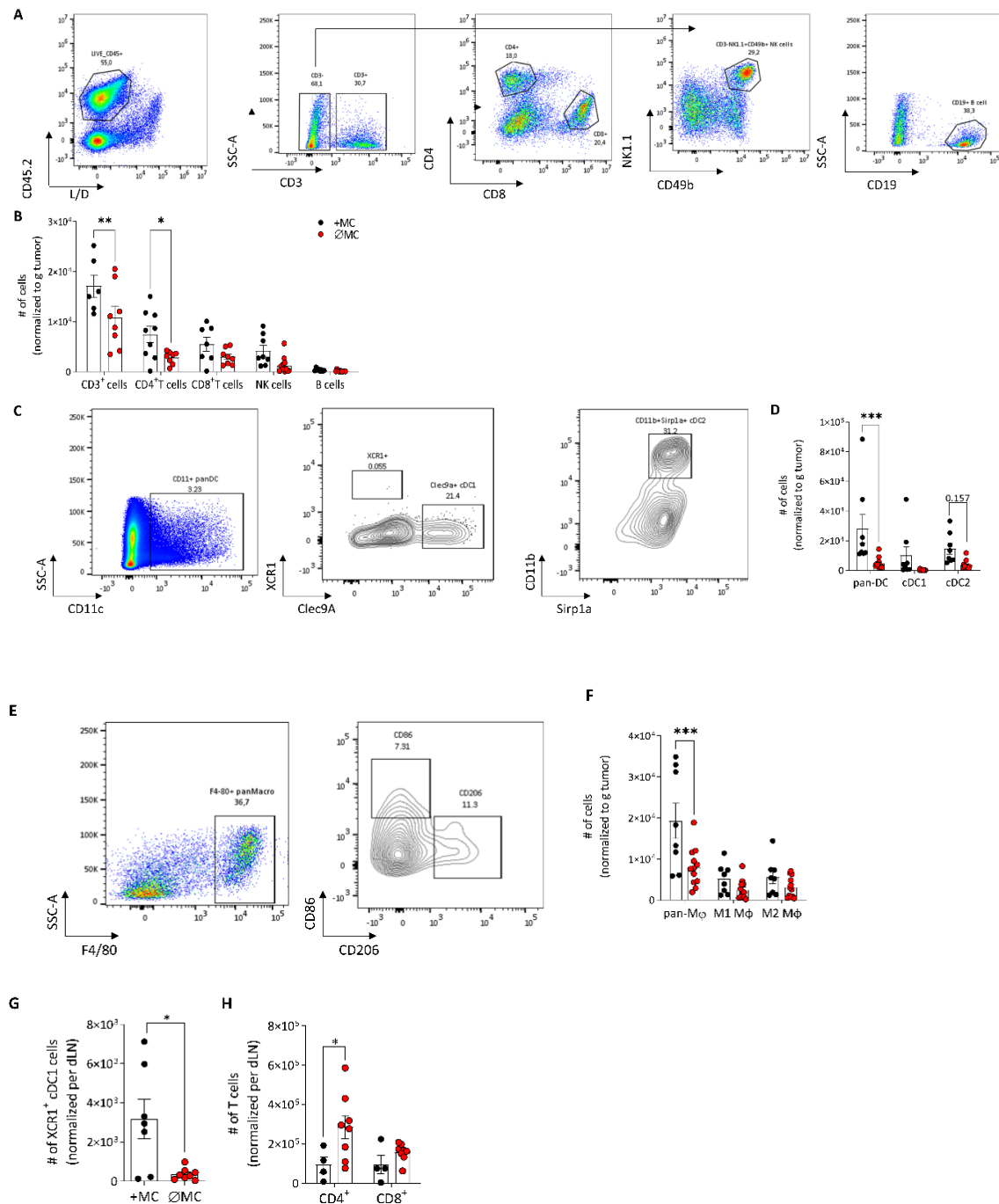


### Figure 19: Altered immune cell composition in tumors of MC-deficient mice

(A) Gating scheme used for the analysis of immune cells. (B) Flow cytometry analysis of tumors between MC-competent (+MC, black) and MC-deficient ( $\emptyset$ MC, red) mice in CD3<sup>+</sup> cells, CD3<sup>+</sup>CD4<sup>+</sup> T cells, CD3<sup>+</sup>CD8<sup>+</sup> T cells, CD3<sup>+</sup>NK1.1<sup>+</sup>CD49b<sup>+</sup> NK cells and CD3<sup>+</sup>CD19<sup>+</sup> B cells. (C) Representative gating scheme for DC. (D) Flow cytometry analysis of CD11c<sup>+</sup> DC and CD11c<sup>+</sup>CD11b<sup>+</sup> cDC2 and CD11c<sup>+</sup>Clec9a<sup>+</sup> cDC1. All cells were pre-gated on living<sup>+</sup>CD45.2<sup>+</sup> and shown as total cell number normalized to gram tumor. (E) Representative gating scheme for macrophages. (F) Flow cytometry analysis of F4/80<sup>+</sup> Macrophages and F4/80<sup>+</sup> CD86<sup>+</sup> M1-like macrophages and F4/80<sup>+</sup> CD206<sup>+</sup> M2-like macrophages. Cells were pre-gated on living CD45.2<sup>+</sup> cells and shown as total cell number normalized to gram tumor (n=7-12, mean with SEM, 2way ANOVA\*\*\*p<0.005). (G) Composition of dLN was analyzed by flow cytometry. Analysis of CD11c<sup>+</sup>Clec9a<sup>+</sup>XCR1<sup>+</sup> cDC1 and (H) CD3<sup>+</sup>CD4<sup>+</sup> T-helper cells and CD3<sup>+</sup>CD8<sup>+</sup> cytotoxic T cells. All cells were pre-gated on living CD45.2<sup>+</sup> cells and shown as total cell number normalized per dLN (n=4-8, mean with SEM, 2way ANOVA\*p<0.05).

#### 3.3.2.2 The role of DC and macrophages in metastasis formation

Based on the data presented, we hypothesize that MC recruit immune cells to the TME and conjointly inhibit lymph metastases, thus acting upstream of an immune cascade controlling melanoma growth and metastases. We showed in Chapter 3.3.2 that the absence of MC is sufficient for metastasis formation within only 16 days and that the reintroduction of MC into the TME can rescue mice from developing metastases as described above. To determine whether the hierarchical hypothesis is accurate, tumor progression and metastasis formation were monitored in four different mouse models: i) MC-competent mice (black), ii) MC-deficient mice (red), iii) Batf3KO mice, which lack CD8a<sup>+</sup> cDC1 as well as CD103<sup>+</sup> migratory cDC1 (green) and iv) mice treated with clodronate resulting in transient depletion of macrophages (and to some extent neutrophils) (blue) (Figure 20A). Interestingly, B16 tumors grew equally in MC-competent mice with and without clodronate treatment, while tumor growth in MC-competent mice lacking DC was comparable to that in MC-deficient mice (Figure 20B). Of note, the absence of DC or macrophages alone had no effect on the metastasis formation. Solely in the MC-deficient mice, metastasis in dLN and along the lymphatic vessels were detected (Figure 20C). Flow cytometry analysis of primary tumors from Batf3KO mice showed a reduced infiltration of CD45<sup>+</sup> immune cells to the TME (Figure 20D). The absence of DC consequentially also resulted in aberrant immune signaling, reducing the number of T-helper cells (CD4<sup>+</sup>), cytotoxic T cells (CD8<sup>+</sup>) and NK cells (NK1.1<sup>+</sup>CD9b<sup>+</sup>) (Figure 20F-G). Considering that tumors from MC-deficient mice are significantly larger and, therefore, might show more necrosis, a correlation between size of the tumor and the number of metastases was performed. No correlation between the size of the tumor and the amount of metastasis was found (Figure 20H). Interestingly however, in MC-deficient mice, a negative correlation was found between the total number of DC and macrophages and the number of metastases, indicating that with fewer myeloid cells there are more metastasis (Figure 20H).

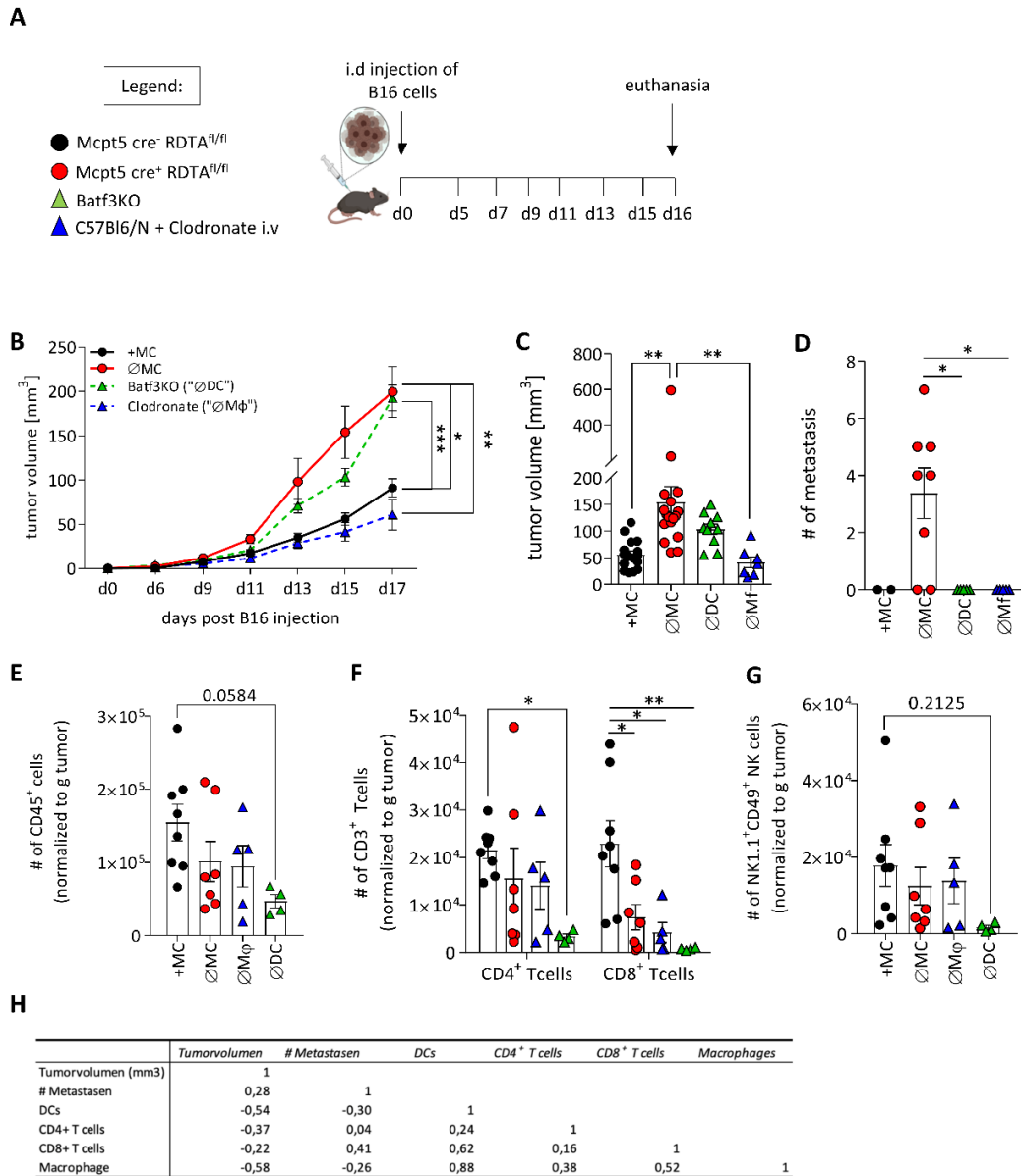


**Figure 20: Depletion of DC and macrophages does not impact metastasis formation**

(A) Schematic outline of the experimental setup. Back skin of MC-competent mice (+MC, black), MC-deficient mice (øMC, red), Batf3KO mice (øDC, green) and clodronate-treated mice (øMacrophages, blue) were injected intradermally with B16-OVA cells in the hind flanks. (B) Tumor volume was measured with a caliper and tumor size shown over 16 days (n=7-20, mean with SEM, 2way ANOVA, \*\*\*p<0.005; \*\*p<0.01; \*p<0.05). (C) End-point comparison of tumor volume in mm<sup>3</sup> at day 16 (n=7-20, mean with SEM, ordinary one-way ANOVA, \*\*p<0.01). (D) Quantification of visible metastasis (dLN and skin combined) in MC-competent (+MC, black), MC-deficient (øMC, red), Batf3KO mice (øDC, green) and clodronate-treated mice (ømacrophages, blue) mice (n=2-8, mean with SEM, ordinary one-way ANOVA, \*p<0.05). (E) TME composition of primary tumors was analyzed by flow cytometry. Differences in living CD45.2<sup>+</sup> cells (n=4-8, mean with SEM, ordinary one-way ANOVA) and (F) CD3<sup>+</sup>CD4<sup>+</sup> and CD3<sup>+</sup>CD8<sup>+</sup> T cells (n=4-8, mean with SEM, 2way ANOVA \*p<0.05, \*\*p<0.01) and (G) CD3<sup>+</sup>Nk1.1<sup>+</sup>CD49b<sup>+</sup> NK cells (n=4-8, mean with SEM, ordinary one-way ANOVA) and. All cells shown as total cell number normalized to gram tumor. (H) Pearson correlation analysis of immune cell infiltration, tumor volume (in mm<sup>3</sup>) and number of metastases. Pearson's r-values as indicated in the table.

### 3.3.2.3 MC repopulation of the skin completely abrogates metastasis formation

Metastasis formation was solely visible upon the lack of MC in our setting. To support the hypothesis that MC indeed mediates metastasis formation, the back skin of MC-deficient mice was reconstituted with in vitro generated BMDC six weeks prior to inoculation with B16 melanoma cells according to a well-established protocol (Figure 21A) [167]. Tumors that grew in skin reconstituted with MC had significantly reduced tumor volumes compared to MC-deficient mice (Figure 21B, C). Of note, no metastasis was detectable in tumor bearing mice from the group of mice reconstituted with MC, indicating that the re-introduction of MC into the skin can rescue the mice from developing metastases (Figure 21D). Further, analysis of the myeloid cell population within the primary tumors showed that the loss of both DC and macrophages was also rescued in mice reconstituted with MC (Figure 21E, F). Since MC inevitably hinder the formation of metastasis, it stands to reason that MC impact EMT. A variety of different epithelial-associated and mesenchymal-associated markers were analyzed by qPCR. The fold-change in mRNA levels was calculated between tumors from MC-deficient mice compared to MC-competent mice and between tumors from mice with reconstituted skin compared to MC-competent mice. Melanomas from MC-deficient mice compared to those from MC-competent mice showed a reduction in epithelial markers associated with cell junction, such as claudin-1, claudin-4 and occludin, while showing a significant upregulation in the mesenchymal marker N-cadherin (Figure 21G). Supportive of the hypothesis that MC are implicated in EMT, qPCR analysis of primary tumors from mice with skin reconstituted with MC showed an upregulation of epithelial markers compared to primary tumors from MC-competent mice, suggesting increased cellular junction and thereby retention of cancer cells at the primary site, as well as lower expression of mesenchymal markers, especially significantly lower fold change of N-cadherin (Figure 21G).

In conclusion, the MC-deficient *Mcpt5-cre-RDTA<sup>fl/fl</sup>* mice can be used as a new model to investigate the formation of lymphatic metastasis in melanoma.

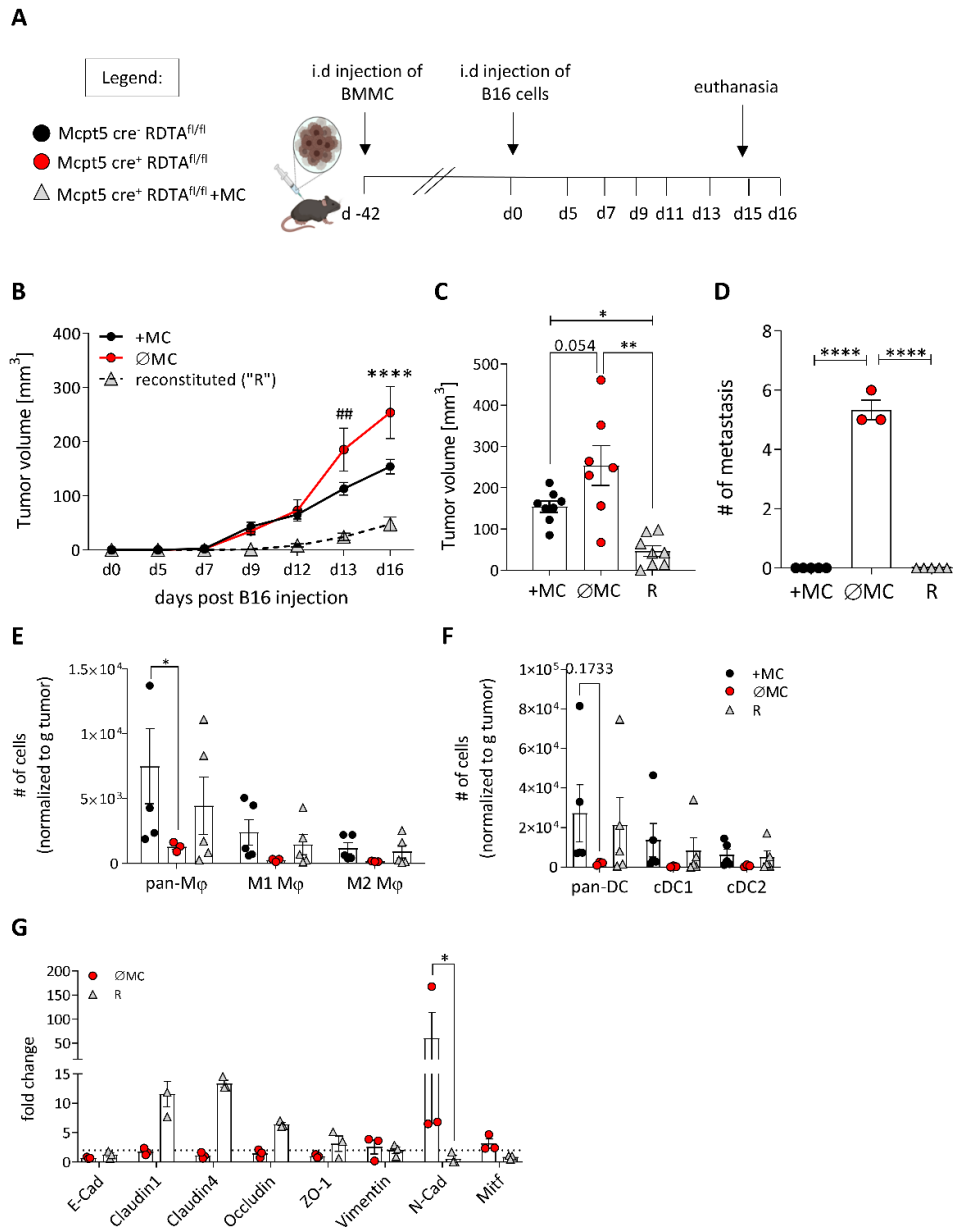


**Figure 21: MC-reconstitution of the skin rescues non-metastasis phenotype**

(A) Schematic representation of experimental set up. Back skin of Mcpt5-cre<sup>-</sup>-RDTA<sup>fl/fl</sup> mice were reconstituted with BMMC prior to B16 inoculation. Reconstituted mice (R, red), MC-competent mice (+MC, black) and MC-deficient mice (∅MC, red) were injected intradermally with B16-OVA cells in the hind flanks. (B) Tumor size in mm<sup>3</sup> shown over 16 days (n=7-10, mean with SEM, 2way ANOVA, \*\*\*p<0.005). (C) Endpoint comparison of tumor volume in mm<sup>3</sup> at day 16 between reconstituted (R, grey), MC-competent (+MC, black) and MC-deficient (∅MC, red) (n=7-10, mean with SEM, ordinary one-way ANOVA, \*\*p<0.01). (D) Quantification of visible metastases (dLN and skin) in reconstituted (R, grey), MC-competent (+MC, black) and MC-deficient (∅MC, red) mice (n=3-5, mean with SEM, unpaired students t-test, \*\*\*\*p<0.001). (E) TME immune cell composition of primary tumors was analyzed by flow cytometry. Differences in F4/80<sup>+</sup> macrophages, F4/80<sup>+</sup> CD86<sup>+</sup> M1-like macrophages and F4/80<sup>+</sup> CD206<sup>+</sup> M2-like macrophages and (F) CD11c<sup>+</sup> DC, CD11c<sup>+</sup> CD11b<sup>+</sup> cDC2 and CD11c<sup>+</sup> Clec9a<sup>+</sup> cDC1. All cells were pre-gated on living CD45.2<sup>+</sup> cells and shown as total cell number normalized to gram tumor (n=3-5, mean with SEM, 2way ANOVA \*p<0.05). (G) qPCR analysis of primary tumors from MC-deficient mice (red) and those mice reconstituted with MC (grey). Fold change of genes was normalized against primary tumors of MC-competent mice (n=3, mean with SEM, 2way ANOVA, \*p<0.05).

### **3.4 Distinct shift of T cell subtypes during cutAE in melanoma patients under ICI**

The data in Chapters 3.2 and 3.3 showed that MC are crucial for recruiting T cells to the TME of melanoma in a mouse model. Also, in humans, an accumulation of MC in areas of immune regression was shown in patients with melanoma, by us and others [99]. Immune checkpoint therapy (ICI) has revolutionized the treatment landscape for melanoma. This therapy harnesses the body's immune system by targeting specific checkpoint proteins, primarily CTLA-4 and PD-1/PD-L1, to enhance the immune response against cancer cells. During immune checkpoint therapy, blocking antibodies targeting checkpoint proteins like PD-1 or CTLA-4 aim to revitalize exhausted T cell responses against cancer cells [193]. These ICI have significantly improved overall survival and progression-free survival rates compared to traditional treatments. However, not all patients respond equally well, and some may experience irAE due to the activation of the immune system against healthy tissues resulting in autoimmune-like reactions [194]. Thus far, cutaneous adverse events (cutAE) have been briefly referred to as “rashes” but have not been investigated in more detail. Thus, we aimed to decipher immune mechanisms behind cutAE in melanoma patients undergoing ICI.

#### **3.4.1 Clinical characteristics of the patient cohort**

Between September 2018 and October 2019, thirty patients (12 females and 18 males) with stage III/IV malignant melanoma were enrolled in this study with a mean age of 66.6 ( $\pm$ 13.3) years. Detailed clinical characteristics are summarized in Table 12. The majority of 20 patients were treatment naïve prior to ICI. The other 10 patients received pre-treatment with targeted therapy (BRAF/MEK inhibition), interferon alpha, radiotherapy or a combination which was followed by disease progression. One patient also received three chemotherapy cycles with dacarbazine followed by targeted therapy. BRAF V600E (13 patients), BRAF V600K (three patients) and BRAF G466E (one patient) mutations were detected. PD-L1 as a potential biomarker for ICI responsiveness was expressed by at least 2% of tumor cells in 12 patients, while tumor cells of six patients were negative for PD-L1. In five patients, the PD-L1 expression status was unknown. The schematic outline of the study setup is depicted in Figure 21A. From each melanoma patient willing to participate in the study blood samples were taken. The first sample was taken before initiation of ICI, to determine the pre-therapeutic levels of immune cells and cytokines as a baseline reference. At the onset of a cutAE, another sample was taken. The last blood sample was taken six months after initiation of therapy to determine the effects of ICI on immune cells (Figure 22A). Eight patients received ipilimumab/nivolumab combination therapy, fourteen patients were treated with anti-PD-1 monotherapy in an adjuvant and

eight in a therapeutic setting. The clinical response of the patients to ICI was determined and the cohort stratified into responders and non-responders post-hoc. In patients receiving adjuvant treatment complete response was achieved in four patients; in patients receiving therapeutic treatment, nine patients were tumor-free, and two patients showed a partial response. These patients were summarized as responders. Fifteen patients showed progressive disease (five in the adjuvant anti-PD-1 monotherapy setting), defined as non-responders. Within the monitoring time, cutAE occurred in twelve patients (43%). Of these, eight patients solely developed cutAE; in four patients, both skin and gut were affected, with colitis symptoms parallel to the cutAE. One patient only presented with colitis. The observed severity of colitis varied between mild to severe (grade 1-3 according to Common Terminology Criteria for Adverse Events, CTCAE v5.0), leading to discontinuation of ICI therapy in 3 cases. The patients with moderate and severe colitis were treated with systemic corticosteroids, and one severe course resulted in additional treatment with TNF- $\alpha$  inhibitor. All cutAE were mild or moderate (grade 1 or 2) and were treated exclusively with topical steroids and oral antihistamines. We observed three cases each of urticaria, acantholytic dermatosis and maculopapular exanthema and two cases of lichenoid dermatitis and psoriasis each.

To understand immune alterations in ICI-treated patients, PBMC were analyzed by flow cytometry and plasma levels of cytokines were determined. The group of melanoma patients before treatment showed more CD4<sup>+</sup>CCR3<sup>+</sup>CCR8<sup>+</sup> cells (Th2 cells) compared to CD4<sup>+</sup>CXCR3<sup>+</sup> cells (Th1 cells). This shifted towards a Th1-dominated immune profile under ICI (Figure 22B-C). Th1 cytokines are believed to play a major role in the initiation of an anti-tumor immune response. Interestingly, an increase in serum level concentrations of both IFN- $\gamma$  and TNF- $\alpha$  was observed over the course of ICI for a subset of patients (Figure 22D, E).

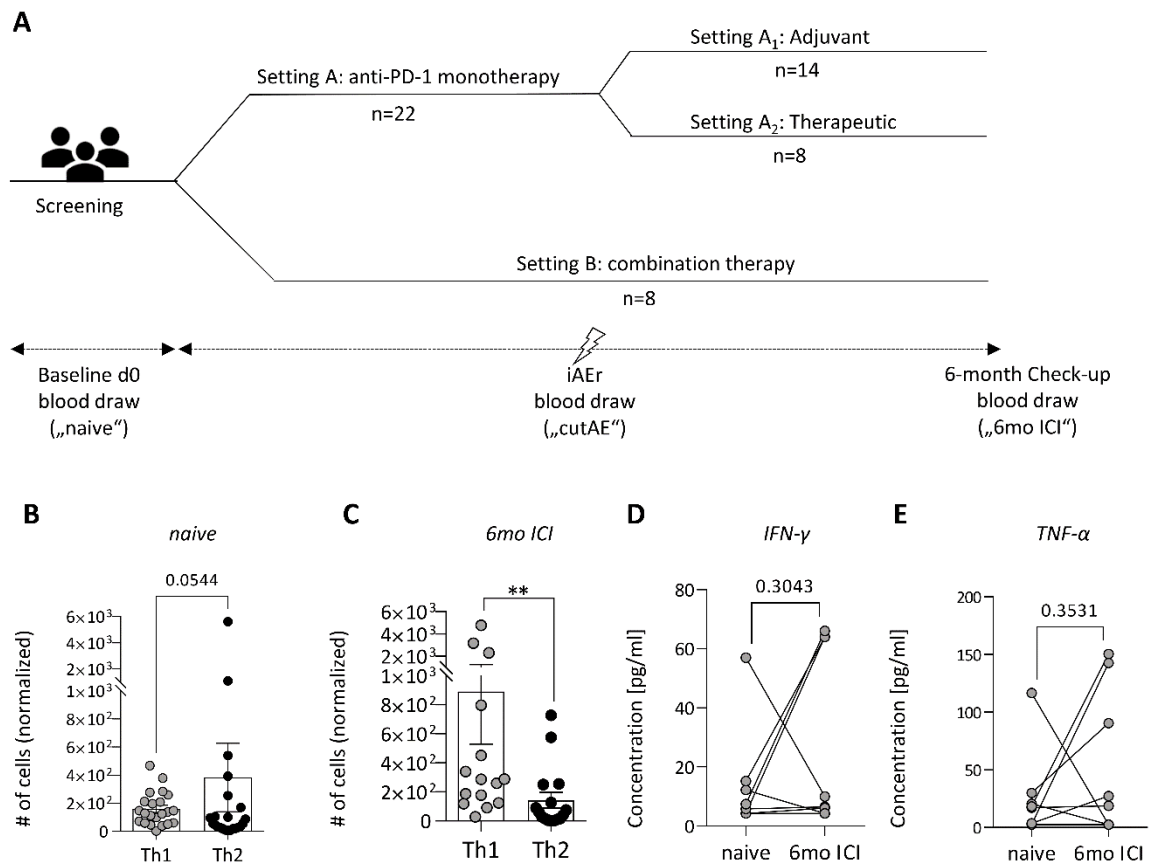


**Figure 22: Study design and Th1/Th2 immune profile of patients**

(A) Clinical Study Design (B) Th1 and Th2 cells in melanoma patients' PBMCs prior to ICI (naïve) and (C) after 6 months of treatment (6mo ICI) was analyzed by flow cytometry (n= 14, mean with SEM, students t-test with Mann-Whitney correction, \*\* $p < 0.01$ ). (D) Serum levels of Th1-associated cytokines IFN- $\gamma$  and (E) TNF- $\alpha$  over the course of ICI. (n=15, student's paired t test)

**Table 12:** Clinical characteristics of melanoma patients included in this study

Patient	Gender/ Age <sup>a</sup>	Melanoma Subtype/ Site/Breslow in mm <sup>b</sup>	BRAF/ PD-L1 <sup>c</sup>	Involved Sites <sup>d</sup>	Pre-Treatment <sup>e</sup>	Treatment Group <sup>f</sup>	Response <sup>g</sup>	irAE <sup>h</sup>	c-irAE <sup>i</sup>	irAE Grade <sup>k</sup>
1	83/F	snSSM/ T/ 1.1	V600E/unk	CUT	none	PD1-a	R	cut	L	1
2	80/M	NM/ HN/ 1.9	WT/7%	LN	none	PD1-a	R	cut	G	1
3	81/F	NM/ UE/ 6.8	WT/2%	CUT, LN	none	PD1-t	R	col		3
4	39/M	NM/ AN/ >8	V600E/<1%	LN	none	PD1-a	R	none		
5	57/M	uNM/ T/ 2.1	V600K/1%	LN	none	PD1-a	R	none		
6	66/M	unk/ T/ 1	WT/<1%	LN, PUL, ST	none	combi	NR	cut	G	1
7	65/M	uNM/ HN/ 1.9	G466E/2%	CUT, LN	none	combi	R	cut/col	P	1 / 2
8	38/M	unk/ UE/ 7	V600E/unk	LN, ST, PUL, HEP, OSS, CUT	DTIC, TT	combi	NR	none		
9	81/M	unk/ LE/ >8	WT/0%	LN, OSS	none	PD1-t	NR	none		
10	77/F	snSSM/ LE/ 1.6	V600K/15%	CUT, LN, ADR, INT	RT, TT	PD1-t	NR	none		
11	68/M	unk/ T/ >8	V600E/2%	LN, CUT, HEP, OSS	none	PD1-a	NR	none		
12	64/F	unk/ T/ 0.7	V600E/6%	LN, PUL	TT	PD1-t	R	none		
13	62/F	ALM/ UE/ 8	V600E/2%	LN	IFN	PD1-a	NR	none		
14	62/M	PM/ T/ >8	V600E/0%	ST, HEP, ADR, PAN, LN, OSS	TT	combi	NR	cut	E	2
15	88/F	uALM/ UE/ >8	WT/<1%	LN, ADR	RT	PD1-t	R	none		
16	78/M	LMM/ HN/ 0.7	V600K/2%	LN, SC	none	PD1-t	NR	none		
17	48/M	ALM/ UE/ 2.1	V600E/20%	LN, CUT	none	PD1-t	NR	none		
18	59/F	ALM/ UE/ 4.9	WT/unk	CUT	none	PD1-a	NR	none		
19	62/M	uNM/ UE/ 2.5	WT/1%	CUT	none	PD1-a	R	cut	E	1
20	81/M	unk/ T/ 2	WT/unk	SC, LN, PUL	RT, IFN	PD1-t	R	cut	U	1
21	77/M	uNM/ UE/ >8	WT/0%	LN	none	combi	NR	cut/col	G	1 / 2
22	51/F	SSM/ T/ 1.1	V600E/unk	LN	IFN	PD1-a	R	cut	U	1
23	64/M	SSM/ T/ 2	WT/0%	LN	none	PD1-a	R	none		
24	51/F	SSM/ HN/ 1.5	V600E/<1%	LN, SC, ADR, BIL, OSS, ST	IFN	combi	NR	none		
25	84/M	snSSM/ T/ >8	WT/2%	PUL	none	combi	NR	none		
26	59/F	NM/ T/ >8	V600E/<1%	LN	none	PD1-a	NR	cut/col	L	1 / 1
27	76/M	uNM/ T/ 4.9	WT/0%	LN	none	PD1-a	R	none		
28	74/M	NM/ T/ 1.3	V600E/30%	LN	none	PD1-a	NR	none		
29	55/F	NM/ UE/ 1.2	V600E/0%	LN, CUT, PUL, CER	IFN	combi	R	cut/col	U, E	2 / 3
30	68/F	uNM/ T/ 3.2	WT/60%	LN	none	PD1-a	R	cut	P	1

<sup>a</sup> gender female (F) or male (M); patients' age at time of study inclusion. <sup>b</sup>melanoma subtype: ulcerated (u), secondary nodular (sn), superficial spreading melanoma (SSM), nodular melanoma (NM), acral lentiginous melanoma (ALM), lentigo maligna melanoma (LMM), polypoid melanoma (PM), subtype unknown (unk); site of primary: head and neck (HN), upper extremities (UE), torso (T), lower extremities (LE), anal (AN); Breslow thickness in mm. <sup>c</sup>BRAF mutation (V600E, V600K, G466E) or wild type (WT); PD-L1 positivity expressed through tumor proportion score. <sup>d</sup>in metastasis involved sites: adrenal (ADR), gallbladder/bile (BIL), cerebral (CER), cutaneous (CUT), hepatic (HEP), intestinal (INT), lymph node (LN), skeletal (OSS), pancreatic (PAN), pulmonary (PUL), soft tissue (ST), subcutaneous (SC). <sup>e</sup>pre-treatment: targeted therapy with BRAF(MEK-inhibitors (TT), radiotherapy (RT), interferon- $\alpha$  (IFN), dacarbazine (DTIC). <sup>f</sup>treatment group: PD1 monotherapy in adjuvant setting (PD1-a), PD1 monotherapy in therapeutic setting (PD1-t), ipilimumab/nivolumab combination therapy (combi). <sup>g</sup>Response: responder (R: no evidence of disease in adjuvant setting; complete response and partial response in therapeutic setting), non-responder (NR: progressive disease). <sup>h</sup>immune related adverse events affecting skin and/or mucous membrane: cutaneous (cut), colitis (col). <sup>i</sup>subtype of cutaneous immune related adverse event: lichenoid (L), exanthema (E), urticaria (U), psoriasis (P), Grover's disease (G). <sup>k</sup>grade of mucocutaneous immune-related adverse events according to CTCAE v5.0 (G1-5)

### 3.4.2 Shift towards Th1 cells in PBMC during ICI is not associated with a favorable clinical response

Since we observed a shift towards Th1 cells in PBMC upon ICI, we next wondered if the shift towards a Th1 profile is detectable more or less in anti-PD1 monotherapy and anti-PD1/anti-CTLA4 combination therapy, as well as responders vs. non-responders. Anti-PD1- monotherapy restored immune responses, which was reflected by an increase in Th1 cells in the peripheral blood of melanoma patients over the course of six months of treatment, which was not observed in the four patients receiving combination therapy with ipilimumab (anti-CTLA4) (Figure 23A). Patients under combination therapy had a 10-fold lower number of Th1 cells than those with monotherapy (Figure 23B). Th2 cells carrying the skin-homing receptor cutaneous lymphocyte-associated antigen (CLA) are a subset of memory T cells which are functionally related to skin physiology. CLA<sup>+</sup> Th1 cells are known to re-circulate between the blood and skin during cutaneous inflammation [195]. Interestingly, we found significantly more CLA<sup>+</sup> Th1 cells in the blood of patients receiving monotherapy compared to patients receiving combination therapy (Figure 23C, D). There was no significant difference between responders and non-responders in the number of Th1 cells, nor in CLA<sup>+</sup> Th1 cells (Figure 23E, F).

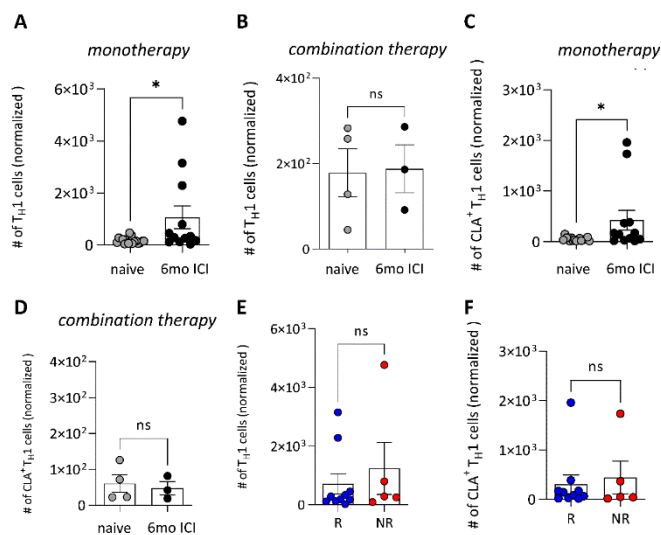


**Figure 23: Shift towards Th1 cells in PBMC during ICI**

T cell subsets in patient's blood were analyzed by flow cytometry to define CD3<sup>+</sup>CD4<sup>+</sup>CXCR3<sup>+</sup> Th1 cell numbers in patients receiving (A) anti-PD1 monotherapy (n=17, mean with SEM, unpaired t-test with Welch's correction) or (B) anti-PD1/anti-CTLA4 combination therapy (n=3-4, mean with SEM, unpaired t-test with Welch's correction). (C) CD3<sup>+</sup>CD4<sup>+</sup>CXCR3<sup>+</sup> CLA<sup>+</sup> skin-homing Th1 cells were analyzed in patients receiving anti-PD1 monotherapy (n=22, mean with SEM, Mann-Whitney test, \* p>0.05) or (D) anti-PD1/anti-CTLA4 combination therapy (n=3-4, mean with SEM, unpaired t-test with Welch's correction). (E) Comparison of Th1 cells between responders (R, blue) and non-responders (NR, red) and (F) CD3<sup>+</sup>CD4<sup>+</sup>CXCR3<sup>+</sup> CLA<sup>+</sup> skin-homing Th1 cells between responders (R, blue) and non-responders (NR, red) (n=5-9, mean with SEM, unpaired t-test with Welch's correction).

### 3.4.3 cutAE show a Th17/Th22-related immune profile

Next, we explored changes in plasma levels of inflammatory cytokines during episode of cutAE to determine potential biomarkers of cutAE during ICI therapy. As was expected, baseline levels prior to ICI showed low concentrations of inflammatory cytokines (Figure 24A). During the acute phase of a cutAE however, an increase in plasma level concentrations for all cytokines was measured. Especially IL-1 $\beta$  (p=0.09), IL-18 (p<0.001) and IL-23 (p=0.17) were elevated in the plasma of patients during an cutAE. While cytokine levels in general fell back to baseline levels over the course of therapy, IL-18 levels remained high for the remaining study duration showing a 3-fold higher concentration than in the naïve state (Figure 24A). The cytokine IL-23 is a key mediator of the IL-23/IL-17 pathway and is central in some inflammatory skin diseases such as psoriasis [196]. Many of the cytokines elevated in the plasma of patients during cutAE are known for being associated with the development and expansion of Th17 cells, making the Th17/Th22 pathway a logical player involved during cutAE. In line with this, the patient cohort showed a significant increase in CD3<sup>+</sup>CD4<sup>+</sup>CCR4<sup>+</sup>CCR6<sup>+</sup> Th17 cells during an acute cutAE (Figure 24B). 4 out of 7 patients also showed a trend for an increase of the associated pro-inflammatory cytokines IL-17A and IL-8 during cutAE in the plasma of patients, while the remaining three patients showed steady levels of cytokines over time (Figure 24C, D). This difference was not as substantial for CD3<sup>+</sup>CD4<sup>+</sup>CCR10<sup>+</sup> Th22 cells, although responders showed a trend towards higher numbers of Th22 cells in the peripheral blood during an acute cutAE, maintaining this level during therapy (Figure 24E). This difference was also backed up by higher serum levels of IL-22, which were four times higher in responders than non-responders (Figure 24F).

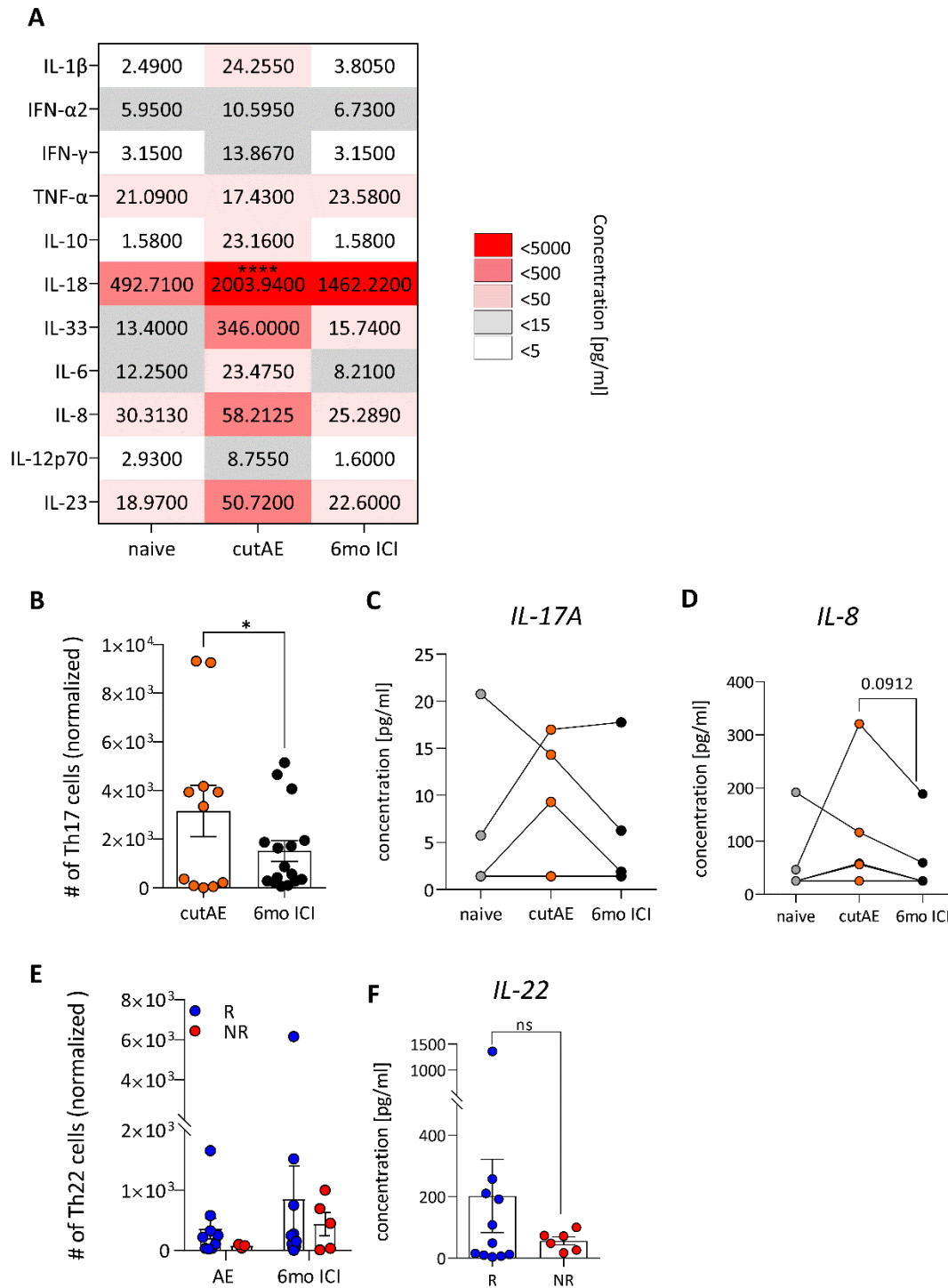


**Figure 24: cutAE show a Th17/Th22-related immune profile**

(A) Cytokines in the plasma of patients were measured with an enzyme-linked immunosorbent assay before ICI (“naïve”), during a cutAE and after 6 months of therapy (“6mo ICI”). Heatmap representation of median concentrations given in pg/mL. Color gradient is depicted from 0–5000 pg/mL. (B) Flow cytometry analysis of PBMCs for CD3<sup>+</sup>CD4<sup>+</sup>CCR4<sup>+</sup>CCR6<sup>+</sup> Th17 cells (n=10, mean with SEM, paired t-test, \* p>0.05). Plasma level analysis of (C) IL-17A and (D) IL-8 in patients (n=7, paired t-test). (E) Flow cytometry analysis of PBMCs for CD3<sup>+</sup>CD4<sup>+</sup>CCR10<sup>+</sup> Th22 cells in responders (R, blue) and non-responders (NR, red) (n=30, mean with SEM, 2way ANOVA). (F) Plasma levels of IL-22 between responders (R, blue) and non-responders (NR, red) (n=17, mean with SEM, unpaired t test).

### 3.4.4 Plasma levels of IL-10 is associated with cutAE and response to ICI

One of the aims of this study was to investigate in more detail the underlying immunological differences between various cutAE. Therefore, at the onset of cutAE, patients were grouped based on the clinical manifestation, namely T-cell mediated maculopapular exanthema, lichenoid dermatitis, acantholytic dermatosis and mast cell-driven urticaria. Immune signatures of plasma inflammatory cytokines were compared between the different clinical manifestations. Comparing the different skin inflammatory diseases showed significantly increased concentrations of IL-18, especially in patients diagnosed with urticaria (Figure 25A). IL-18 is released by cells upon the activation of the inflammasome [197]. It is known that IL-18 activates MC and can lead to the formation of mucosal mastocytosis [198]. Furthermore, MC play a key role in inflammatory bowel diseases, such as Morbus Crohn and ulcerative colitis [199]. To determine whether MC-dependent adverse events have similar underlying immune mechanisms, we compared the plasma levels of IL-18 with cT-cell-driven cutAE and colitis. Interestingly, it became apparent that the cytokine inflammatory profile of urticaria resembles that of colitis (Figure 25B).

IL-18 belongs to the IL-1 family. Other members involve the cytokines IL-1 $\beta$  and IL-33. Interestingly, while the inflammasome-related cytokine IL-1 $\beta$  was also significantly upregulated in patients with urticaria, the plasma levels of the alarmin IL-33 were comparable between all cutAE (Figure 25A). As shown in Figure 23B, patients during a cutAE show a dominance in Th17 cells. The highest level of the pro-inflammatory Th17 cytokine IL-23 was detected in maculopapular exanthema, while acantholytic dermatosis was significantly reduced compared to maculopapular exanthema (Figure 25C).

IL-10 is a potent anti-inflammatory cytokine, which can be produced by many cell types including melanoma cells and Tregs, thereby playing an essential role in dampening the immune responses and inhibiting pro-inflammatory signals [200, 201]. In our cohort, plasma levels of IL-10 were elevated during a cutAE (Figure 25D), which may reflect a counter-regulation against the skin inflammation associated with cutAE. Unexpectedly, however, the concentration level of IL-10 during a cutAE was significantly higher in non-responders compared to responders, potentially because the immune system is inhibited by IL-10 (Figure 25E). Patients might be predisposed to get cutaneous inflammation, as baseline IL-10 levels tended to be lower in patients that later developed cutAE (Figure 25F). Patients were grouped into IL-10 high and IL-10 low, based on their baseline IL-10 levels measured before initiation of ICI, with a plasma concentration >1.58 pg/ml being considered high. This predisposition is also seen in patients with high baseline IL-10 before ICI, as IL-10 levels were still increased upon appearance of

cutAE and at 6-month follow-up (Figure 25G). High levels of IL-10 in patients before ICI correlated negatively with the response to therapy ( $p < 0.09$ ), supporting that a pre-existing pro-tumoral immune environment influence the outcome of therapy (Figure 25H).

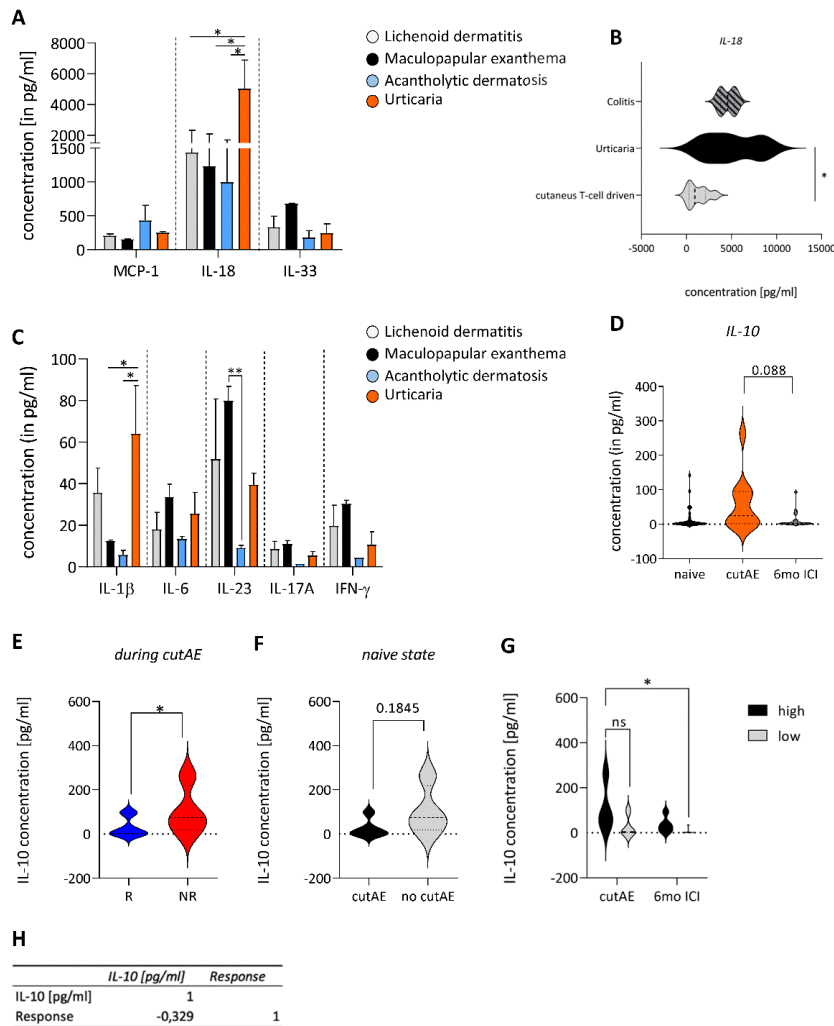


**Figure 25: IL-10 as prognostic marker.**

(A) Serum levels of inflammation-associated cytokines MCP-1 (CCL22), IL-18 and IL-33 in different subtypes of cutAE (lichenoid dermatitis=grey, maculopapular exanthema=black, acantholytic dermatosis=blue and urticaria=orange) ( $n = 2-3$ , mean with SEM, 2way ANOVA, \*\*  $p < 0.01$ ; \*\*\*  $p < 0.005$ ). (B) Serum levels of IL-18 in T-cell driven cutAE compared (light grey) compared to MC-driven urticaria (black) and gastric colitis (striped) ( $n = 2-3$ , mean with SEM, 2way ANOVA, \*  $p < 0.05$ ). (C) Serum levels of Th17-associated cytokines IL-1 $\beta$ , IL-6, IL-23, IL-17A and IFN- $\gamma$  in different subtypes of cutAE (lichenoid dermatitis=grey, maculopapular exanthema=black, acantholytic dermatosis=blue and urticaria=orange) ( $n = 2-3$ , mean with SEM, 2way ANOVA, \*  $p < 0.05$ ). (D) High serum IL-10 in patients during cutAE ( $n = 24$ , mean with SEM, paired t-test with Wilcoxon correction, ns). (E) Higher serum IL-10 levels in non-responding patients during AE ( $n = 11$ , mean with SEM, unpaired t test, \*  $p < 0.05$ ). (F) High serum levels of IL-10 in patients during ICI that develop cutAE as compared to patients not developing cutAE during ICI (ns). (G) Naive patients were grouped in IL-10<sup>high</sup> and IL-10<sup>low</sup> patients and the development of IL-10 in the serum analyzed during ICI. Naive IL-10<sup>high</sup> patients show a higher increase of IL-10 during a cutAE ( $n = 11$ , mean with SEM, 2way ANOVA, \*  $p < 0.05$ ). (H) Pearson correlation analysis of baseline IL-10 levels (in pg/ml) and response. Pearson's r-values as indicated in the table ( $p < 0.09$ ).

## 4. Discussion

### 4.1 Fetal Tissue-derived MC as experimental surrogate for in vitro CTMC

The intricate biology and versatile functions of MC have interested researchers for years, as they play a multifaceted role in health and disease. With their remarkable plasticity, MC can serve as direct effectors or orchestrate the recruitment of innate and adaptive immune cells to modulate immune responses. Extensive research has highlighted MC as indispensable in allergic reactions, autoimmune inflammation, and cancer [81, 202]. Notably, our recent publication unveiled an anti-tumorigenic role of MC in melanoma, which secreted the tumor-attracting chemokine CXCL10 upon activation with the TLR4 agonist LPS [99]. As a result, interest in MC continues to surge, encompassing comprehensive in vitro and in vivo analyses.

Given the challenges in obtaining primary MC in large quantities, generating MC in vitro has become a widely accepted approach. In murine investigations, conventional BM cells serve as the foundation for these cultures, yielding abundant MC populations that mimic critical characteristics of bona fide MC. Nonetheless, these in vitro-generated MC only mimic mature tissue-specific MC to a certain extent due to inherent limitations [47]. Recent investigations employing single-cell sequencing methods have unraveled the lineage tracing of MC, confirming the presence of MC progenitors in fetal tissues and revealing that a significant portion of MC does not originate from the BM as previously thought but from the yolk sac [2]. Therefore, MC derived from fetal liver and fetal skin have been introduced as an alternative surrogate for in vitro experimentation. Based on this, a direct comparison of BMMC, FSMC, and FLMC was performed in Chapter 3.1 to determine the most compatible surrogate for CTMC for in vitro analysis.

Several culture conditions under which BMMC are generated are used in different labs, with varying FCS concentrations and with or without SCF in the medium [203-205]. However, our data demonstrate that only the culture in a complete MC medium containing FCS, SCF, and IL-3 is sufficient for generating mature MC expressing FcεRI and CD117. The cultivation of BM cells in a medium containing only IL-3 generates cells that are FcεRI<sup>+</sup>CD117<sup>-</sup>, which instead mimic basophils, which in vitro can undergo similar reactions to MC, thereby falsifying the data. The importance of IL-3 and SCF in the culture of MC is also supported by another group, which further identified the lack of SCF as favorable for the generation of basophils [206]. SCF is essential in generating MC from BM and maintaining mature MC in culture, and depriving mature MC of SCF results in the downregulation of FcεRI as early as 12 hours after deprivation. Mature MC can be generated from all three tissues, while FSMC resemble mature CTMC the

closest based on histological morphology and expression of surface markers. Even though BMMC generates the highest yield, resulting from the increased proliferation rate. Nonetheless, the yield of FLMC and FSMC are sufficient for repetitive in vitro experiments.

#### **4.1.1 Different functionalities of MC types are based on transcriptional heterogeneity**

Due to the IgE-dependent pathway, MC are primarily investigated in immediate type I allergic reactions, making this an important aspect to compare between the different MC types [207]. Functional analysis of IgE-crosslinking of the FcεRI receptor was performed by measuring the intracellular Ca<sup>2+</sup> influx before and after DNP-HSA addition, which revealed unequivocal immediate Ca<sup>2+</sup>-influx for all three MC types. Strikingly, however, significant differences in mRNA expression of *Hdc*, the gene for histidine decarboxylase, and *Tpsb2*, the gene encoding for MC-tryptase, were observed in steady-state FSMC. This difference also has experimental relevance, as electron microscopy showed significantly larger granules in the cells, resulting in a considerable difference in histamine release from FSMC upon IgE-crosslinking of the FcεRI receptor (Figure 9). This difference must be considered when the field of research is linked to the IgE-functionality of MC and the histamine release. More potent and subtle differences in FcεRI receptor pathway analysis can be evaluated when working with FSMC instead of BMMC. Supportive of this, transcriptome analysis revealed a higher fold change of mRNA levels of *mrgprb2* (the mouse equivalent of *mrgprx2*) in both fetus-derived MC, making them invaluable tools for investigating MC roles in skin-related ailments such as atopic dermatitis, allergic contact dermatitis, and urticaria [208].

Due to the sentinel function of MC, research relating to TLR-stimulation of MC and host defense against pathogens is also a common research field [209, 210]. qPCR analysis of the TLR profile of each MC type showed differences in ct value for the receptors TLR1, TLR2, and TLR4. The ct value is inversely proportional to the amount of target nucleic acid in the sample, so the lower the ct value, the higher the amount of the target gene. This means that FLMC have higher mRNA levels for TLR1, TLR2, and TLR4. Interestingly, after stimulating MC from all three tissue origins with TLR agonists, BMMC and FLMC showed comparable responsiveness upon stimulation with Pam3Cys (TLR1/2), Pam2Cys (TLR2/6), and LPS (TLR4).

Interestingly, in a proteomic analysis of human MC, a lack of innate immune sensors, including TLR4, was detected [74]. Further, the relative expression of IL-6 in resting murine BMMC was also reported to be greater than human cord-blood-derived MC [211]. FSMC exhibited the lowest IL-6 secretion into the supernatant upon innate stimulation, significantly lower when stimulated with LPS. A possible reason for this might be the decreased fold change of mRNA for

*s100a8* and *s100a9* found in (Figure 10). S100A8/A9 is an endogenous ligand for TLR4 and is implicated in the pathogenesis of inflammatory disorders.

Interestingly, S100a8 diminished MC degranulation and produced IL-6 and IL-4 cytokines in response to IgE crosslinking in vitro [212]. This data suggests that FSMC might be more closely related to human MC, offering a more suitable surrogate when generating research with translational relevance. Overall, FSMC responded weaker towards stimulation with LPS and MDP, which targets the NOD receptor, as only a few cytokines could be detected in the supernatant of FSMC compared to BMMC.

Another sentinel function of MC is the response to danger signals. MC, ILC2, and Tregs are immune cells that constitutively express the ST2 receptor on their cell surface, allowing them to respond to the alarmin IL-33 [59]. While all three MC types express ST2 on the cell surface, fetal tissue-derived MC have a reduced expression. Interestingly, this difference is only apparent in FLMC upon stimulation with IL-33. Analysis of the BMMC and FSMC supernatants showed similar cytokine secretion levels. A summary of the differences between BMMC, FLMC, and FSMC is depicted in Table 13. The summary indicates that the primary features, including histological staining and protease content, align with CTMC [21, 213]. Our findings indicate that FSMC exhibits the highest level of maturity, which is reasonable given that these cells have already been subjected to the skin's external environment.

**Table 13:** Summarized data of MC surrogate characteristics

	<b>BMMC</b>	<b>FLMC</b>	<b>FSMC</b>
<b>Histology:</b>			
Alcian blue/safranin staining	Blue	Blue/Red	Red
Toluidine staining	Violet	Violet	Violet
<b>Granule Content:</b>			
Granules	+	++	+++
Histamine content	+	++	+++
Proteases	Mcpt4-9, Cpa3	Mcpt4-9, Cpa3	Mcpt4-9, Cpa3
Degranulation by IgE	+++	+++	+++
<b>Expression Profile:</b>			
TLRs	TLR1-4 & 6-9	TLR1-4 & 6-9	TLR1-4 & 6-9
CD45	+	+	+
CD117	+	+	+
FcεRI	+	+	+
ST2	++	+	++
<b>Cytokine secretion upon:</b>			
LPS stimulation	+++	++	+
IL-33 stimulation	+++	+	+++

MC are known to be tissue-resident and achieve their final tissue-specific maturation state based on environmental factors, such as cytokines and transcription factors. Therefore, MC heterogeneity results from the microenvironment, which educates the cells. Consequently, the effector functions of MCs differ depending on the tissue in which the cell matures and differentiates [21, 203, 214]. Hence, the functional roles of MCs exhibit variation contingent upon the specific tissue where their maturation and differentiation occur. In conclusion, the data described in Chapter 3.1 underlines the disparities among MC generated in vitro from distinct tissues, necessitating careful consideration, particularly in studying MC immune functions. Overall, differences in maturity and responsiveness were determined between the MC types, with FSMC resembling mature CTMC the closets. This indicates that there is already an imprinting of the precursor cells for MC in fetal tissues that remains effective even during in vitro cultivation. Thus, the tissue of origin imprints MC precursor cells so that these cells, despite identical culture conditions and consecutive equal surface expression of CD117 and FcεRI, acquire distinct phenotypes and signatures.

#### **4.1.2 Limitations of the study**

Most of the experiments conducted within this study were executed using biological triplicates, ensuring the mitigation of any potential batch effects. However, limitations to this study are the need for more appropriate controls. To determine whether the generated MC types do resemble mature CTMC, a positive and negative control would have been necessary. As a positive control, mature CTMC from murine skin would have been essential, as this is the desired cell type for which an appropriate surrogate was searched. CTMC from human skin would have been interesting; however as existing data suggest, the genetic overlap between murine and human MC are limited. Since the MC types were excluded as MMC, a comparison with peritoneal derived MC would have further supported the claims. Overall, this study supports the existing data of MC heterogeneity and shows that this plastic cell type is still not fully characterized and is highly variable depending on the tissue origin and the mode of cultivation.

## **4.2 ST2/TLR2 activated MC promote anti-tumoral functions in the TME of melanoma**

The research findings presented in this study shed light on the role of MC and IL-33 in shaping the TME of melanoma and their impact on tumor progression.

### **4.2.1 High levels of IL-33 are associated with better survival in melanoma**

Although MC have mainly been investigated in the context of allergic events, their relevance within tumors has emerged [215]. MC have lately been analyzed for their involvement in different cancer entities. However, depending on the cancer entity, the results are controversial. The conflicting prognostic value of MC in the TME may stem from the heterogeneous nature of MC themselves and the investigated tumors. Immune surveillance refers to the capacity of the immune system to sense cellular dysregulation and respond by initiating a stress response to restore homeostasis. In tumorigenesis, epithelial cells release the alarmin IL-33 upon tissue damage and can cause MC degranulation [216, 217]. IL-33 is involved in Type 1, Type 2 and regulatory immune responses through signaling via the ST2 receptor on various immune cells, promoting inflammation and repair [218]. Not surprisingly, the published studies on the role of IL-33 in cancer are conflicting, depending on the models used for analysis. The role of IL-33 in melanoma has also been controversially discussed. Some investigations determined that IL-33 overexpression can promote anti-tumor type I immunity, inhibiting melanoma lung metastasis by CD8<sup>+</sup> T cells and NK cells [219] [220]. In another study, IL-33 was found to recruit eosinophils, mediating an anti-tumoral role and inhibiting metastasis [221].

On the other hand, contradicting reports have shown that IL-33 can induce ILC2, which inhibits NK cells and results in enhanced metastasis formation [222]. However, IL-33 is elevated in many human cancers, including hepatocellular carcinoma (HCC), pulmonary adenocarcinoma, and lymphoma, associated with a good prognosis [223-225]. The investigation using publicly available data from the TCGA database into the effects of IL-33 demonstrated that high levels of IL-33 were associated with improved overall survival in skin cutaneous melanoma patients. We could confirm this in our mouse model, as treatment of B16 tumors with IL-33 significantly reduced tumor volume, and this effect was accompanied by a considerable accumulation of MC (Figure 12). In breast cancer, MC have been shown to localize at the margin of tumors, especially near vessels [226]. In our murine melanoma model, accumulation of MC was determined peritumoral, located underneath the epidermal layer of the skin, but not infiltrating the tumor. These MC exhibited signs of granular release, indicative of an active state.

#### **4.2.2 Treatment of B16 melanoma with IL-33/Pam2Cys attenuates tumor progression**

Mechanisms of immune surveillance include the recognition of microbial stresses at epithelial barriers by PAMPs or detecting self-danger signals, known as alarmins, secreted upon damage. Based on the broad spectrum of receptors that MC carry and their sentinel role, it is evident that MC can respond to endogenous signals in the TME of melanoma.

In vitro experiments revealed that IL-33-activated MC secrete various immune-recruiting chemokines upon stimulation. This suggests that MC are crucial in promoting immune cell recruitment within the TME, particularly in response to IL-33. In DC, stimulation via TLR2-signaling induces the production of pro-inflammatory cytokines [227]. In MC, however, a synergistic effect of IL-33 and TLR2/6 agonist (Pam2Cys) stimulation was evident, resulting in enhanced cytokine secretion, especially of cytokines involved in immune cell recruitment (Figure 14). This effect depended on IL-33, as *ST2*<sup>-/-</sup> MC did not respond similarly (Figure 15). In vivo experiments using mouse models further validated the importance of MC in tumor progression. The combined treatment of IL-33 and Pam2Cys showed a significant impairment of tumor progression. Importantly, this effect was observed only in the presence of MC, emphasizing their essential role in the anti-tumoral response. We observed a MC-dependent recruitment of CD8<sup>+</sup> cytotoxic T cells and NK cells to the tumors and an upregulation of associated cytotoxic cytokines IFN- $\gamma$ , Granzyme B, and Perforin. In conclusion this study shows that MC are essential for recruiting T cells to the TME, thereby inducing an effective anti-tumor effect (Figure 26).

Furthermore, genes associated with T-cell recruitment were upregulated in tumors from MC-competent mice, which have previously been shown to be secreted by MC [99]. Corresponding to the in vitro data, this phenomenon in vivo was attributed mainly to IL-33, as mice reconstituted with *ST2*<sup>-/-</sup> MC before tumor inoculation showed only a partial response towards IL-33/Pam2Cys treatment.

#### **4.2.3 IL-33 stimulated MC recruit T cells and induce hot tumors in a murine melanoma model**

The TME represents a dynamic network structure comprised of pro- and anti-tumorigenic immune cells, tumor cells, and ECM, displaying inherent complexity during cancer progression or therapeutic modulations [228]. It is therefore crucial to comprehend the intricate interplay between TME components for optimized treatments. Furthermore, cancer heterogeneity across different patients underscores the necessity of mapping immune infiltrates for diagnostics and

personalized treatment adaptation [229]. Based on the infiltration of T cells, tumors are classified as hot (T cell inflamed) or cold (not T cell inflamed). As hot tumors are immune-activated, new therapies aim to convert them into hot tumors, which exhibit higher response rates to checkpoint immunotherapy [230-232]. In this study, flow cytometry data revealed that some tumors treated with IL-33 alone responded to treatment while others did not. Differentiating between responders and non-responders was possible through analysis of T-cell infiltration. Hot tumors, exhibiting enhanced T cell infiltration, displayed significantly smaller tumor sizes than cold tumors, which showed T cell exclusion. Double treatment of tumors with both IL-33 and Pam2Cys led to increased conversion of B16 tumors into hot tumors compared to single treatment. Analysis indicated that MC are essential for this transformation, as no T-cell infiltration based on treatment was detectable in their absence.

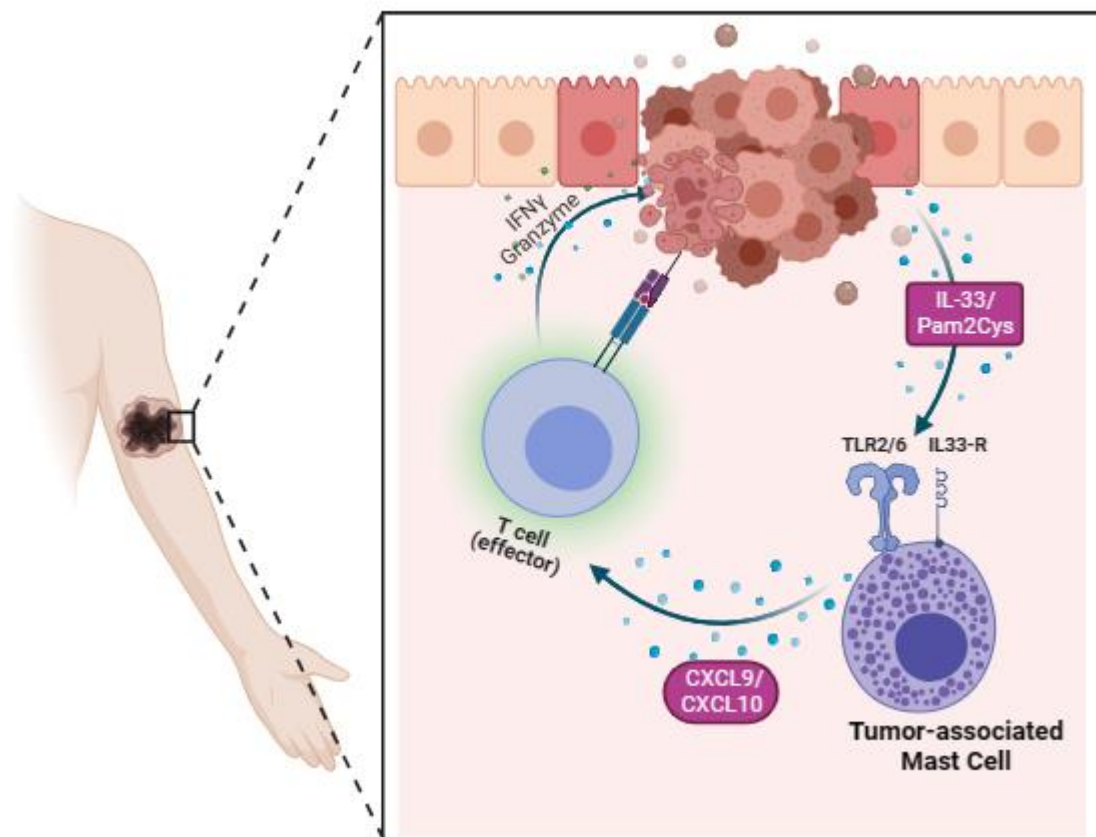


**Figure 26: Graphical abstract for IL-33-activated MC in melanoma**

Graphical Abstract depicting that IL-33/Pam2Cys activated MC in the TME of melanoma secrete immune modulatory chemokines, such as CXCL9 and CXCL10, inducing the recruitment of T cells, which elicit an anti-tumoral immune response. Own illustration.

#### 4.2.4 MC as a target for novel combination therapy in melanoma

Due to the high therapeutic resistance of metastatic melanoma, new treatment options are necessary. Recent research in different tumor entities has identified that IL-33 in the TME can enhance anti-tumor responses by recruiting CD8<sup>+</sup> T cells and NK cells mediated through IFN- $\gamma$ . The role of endogenous IL-33 in mediating CD8<sup>+</sup> T cell-dependent antitumor responses was demonstrated in mouse models of colon carcinoma and hepatocellular carcinoma [233, 234]. First experiments using IL-33 as an immunoadjuvant vaccine successfully showed the induction of CD8<sup>+</sup> T cells co-expressing IFN- $\gamma$  and TNF- $\alpha$  [235]. Also, the use of TLR-agonists as vaccine adjuvants in cancer treatment has been investigated due to their ability to activate immune cells [57, 58].

The engagement of TLR2 on CD8<sup>+</sup> CTLs dramatically increases the production of IFN- $\gamma$  and enhances the production of granzyme B and perforin [236, 237]. The physiological significance of TLR signaling in T cells is highlighted in experiments demonstrating that MC are crucial for TLR2-induced tumor inhibition [100]. The TLR1/6 agonist Pam3Cys has shown limited application for immunotherapy because of inconsistent anti-tumor efficacy and unconvincing in vivo safety [238, 239]. The distressing in vivo results of TLR agonists could be bypassed using bioactive alternatives [240]. The study's findings collectively suggest that the synergistic activation of MC via ST2 and TLR2/6 mediates an anti-tumoral effect by promoting the recruitment of immune cells to the TME. This phenomenon results in hot tumors with increased immune cell infiltration and suppressed tumor growth. These insights into the role of MC and IL-33 in melanoma regulation open avenues for immunotherapeutic strategies aimed at harnessing the anti-tumoral potential of these immune components.

Further research is warranted into the detailed mechanisms involved in this process and potential clinical applications. While initially, anti-PD1 therapy had shown impressive results, only a subset of patients initially responded, and increasing clinical evidence indicates that a substantial proportion of initial responders ultimately relapse with lethal, drug-resistant disease due to de-novo and acquired resistance [241]. In a B16 melanoma model, the systemic administration of IL-33 and PD-1 expression in tumor-specific CD4<sup>+</sup> T cells were shown [242]. We hypothesize that the combination of neo-adjuvant anti-PD1 immunotherapy and peritumoral administration of IL-33/Pam2Cys can enhance the efficacy of the checkpoint therapy. While the PD1 therapy induces activation of T cells, allowing the identification of the tumor-reactive CD8<sup>+</sup> T cell, the stimulation of tumor-associated MC within the TME with IL-33/Pam2Cys will recruit the T cells, transforming the TME into an immune active state.

#### **4.2.5 Limitations of the study**

One limitation of our study is using a single melanoma cell line. All experiments were conducted with the B16 model. Repeated experiments using the YUMM cells would be beneficial to verify the data further. YUMM cells are available in various mutations, allowing for discrimination between BRAF and NRAS mutated melanoma cells [243]. In addition, only low-metastasizing B16-F1 cells were used. It would be interesting to see whether the therapeutic function of ST2-TLR2/6 activated MC still outweighs the high metastasizing B16-F10 cells. Another limitation is the use of the *Mcpt5cre<sup>+</sup>-RDTA<sup>fl/fl</sup>* mouse model. This mouse line has a constitutive deficiency in MC. Therefore, kinetic analysis of immune cell recruitment cannot be performed. Using the new inducible mouse model using the diphtheria toxin would allow for depletion of MC at various time points before or after tumor inoculation, which helps decipher the aberrant immune signaling [244].

#### **4.3 Melanoma education by MC impairs lymphatic metastasis**

The incidence of melanoma is steadily rising. What differentiates melanoma from other skin cancers, such as basal cell and squamous cell carcinoma, is the high potential and tendency of the primary tumor to spread locally and distantly [245]. While most melanomas are detected during an early disease stage, many patients develop metastasis over time. The most common sites of metastasis are skin and subcutaneous tissue, followed by lungs, liver, and brain. Metastasis in human melanoma patients traffics via the lymphatic vessels. Lymphatic vessels are recognized as important regulators of immunity and inflammation and represent an essential route for metastatic dissemination [246]. Single-cell transcriptomic analysis of acral melanoma, a rare subtype of melanoma characterized by a severe immunosuppressive state and a high incidence of LN metastasis, identified lymphatic metastasis, was mediated by MITF and a subsequent metabolic shift towards fatty acid oxidation [247]. Further studies analyzing lymphatic metastasis found WNT5B a key mediator in promoting the metastatic potential of melanoma cells through its effects on lymphatic endothelial cells [248].

Activating invasion and metastasis formation is one of the hallmarks of cancer [180]. The metastatic cascade is a multi-step process initiated by a local invasion of the surrounding stroma. For this to happen, melanoma cells undergo a process called EMT, whereby the tight connection between cancer cells and the extracellular matrix is lost, enabling the dissemination of cancer cells. However, instead of a binary process, recent research has proposed that EMT occurs in

various intermediate stages, with tumor cells that express both a mixture of epithelial and mesenchymal phenotypes being more effective in circulating and metastasis formation [249]. Melanoma has a high metastatic potential, as the cancer originates from melanocytes derived by neural crest. Since the conversion from an epithelial to mesenchymal cell type is essential during normal embryogenesis and mainly attained by the neural crest, melanocytes are epithelial cells that have already been subjected to EMT during their normal development. Thus, melanocytes are thought to possess an inherent predisposition to gain EMT-induced invasive potential [250, 251].

MC are tissue-resident sentinel cells with some unique properties. For example, MC are equipped with many innate immune receptors. They are part of the adaptive immune system through the binding of immunoglobulins. Through the storage and release of mediators in their granules, MC can contribute to shaping the TME and directly or indirectly melanoma behavior. Our observations demonstrate that MC play a crucial role in preventing lymphatic metastases of melanoma. *Mcpt5cre<sup>+</sup>-RDTA<sup>fl/fl</sup>* mice, deficient in CTMC, showed a metastatic phenotype after the injection with B16 melanoma cells, with visible infiltration of the lymphatic vessels and the draining lymph nodes. We proved that this phenotype depends on the presence of MC in the skin, as reconstituting the skin of MC-deficient mice with MC before tumor cell inoculation rescued this phenotype completely. Based on the data in this study, we propose a dual role of MC in preventing metastasis, on the one side through direct education of the melanoma cells and on the other hand through chemotactic recruitment of immune cells to the TME.

#### **4.3.1 Education of melanoma cells by MC**

Our investigation of bulk RNA sequencing data from primary tumors of MC-deficient mice revealed modifications in genes related to interferon signaling and GTPase activity, which may explain the increased metastatic potential [252]. Further RNA analysis of primary tumors identified a downregulation of epithelial-associated markers and an upregulation of mesenchymal markers in tumors from MC-deficient mice. This phenotype was reversed upon reconstitution with MC prior to tumor cell inoculation, indicating that MC are essential for maintaining melanoma cell junctions with the extracellular matrix, thus preventing metastasis. It is worth noting that the EMT markers analyzed in this study, such as cadherins, occluding, and vimentin, are primarily associated with type 2 EMT. However, to further support the EMT hypothesis, deeper analysis of Type 3 EMT molecules, such as transcriptional factors Snail, Slug, zinc finger E-box binding homeobox 1 (ZEB1), and Twist [58], as well as intracellular factors, such as changes in intracellular Erk signaling, RhoB, and  $\beta$ -catenin, whose differential expression

should also be analyzed in MC-deficient mice would be necessary [253, 254]. Rho enzymes were found to be altered in MC-deficient mice, as shown by RNA sequencing data; however,  $\beta$ -catenin is an exciting candidate for further studies, as its involvement with DC is well known. Transplantation experiments should be performed to investigate further whether immune education of melanoma can be achieved. Primary tumors from MC-competent mice can be harvested and re-injected intra-dermally into MC-deficient mice, and tumor growth and metastasis formation can be observed. Through RNA analysis of the re-transplanted tumors, the impact of tumor cell education on the environment and, thus, changes in EMT markers can be determined.

#### **4.3.2 Chemotactic recruitment of immune cells by MC to the TME**

The manipulation of chemokine axes in melanoma can also create a more immunoregulatory environment independent of immune cell recruitment. RNA sequencing analysis of primary tumors from MC-deficient mice showed downregulation in *Irf7* and differential gene expression in signaling pathways associated with interferon-signaling. It has been demonstrated in breast cancer that silencing the *Irf7* pathway helps metastatic cells escape immune surveillance, and that restoration of *Irf7* in tumor cells or administration of IFN $\gamma$  reduces metastasis formation. It enhances the overall survival [255]. Our data suggests that *Irf7*-driven metastasis suppression and the corresponding IFN-signaling to host immune cells depend on the presence of MC in the skin. Controversially, the sequencing data also revealed a decreased expression of *Ccl2* in primary tumors from MC-deficient mice. Data also from research in breast cancer has shown that the recruitment of specific Gr-1<sup>+</sup> inflammatory monocytes and metastasis-associated macrophages to the pulmonary metastatic site is dependent on CCL2 and that the depletion of tumor-derived CCL2 inhibits metastasis [256].

On the other hand, the RNA data correlates with the flow cytometry analysis of the primary tumors. In MC-deficient mice, we found a significant reduction in the recruitment of macrophages to the tumors, and CCL2 is the most potent chemoattractant in macrophage recruitment. Further, RNA sequencing data revealed a downregulation in *Ccl7* in primary tumors from MC-deficient mice. The role of CCL7 in cancer has been diversely discussed, as the chemokine can act pro- or anti-tumoral, depending on the tumor entity. For example, tumor-derived CCL7 can promote tumor growth, invasion, and metastasis in renal cell carcinoma in an autocrine manner by recruiting TAMs [257]. In colorectal cancer, CCL7 is secreted by Mo-MDSC, which acti-

vates dormant cells and thus causes metastasis formation [258]. Our study shows that the downregulation of mRNA levels of *ccl7*, as a direct effect of the absence of MC, leads to the failed recruitment of anti-tumoral lymphocytes.

The downregulation of CCL7 supports the flow cytometry data, which showed impaired recruitment of DC to the TME in the absence of MC. The receptor for CCL7, CCR7, is expressed on migratory CD103<sup>+</sup> DC that have encountered antigens, facilitating the migration from the TME to the tumor-draining LN [259]. Our data suggest an education of melanoma cells by MC, with the absence of MC resulting in aberrant immune signaling. In this case, the downregulation of CCL7 results in the malfunction of DC recruitment to the TME.

The analysis conducted in this thesis focuses on MC cell recruiting functions in the context of melanoma. However, it remains unclear as to which mechanism MC inhibit metastasis formation. MC are a potent source of extracellular vesicles (EV) released into the TME. Based on the impact of MC on metastasis development in the absence of apparent signs of activation, identification of potentially relevant mediators released by MC via piecemeal degranulation through secretome analyses and single cell sequencing would further aid in deciphering the role of MC in metastasis.

In many solid tumors, CXCL5 is overexpressed and promotes distant metastasis by recruiting neutrophils [260]. CXCL5 has also been implicated in metastasis through inducing EMT, as neutrophils aid in tumor intravasation into lymphatic vessels [261, 262]. In our model, MC-deficient mice presented with significantly increased concentrations of CXCL5 in the serum, indicating a systemic increase in this chemokine. This correlates with a significant increase in CD11b<sup>+</sup>Gr1<sup>+</sup> neutrophils detected in the primary tumors of MC-deficient mice through flow cytometry. Therefore, the loss of MC reveals a strong production of CXCL5, resulting in the increased recruitment of neutrophils to the TME, supporting EMT, intravasation, and metastasis formation.

Based on this metastatic phenotype, we hypothesized that MC are at the top of a hierarchical model, thereby influencing aberrant immune signaling in the TME. While tumor progression in macrophage-deficient mice was comparable to that of MC-competent mice, the absence of DC (Bat3KO mice) showed tumor progression like that of MC-deficient mice. Notably, metastasis was only evident in MC-deficient mice independent of the tumor size, supporting the hypothesis that MC are the top of the signaling cascade. Interestingly, Batf3KO mice showed a significant reduction in overall lymphocyte composition in the primary tumor, significantly reducing recruitment of T cells and NK cells in the TME. The similar tumor progression in MC-deficient and DC-deficient mice leads us to believe there is a connection between the cells.

Further, primary tumors of MC-deficient mice showed a significant reduction in DC recruitment to the TME. It has been demonstrated that MC support adaptive immune responses by promoting DC migration to skin-draining LN in contact hypersensitivity and bacterial response [263, 264]. Furthermore, it has been shown that MC granules are engulfed by DC, which leads to DC maturation and conditioning [265]. Our data shows that the reduction of DC in the TME of melanoma, because of MC deficiency, leads to an aberrant immune signaling, resulting in reduced recruitment of T cells and NK cells, thereby orchestrating a pro-tumoral microenvironment.

In this study, cDC1 were defined using the surface marker CD11c<sup>+</sup>Clec9a<sup>+</sup> and divided into migratory DC using the surface marker XCR1. However, the surface marker CD103 would have supported a more accurate picture since tumor-draining DC are known to carry this marker. In addition, tumor-infiltrating CD103<sup>+</sup> DC have been implicated with tumor-intrinsic upregulation of  $\beta$ -catenin, which supports the hypothesis that MC not only impacts the infiltration of immune cells into the TME but is also interlinked with the education of melanoma itself [266].

### 4.3.3 Outlook

Our data have shown a metastatic phenotype based on the absence of MC. Metastasis formation in this study was observed solely on a macroscopic level. Using fluorescently labeled B16 cells would allow for live cell tracking. Data from bulk RNA sequencing suggest that GTPases are involved in the metastasis formation without MC. Possible candidates involved in this context could be RHO-GTPases or Ran GTPases, both known to be involved in metastasis [267, 268]. To validate this finding, further qPCR analysis is required. To further decipher the interaction between DC and MC and the potential involvement in metastasis, single-cell sequencing would aid in detangling the interconnection of both cell types, especially in understanding possible changes between resting and tumor-associated MC, to clearly define the mode of communication that MC have in the TME. Also, the composition of the TME was determined by flow cytometry, which allows for the determination of cell quantity but not cell distribution. Visualization methods such as immunohistochemistry would be beneficial in defining communication clusters of immune cells. This would help to determine whether the role of MC is through direct cell-to-cell interactions or chemokine signaling. One open question remains: What compensatory methods are acting in place of the MC absence? To answer this question, the Mcpt5-DTR

mouse model can be useful [244]. Using this inducible model allows for the depletion of MC at various time points before or during melanoma manifestation.

In conclusion, using the  $Mcpt5\text{-cre}^+\text{-RDTA}^{fl/fl}$  as a model allows the analysis of melanoma lymphatic metastasis. So far, available mouse models for metastasis in melanoma focus on intravenous injections or xenotransplantations [269]. However, these models need to be more adequate representations of the actual situation in humans. Using this metastatic model allows for in-depth analysis of the dissemination of cancer cells from the primary site using in vivo live imaging tools.

#### **4.4 Distinct shift of T cell subtypes during cutAE in melanoma patients under ICI**

ICI has become a pillar of melanoma therapy, but the immunological consequences of ICI still need to be adequately investigated. An extensive literature research conducted by Khoja et al. showed that different tumour entities (melanoma, renal cell and NSCLC) present with different irAE profiles when treated with the same anti-PD-1 agent [270]. Therefore, the pilot study aimed to identify immune cell subsets and cytokines responsible for different cutAE in melanoma patients to define potential biomarkers. Furthermore, a recent study analysing common immunological states preceding distinct manifestations of ICI-induced toxicity identified two baseline features essential for the determination of ICI-induced cutaneous AE: the abundance of activated  $CD4^+$  memory T cells and a clonally diverse TCR repertoire in the peripheral blood [271]. Therefore, the basis of this study was the analysis of  $CD4^+$  T helper subsets in the peripheral blood of melanoma patients.

In the patient cohort, a shift from Th2 towards Th1 cells was induced through ICI in all patients regardless of cutAE and irrespective of response to ICI therapy (Figure 22). Skin-homing  $CLA^+$  Th1 cells migrate to the skin via their homing receptor CLA and recirculate between the blood and the skin. The significant increase in  $CLA^+$  Th1 cells in patients' peripheral blood during monotherapy mirrors an increased potential for recruitment of skin-associated T cells to the site of inflammation (Figure 23). Nivolumab and pembrolizumab block PD-1 on the T cell, activating T cells and restoring the immune response of effector T cells, whereas ipilimumab activates the immune system by targeting CTLA-4. CutAE have been reported to correlate with clinical response to ICI therapy [272]. Even though it burdens the patient, cutAE are a promising prognostic biomarker for a competent immune system. ICI primarily aims to enhance cytotoxic re-

sponses by CD8<sup>+</sup> T cells. Thus, other studies have mainly concentrated on PD1<sup>+</sup> T cell subfractions as response markers for clinical response associated with rescuing exhausted CD8<sup>+</sup> effector T cells by ICI rather than identifying T helper cell subtypes responsible for cutAE.

#### **4.4.1 Cutaneous adverse events show a Th17 phenotype**

During ICI, an increase in inflammatory cytokines, which were elevated even further during a cutAE, was observed in the plasma of patients. Particularly IL-1 $\beta$ , IFN- $\gamma$ , IL-33, IL-6, IL-18 and IL-23 were strongly elevated during cutAE. This finding is in line with recent studies conducted on melanoma patients. In a longitudinal study, Lim et al. found an increase in eleven circulating cytokines, including the proinflammatory cytokines IL-1 $\alpha$ , IL-2, and IFN- $\alpha$ 2, in patients with severe immune-related toxicities. The expression of these 11 cytokines was integrated into a single toxicity score, which showed predictive utility and correlation with grade 3 or greater cutAE in melanoma patients receiving anti-PD1 ICI [273]. Another multi-omics study analyzing different ICI-induced cutAE identified an early increase in CXCL3-related CXCL9/CXCL10/CXCL11 and IFN- $\gamma$  indicative of developing cutAE [274].

Interestingly, IL-6, IL-1 $\beta$ , IL-23, and TGF- $\beta$  are crucial for differentiating Th17 and Th22 cells from naïve CD4<sup>+</sup> T cells [275]. Indeed, a significant increase of Th17 cells was detected in the peripheral blood of patients during a cutAE, as well as increased plasma levels of IL-17A and IL-8 (Figure 27). It was reported that Th17 cells were increased after CTLA-4 blockade in patients with metastatic melanoma, suggesting a possible role for Th17 cells in ICI-induced toxicities [276]. Similar results were obtained in another study performed in melanoma patients treated with ipilimumab, in which pre-treatment IL-17 levels were associated with the development of severe intestinal inflammation [277]. Th17 cells play an essential role in defence against extracellular pathogens. Unfortunately, no microbiome analysis of the lesional skin sites was performed to determine whether the cutAE was also accompanied by a shift in the skin microbiome.

Further, Th22 cells increased in our patients with the onset of cutAE, particularly in responders, and remained high after six months. This was further supported by the higher levels of IL-22 in the plasma of patients responding to ICI. IL-22 is primarily secreted by lymphoid cells, mainly group 3 innate lymphoid cells, NKT cells, and CD4<sup>+</sup> T helper cells [278]. IL-22 promotes barrier integrity and repair by mediating communication between the skin barrier and the immune system, thereby playing a pivotal role in skin homeostasis and inflammation. It has become clear, however, that Th17 cells can also secrete IL-22 [279]. Considering the lack of intracellular staining, the origin of IL-22 in patients' plasma still needs to be determined. Interestingly,

recent studies in melanoma have shown that IL-22 promotes tumor cell proliferation, migration, and invasion, thereby challenging the hypothesis that high plasma levels of IL-22 might be able to raise a better anti-tumor response in the skin [280].

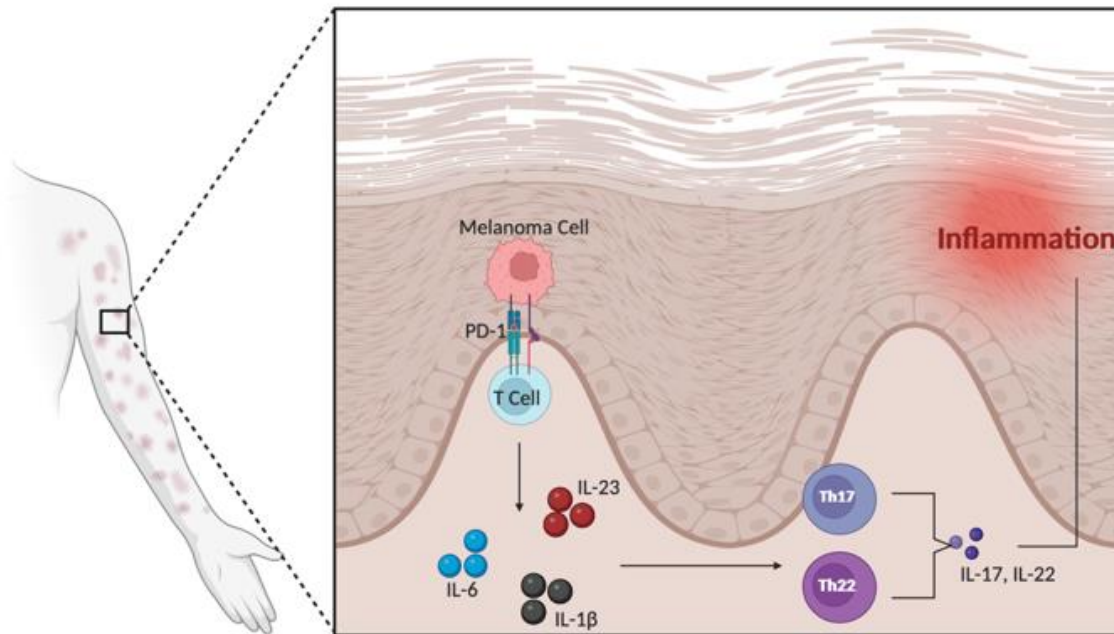


**Figure 27: Graphical abstract for cutAE study**

Graphical abstract showing melanoma patients undergoing ICI show a shift in T cell subsets. During the acute onset phase of a cutAE, patients present with an increased Th17/Th22 profile, resulting in elevated serum levels of IL-17 and IL-22 and skin inflammation (own illustration).

#### 4.4.2 Each cutAE presents with a unique cytokine profile

The skin is a significant location for irAE due to several compelling factors. Dermatologic toxicities manifest the earliest, with an average onset between 21- and 42-days post-initiation of therapy. Subsequently, gastrointestinal toxicity usually arises at 35 to 49 days after the commencement of treatment [281]. Given the skin's richness in lymphocytes, it frequently becomes a target, leading to cutAE appearing in as little as four weeks after treatment initiation [282]. Another crucial aspect is that the skin is the sole site where local reactions like vitiligo and dermatitis consistently align with a positive systemic response to checkpoint inhibition and enhanced treatment response [139, 283]. These findings underscore the possibility that the immune-based mechanisms triggering localized skin toxicity in response to ICI therapy could support antitumoral immune activity. The cutAE presented in the patient cohort were urticaria, acantholytic dermatosis, maculopapular exanthema, lichenoid dermatitis, and psoriasis. These

adverse events appear to be recurrent inflammatory eruptions in patients with melanoma undergoing ICI [284]. Although the immunological mechanisms underlying cutAE are being investigated, research has mainly analysed heterogeneous patient cohorts with ill-defined cutAE described as “rashes” or “exanthemas.” However, some cytokine signatures in the study were tailored to specific clinical manifestations. For example, patients with urticaria showed a significant increase in serum concentrations of IL-18 and IL-1 $\beta$  compared to other cutAE. The serum levels of IL-18 in urticaria patients were comparable to those in patients with colitis. IL-18 is an immune-regulatory cytokine shown to play a role in the pathomechanism of chronic urticaria [18]. This underlines that ICI-related cutAE do not necessarily share single immunological patterns and must be analysed separately. Also, the high levels of IL-1 $\beta$  in patients presenting with urticaria are interesting. A study in neonatal mice found that the colonization of newborn mice by the microbiota induces local production of TNF- $\alpha$ , which primed MC to elicit dysregulated production of IL-1 $\beta$ , thereby causing skin and systemic disease [285]. Further microbiota analysis in our patient cohort would, therefore, be of interest to elicit potential correlations between skin microbiota disbalance and the onset of urticaria under ICI.

#### **4.4.3 Serum IL-10 levels as a potential diagnostic marker for cutAE**

In our cohort, plasma levels of IL-10 were elevated during a cutAE, which may reflect a counter-regulation against the skin inflammation associated with cutAE (Figure 25). Of note, IL-10 was elevated in non-responders. IL-10 is a potent anti-inflammatory cytokine that plays a central role in limiting the host's immune response to pathogens, thereby preventing damage to the host. It downregulates the expression of Th1 cytokine secretion, antigen presentation, and CD4<sup>+</sup> T cell activation against inflammation, which could also be the case in cutAE. Thus, high levels of IL-10 may create an immunosuppressive tumor microenvironment, hindering the body's ability to fight the cancer effectively.

The data further suggests a predisposition, as patients with initially lower IL-10 levels tended to develop cutAE compared to patients with high baseline IL-10 levels. This would align with the hypothesis that cutAE are beneficial for ICI, as elevated IL-10 levels have been reported to correlate with poor survival in melanoma patients [286]. Contrary to this data, however, higher levels of plasma IL-10 were detected during cutAE. However, this result might indicate a bias in the data set, as patients with high baseline levels of IL-10 maintained these elevated levels over 6 months of ICI treatment, thereby leading to higher overall IL-10 levels during the measurement of all patients. Thus, increased IL-10 expression associated with cutAE may be tumor-promoting and not beneficial for the patient.

In conclusion, this exploratory study implies that cutAE in melanoma should be treated fast and effectively to reduce cutAE early and to prevent further production of IL-10. Common treatment strategies include topical corticosteroids and systemic immunomodulators.

#### **4.4.3 Outlook and limitations**

One aspect that needs to be evaluated critically when interpreting the data is the potential effect that the therapeutic corticosteroid intervention used to treat cutAE may play a negative role for the anti-tumoral immune responses. Not all dermatologic toxicities, such as vitiligo, are considered harmful and require treatment.

Limitations of this study include the monocentric setting and the low number of patients, which may have prevented the finding of significant differences. Unfortunately, however, over three years, only a limited number of patients were willing to follow through with the study. Therefore, some data points still need to be improved, making statistical pairwise analysis difficult. Furthermore, only a limited number of inflammatory cytokines and T cell immune cell subsets were analysed at three-time points, and a broader approach, including effector T cells, memory cells, and other immune cell subsets such as NK and NKT cells, may have led to a more in-depth understanding of the cutAE. On the other hand, preliminary results in limited populations may pave the way for more directed and more extensive studies. This prospective study, designed as an exploratory study to be followed up by more extensive studies in the future, provided several significant results and offered important insights. The study's strength is the analysis of T cellular mechanisms and cytokines before and during ICI and at the onset of cutAE, allowing for first investigations in immune signatures relevant to the onset of a diverse spectrum of cutAE. Data from this pilot study showed that each cutAE is individual, with specific cytokine signatures. Therefore, further studies deciphering individual cutAE would benefit patients and clinicians in adequately adjusting therapy options.

## 5. Conclusion

The current research aimed to identify the aberrant immune signaling in melanoma and the involvement of MC in the TME of melanoma.

The central questions for this research were:

- i) Determine appropriate in vitro MC surrogates that best resemble CTMC.
- ii) Investigate the role of MC in the TME of melanoma through stimulation with endogenous factors.
- iii) Identify immunological mechanisms underlying cutAE in patients with melanoma undergoing ICI.

Through intensive in vitro studies, we identified that MC can be generated successfully from bone marrow precursors, as well as from fetal livers and fetal skin. Although all three cell types can be classified as MC based on their surface expression of CD117 and FcεRI, FSMC are the most mature form of in vitro generated MC and resemble connective tissue MC the closest, as fetal skin cells have already been exposed to tissue-specific environmental factors and thus have already been primed.

Through combined stimulation of MC with IL-33 and the TLR2/6 agonist Pam2Cys, an anti-tumoral effect on the progression of melanoma was identified in a murine B16 model. MC-dependent recruitment of T cells and NK cells to the TME of melanoma was identified upon treatment with IL-33 and Pam2Cys, potentially mediated through IFN-γ and Perforin, as well as through T cell recruiting chemokines CXCL9/CXCL10. Furthermore, MC have been identified as key regulators of lymphatic metastasis in melanoma, as MC-deficient mice present with a metastatic phenotype. In conclusion, this research showed that MC are essential for the immune signaling in melanoma by mediating cell recruitment and, therefore, play an important role as anti-tumoral immune cells.

Lastly, a pilot clinical study analyzed melanoma patients undergoing immune checkpoint therapy. Patients presenting with cutaneous adverse events showed a shift in T cell subtypes, implicating that cutaneous adverse events are mediated by Th17 cells.

## List of References

1. St. John, A.L., A.P.S. Rathore, and F. Ginhoux, *New perspectives on the origins and heterogeneity of mast cells*. Nature Reviews Immunology, 2022.
2. Gentek, R., et al., *Hemogenic Endothelial Fate Mapping Reveals Dual Developmental Origin of Mast Cells*. Immunity, 2018. **48**(6): p. 1160-1171.e5.
3. Dahlin, J., et al., *The Ingenious Mast Cell: Contemporary insights into mast cell behavior and function*. Allergy, 2021. **77**.
4. Grootens, J., J.S. Ungerstedt, G. Nilsson, and J.S. Dahlin, *Deciphering the differentiation trajectory from hematopoietic stem cells to mast cells*. Blood Advances, 2018. **2**(17): p. 2273-2281.
5. Dahlin, J.S., et al., *A single-cell hematopoietic landscape resolves 8 lineage trajectories and defects in Kit mutant mice*. Blood, 2018. **131**(21): p. e1-e11.
6. Tusi, B.K., et al., *Population snapshots predict early haematopoietic and erythroid hierarchies*. Nature, 2018. **555**(7694): p. 54-60.
7. Jardine, L., et al., *Blood and immune development in human fetal bone marrow and Down syndrome*. Nature, 2021. **598**(7880): p. 327-331.
8. Collington, S.J., et al., *The Role of the CCL2/CCR2 Axis in Mouse Mast Cell Migration In Vitro and In Vivo*. The Journal of Immunology, 2010. **184**(11): p. 6114-6123.
9. Hallgren, J., et al., *Pulmonary CXCR2 regulates VCAM-1 and antigen-induced recruitment of mast cell progenitors*. Proc Natl Acad Sci U S A, 2007. **104**(51): p. 20478-83.
10. Weller, C.L., et al., *Chemotactic action of prostaglandin E<sub>2</sub> on mouse mast cells acting via the PGE<sub>2</sub> receptor 3*. Proceedings of the National Academy of Sciences, 2007. **104**(28): p. 11712-11717.
11. Msallam, R., et al., *Fetal mast cells mediate postnatal allergic responses dependent on maternal IgE*. Science, 2020. **370**(6519): p. 941-950.
12. Huber, M., et al., *Regulation of the pleiotropic effects of tissue-resident mast cells*. J Allergy Clin Immunol, 2019. **144**(4s): p. S31-s45.
13. da Silva, E.Z., M.C. Jamur, and C. Oliver, *Mast cell function: a new vision of an old cell*. J Histochem Cytochem, 2014. **62**(10): p. 698-738.
14. Ribatti, D., *The Staining of Mast Cells: A Historical Overview*. Int Arch Allergy Immunol, 2018. **176**(1): p. 55-60.
15. Grigorev, I.P. and D.E. Korzhevskii, *Modern Imaging Technologies of Mast Cells for Biology and Medicine (Review)*. Sovrem Tekhnologii Med, 2021. **13**(4): p. 93-107.
16. Feyerabend, T.B., et al., *Loss of histochemical identity in mast cells lacking carboxypeptidase A*. Mol Cell Biol, 2005. **25**(14): p. 6199-210.
17. Pejler, G., E. Rönnberg, I. Waern, and S. Wernersson, *Mast cell proteases: multifaceted regulators of inflammatory disease*. Blood, 2010. **115**(24): p. 4981-90.
18. Crapper, R.M. and J.W. Schrader, *Frequency of mast cell precursors in normal tissues determined by an in vitro assay: antigen induces parallel increases in the frequency of P cell precursors and mast cells*. J Immunol, 1983. **131**(2): p. 923-8.

19. Friend, D.S., et al., *Mast cells that reside at different locations in the jejunum of mice infected with Trichinella spiralis exhibit sequential changes in their granule ultrastructure and chymase phenotype*. J Cell Biol, 1996. **135**(1): p. 279-90.
20. Jones, T.G., et al., *Antigen-induced increases in pulmonary mast cell progenitor numbers depend on IL-9 and CD1d-restricted NKT cells*. J Immunol, 2009. **183**(8): p. 5251-60.
21. Gurish, M.F. and K.F. Austen, *Developmental origin and functional specialization of mast cell subsets*. Immunity, 2012. **37**(1): p. 25-33.
22. Hayashi, C., et al., *Mast-cell precursors in the skin of mouse embryos and their deficiency in embryos of Sl/Sld genotype*. Dev Biol, 1985. **109**(1): p. 234-41.
23. Dwyer, D.F., N.A. Barrett, and K.F. Austen, *Expression profiling of constitutive mast cells reveals a unique identity within the immune system*. Nat Immunol, 2016. **17**(7): p. 878-87.
24. Frossi, B., et al., *Is it time for a new classification of mast cells? What do we know about mast cell heterogeneity?* Immunol Rev, 2018. **282**(1): p. 35-46.
25. Derakhshan, T., et al., *Lineage-specific regulation of inducible and constitutive mast cells in allergic airway inflammation*. Journal of Experimental Medicine, 2020. **218**(1).
26. Dwyer, D.F., et al., *Human airway mast cells proliferate and acquire distinct inflammation-driven phenotypes during type 2 inflammation*. Sci Immunol, 2021. **6**(56).
27. Motakis, E., et al., *Redefinition of the human mast cell transcriptome by deep-CAGE sequencing*. Blood, 2014. **123**(17): p. e58-67.
28. Galli, S.J., S. Nakae, and M. Tsai, *Mast cells in the development of adaptive immune responses*. Nat Immunol, 2005. **6**(2): p. 135-42.
29. Chen, H.-Y., et al., *Nanoimaging granule dynamics and subcellular structures in activated mast cells using soft X-ray tomography*. Scientific Reports, 2016. **6**(1): p. 34879.
30. Moon, T.C., A.D. Befus, and M. Kulka, *Mast cell mediators: their differential release and the secretory pathways involved*. Front Immunol, 2014. **5**: p. 569.
31. Redegeld, F.A., et al., *Non-IgE mediated mast cell activation*. Immunol Rev, 2018. **282**(1): p. 87-113.
32. Galli, S.J. and M. Tsai, *IgE and mast cells in allergic disease*. Nat Med, 2012. **18**(5): p. 693-704.
33. Raposo, G., et al., *Accumulation of major histocompatibility complex class II molecules in mast cell secretory granules and their release upon degranulation*. Mol Biol Cell, 1997. **8**(12): p. 2631-45.
34. Baram, D., et al., *Synaptotagmin II negatively regulates Ca<sup>2+</sup>-triggered exocytosis of lysosomes in mast cells*. J Exp Med, 1999. **189**(10): p. 1649-58.
35. Varricchi, G., et al., *Are Mast Cells MASTers in Cancer?* Front Immunol, 2017. **8**: p. 424.
36. Noto, C.N., S.G. Hoft, and R.J. DiPaolo, *Mast Cells as Important Regulators in Autoimmunity and Cancer Development*. Front Cell Dev Biol, 2021. **9**: p. 752350.

37. Rivera, J. and A.M. Gilfillan, *Molecular regulation of mast cell activation*. J Allergy Clin Immunol, 2006. **117**(6): p. 1214-25; quiz 1226.
38. Borkowski, T., M.-H. Jouvin, S.-Y. Lin, and J.-P. Kinet, *Minimal Requirements for IgE-Mediated Regulation of Surface Fc RI*. Journal of immunology (Baltimore, Md. : 1950), 2001. **167**: p. 1290-6.
39. Beck, L.A., et al., *Omalizumab-induced reductions in mast cell Fc epsilon RI expression and function*. J Allergy Clin Immunol, 2004. **114**(3): p. 527-30.
40. Yamaguchi, M., et al., *IgE enhances mouse mast cell Fc(epsilon)RI expression in vitro and in vivo: evidence for a novel amplification mechanism in IgE-dependent reactions*. J Exp Med, 1997. **185**(4): p. 663-72.
41. Gilfillan, A.M. and C. Tkaczyk, *Integrated signalling pathways for mast-cell activation*. Nature Reviews Immunology, 2006. **6**(3): p. 218-230.
42. Paruchuri, S., et al., *Leukotriene E4 Activates Peroxisome Proliferator-activated Receptor gamma and Induces Prostaglandin D2 Generation by Human Mast Cells\**. Journal of Biological Chemistry, 2008. **283**(24): p. 16477-16487.
43. Lyons, D.O. and N.A. Pullen, *Beyond IgE: Alternative Mast Cell Activation Across Different Disease States*. Int J Mol Sci, 2020. **21**(4).
44. Kumar, V. and A. Sharma, *Mast cells: emerging sentinel innate immune cells with diverse role in immunity*. Mol Immunol, 2010. **48**(1-3): p. 14-25.
45. Agier, J., J. Pastwińska, and E. Brzezińska-Błaszczuk, *An overview of mast cell pattern recognition receptors*. Inflamm Res, 2018. **67**(9): p. 737-746.
46. Sandig, H. and S. Bulfone-Paus, *TLR signaling in mast cells: common and unique features*. Front Immunol, 2012. **3**: p. 185.
47. Mrabet-Dahbi, S., et al., *Murine mast cells secrete a unique profile of cytokines and prostaglandins in response to distinct TLR2 ligands*. Exp Dermatol, 2009. **18**(5): p. 437-44.
48. Varadaradjalou, S., et al., *Toll-like receptor 2 (TLR2) and TLR4 differentially activate human mast cells*. Eur J Immunol, 2003. **33**(4): p. 899-906.
49. McCurdy, J.D., T.J. Lin, and J.S. Marshall, *Toll-like receptor 4-mediated activation of murine mast cells*. J Leukoc Biol, 2001. **70**(6): p. 977-84.
50. Supajatura, V., et al., *Differential responses of mast cell Toll-like receptors 2 and 4 in allergy and innate immunity*. 2002. **109**(10): p. 1351-1359.
51. Kulka, M., L. Alexopoulou, R.A. Flavell, and D.D. Metcalfe, *Activation of mast cells by double-stranded RNA: evidence for activation through Toll-like receptor 3*. J Allergy Clin Immunol, 2004. **114**(1): p. 174-82.
52. Takenaka, H., et al., *Synergistic augmentation of inflammatory cytokine productions from murine mast cells by monomeric IgE and toll-like receptor ligands*. Biochem Biophys Res Commun, 2010. **391**(1): p. 471-6.
53. Ren, K. and R. Torres, *Role of interleukin-1beta during pain and inflammation*. Brain Res Rev, 2009. **60**(1): p. 57-64.
54. Teijeira, A., et al., *Differential Interleukin-8 thresholds for chemotaxis and netosis in human neutrophils*. Eur J Immunol, 2021. **51**(9): p. 2274-2280.
55. Bradley, J.R., *TNF-mediated inflammatory disease*. J Pathol, 2008. **214**(2): p. 149-60.

56. Kopf, M., et al., *Impaired immune and acute-phase responses in interleukin-6-deficient mice*. *Nature*, 1994. **368**(6469): p. 339-342.
57. Grimmig, T., et al., *Toll Like Receptor 2, 4, and 9 Signaling Promotes Autoregulative Tumor Cell Growth and VEGF/PDGF Expression in Human Pancreatic Cancer*. *Int J Mol Sci*, 2016. **17**(12).
58. Curtin, J.F., et al., *HMGB1 mediates endogenous TLR2 activation and brain tumor regression*. *PLoS Med*, 2009. **6**(1): p. e10.
59. Eissmann, M.F., M. Buchert, and M. Ernst, *IL33 and Mast Cells—The Key Regulators of Immune Responses in Gastrointestinal Cancers?* *Frontiers in Immunology*, 2020. **11**.
60. Hsu, C.L., C.V. Nielsen, and P.J. Bryce, *IL-33 is produced by mast cells and regulates IgE-dependent inflammation*. *PLoS One*, 2010. **5**(8): p. e11944.
61. Moussion, C., N. Ortega, and J.P. Girard, *The IL-1-like cytokine IL-33 is constitutively expressed in the nucleus of endothelial cells and epithelial cells in vivo: a novel 'alarmin'?* *PLoS One*, 2008. **3**(10): p. e3331.
62. Zhou, Z., F. Yan, and O. Liu, *Interleukin (IL)-33: an orchestrator of immunity from host defence to tissue homeostasis*. *Clin Transl Immunology*, 2020. **9**(6): p. e1146.
63. Schmitz, J., et al., *IL-33, an interleukin-1-like cytokine that signals via the IL-1 receptor-related protein ST2 and induces T helper type 2-associated cytokines*. *Immunity*, 2005. **23**(5): p. 479-90.
64. Liew, F.Y., J.P. Girard, and H.R. Turnquist, *Interleukin-33 in health and disease*. *Nat Rev Immunol*, 2016. **16**(11): p. 676-689.
65. Allakhverdi, Z., D.E. Smith, M.R. Comeau, and G. Delespesse, *Cutting edge: The ST2 ligand IL-33 potently activates and drives maturation of human mast cells*. *The Journal of Immunology*, 2007. **179**(4): p. 2051-2054.
66. Joulia, R., F.E. L'Faqihi, S. Valitutti, and E. Espinosa, *IL-33 fine tunes mast cell degranulation and chemokine production at the single-cell level*. *J Allergy Clin Immunol*, 2017. **140**(2): p. 497-509.e10.
67. Rönnerberg, E., et al., *Divergent Effects of Acute and Prolonged Interleukin 33 Exposure on Mast Cell IgE-Mediated Functions*. *Front Immunol*, 2019. **10**: p. 1361.
68. Lefrançois, E., et al., *Central domain of IL-33 is cleaved by mast cell proteases for potent activation of group-2 innate lymphoid cells*. *Proceedings of the National Academy of Sciences*, 2014. **111**(43): p. 15502-15507.
69. Saluja, R., A. Zoltowska, M.E. Ketelaar, and G. Nilsson, *IL-33 and Thymic Stromal Lymphopoietin in mast cell functions*. *Eur J Pharmacol*, 2016. **778**: p. 68-76.
70. Chhiba, K.D., C.L. Hsu, S. Berdnikovs, and P.J. Bryce, *Transcriptional Heterogeneity of Mast Cells and Basophils upon Activation*. *J Immunol*, 2017. **198**(12): p. 4868-4878.
71. Cardamone, C., R. Parente, G. De Feo, and M. Triggiani, *Mast cells as effector cells of innate immunity and regulators of adaptive immunity*. *Immunology letters*, 2016. **178**: p. 10-14.
72. Zhang, M., J.L. Duffen, K.H. Nocka, and M.T. Kasaian, *IL-13 Controls IL-33 Activity through Modulation of ST2*. *J Immunol*, 2021. **207**(12): p. 3070-3080.

73. Loiarro, M., V. Ruggiero, and C. Sette, *Targeting TLR/IL-1R Signalling in Human Diseases*. Mediators of Inflammation, 2010. **2010**: p. 674363.
74. Plum, T., et al., *Human Mast Cell Proteome Reveals Unique Lineage, Putative Functions, and Structural Basis for Cell Ablation*. Immunity, 2020. **52**(2): p. 404-416.e5.
75. Kovarova, M., *Isolation and characterization of mast cells in mouse models of allergic diseases*. Methods Mol Biol, 2013. **1032**: p. 109-19.
76. Michel, A., et al., *Mast cell-deficient Kit(W-sh) "Sash" mutant mice display aberrant myelopoiesis leading to the accumulation of splenocytes that act as myeloid-derived suppressor cells*. J Immunol, 2013. **190**(11): p. 5534-44.
77. Siebenhaar, F., et al., *Mast Cells as Drivers of Disease and Therapeutic Targets*. Trends in Immunology, 2018. **39**(2): p. 151-162.
78. Elieh-Ali-Komi, D., S. Wöhrl, and L. Bielory, *Mast Cell Biology at Molecular Level: a Comprehensive Review*. Clinical Reviews in Allergy & Immunology, 2020. **58**: p. 1-24.
79. Abraham, S.N. and A.L. St John, *Mast cell-orchestrated immunity to pathogens*. Nat Rev Immunol, 2010. **10**(6): p. 440-52.
80. Biedermann, T., et al., *Mast cells control neutrophil recruitment during T cell-mediated delayed-type hypersensitivity reactions through tumor necrosis factor and macrophage inflammatory protein 2*. J Exp Med, 2000. **192**(10): p. 1441-52.
81. Dudeck, A., et al., *Mast cells as protectors of health*. J Allergy Clin Immunol, 2019. **144**(4s): p. S4-s18.
82. Olivera, A., M.A. Beaven, and D.D. Metcalfe, *Mast cells signal their importance in health and disease*. J Allergy Clin Immunol, 2018. **142**(2): p. 381-393.
83. Spoerl, D., H. Nigolian, C. Czarnetzki, and T. Harr, *Reclassifying Anaphylaxis to Neuromuscular Blocking Agents Based on the Presumed Patho-Mechanism: IgE-Mediated, Pharmacological Adverse Reaction or "Innate Hypersensitivity"?* International Journal of Molecular Sciences, 2017. **18**(6): p. 1223.
84. Mizuno, H., et al., *Mast cells promote the growth of Hodgkin's lymphoma cell tumor by modifying the tumor microenvironment that can be perturbed by bortezomib*. Leukemia, 2012. **26**(10): p. 2269-2276.
85. Soucek, L., et al., *Mast cells are required for angiogenesis and macroscopic expansion of Myc-induced pancreatic islet tumors*. Nat Med, 2007. **13**(10): p. 1211-8.
86. Lampiasi, N., A. Azzolina, G. Montalto, and M. Cervello, *Histamine and spontaneously released mast cell granules affect the cell growth of human hepatocellular carcinoma cells*. Experimental & Molecular Medicine, 2007. **39**(3): p. 284-294.
87. Song, F., et al., *Mast cells inhibit colorectal cancer development by inducing ER stress through secreting Cystatin C*. Oncogene, 2022.
88. Johansson, A., et al., *Mast cells are novel independent prognostic markers in prostate cancer and represent a target for therapy*. Am J Pathol, 2010. **177**(2): p. 1031-41.
89. Fleischmann, A., et al., *Immunological microenvironment in prostate cancer: high mast cell densities are associated with favorable tumor characteristics and good prognosis*. The Prostate, 2009. **69**(9): p. 976-981.

90. Watanabe, S.-i., et al., *High density of tryptase-positive mast cells in patients with renal cell carcinoma on hemodialysis: correlation with expression of stem cell factor and protease activated receptor-2*. Human pathology, 2012. **43**(6): p. 888-897.
91. Fu, H., et al., *Tumor infiltrating mast cells (TIMs) confers a marked survival advantage in nonmetastatic clear-cell renal cell carcinoma*. Annals of surgical oncology, 2017. **24**: p. 1435-1442.
92. Baghban, R., et al., *Tumor microenvironment complexity and therapeutic implications at a glance*. Cell Communication and Signaling, 2020. **18**(1): p. 59.
93. Neophytou, C.M., M. Panagi, T. Stylianopoulos, and P. Papageorgis, *The Role of Tumor Microenvironment in Cancer Metastasis: Molecular Mechanisms and Therapeutic Opportunities*. Cancers (Basel), 2021. **13**(9).
94. Strouch, M.J., et al., *Crosstalk between mast cells and pancreatic cancer cells contributes to pancreatic tumor progression*. Clinical Cancer Research, 2010. **16**(8): p. 2257-2265.
95. Rao, Q., et al., *Recruited mast cells in the tumor microenvironment enhance bladder cancer metastasis via modulation of ER $\beta$ /CCL2/CCR2 EMT/MMP9 signals*. Oncotarget, 2016. **7**(7): p. 7842.
96. Visciano, C., et al., *Mast cells induce epithelial-to-mesenchymal transition and stem cell features in human thyroid cancer cells through an IL-8–Akt–Slug pathway*. Oncogene, 2015. **34**(40): p. 5175-5186.
97. Gounaris, E., et al., *Mast cells are an essential hematopoietic component for polyp development*. Proceedings of the National Academy of Sciences, 2007. **104**(50): p. 19977-19982.
98. Rigoni, A., et al., *Mast cells infiltrating inflamed or transformed gut alternatively sustain mucosal healing or tumor growth*. Cancer research, 2015. **75**(18): p. 3760-3770.
99. Kaesler, S., et al., *Targeting tumor-resident mast cells for effective anti-melanoma immune responses*. JCI Insight, 2019. **4**(19).
100. Oldford, S.A., et al., *A critical role for mast cells and mast cell-derived IL-6 in TLR2-mediated inhibition of tumor growth*. J Immunol, 2010. **185**(11): p. 7067-76.
101. Shikotra, A., et al., *Mast cell phenotype, TNF $\alpha$  expression and degranulation status in non-small cell lung cancer*. Scientific Reports, 2016. **6**(1): p. 38352.
102. Cheng, S., et al., *A pan-cancer single-cell transcriptional atlas of tumor infiltrating myeloid cells*. Cell, 2021. **184**(3): p. 792-809. e23.
103. Tanese, K., E.A. Grimm, and S. Ekmekcioglu, *The role of melanoma tumor-derived nitric oxide in the tumor inflammatory microenvironment: its impact on the chemokine expression profile, including suppression of CXCL10*. Int J Cancer, 2012. **131**(4): p. 891-901.
104. Slominski, R.M., M.A. Zmijewski, and A.T. Slominski, *The role of melanin pigment in melanoma*. Exp Dermatol, 2015. **24**(4): p. 258-9.
105. MacKie, R., A. Hauschild, and A. Eggermont, *Epidemiology of invasive cutaneous melanoma*. Annals of Oncology, 2009. **20**: p. vi1-vi7.
106. Rastrelli, M., S. Tropea, C.R. Rossi, and M. Alaibac, *Melanoma: epidemiology, risk factors, pathogenesis, diagnosis and classification*. In vivo, 2014. **28**(6): p. 1005-1011.

107. Anon, *Global Health Estimates 2020: Deaths by Cause, Age, Sex, by Country and by Region, 2000-2019*. . World Health Organization, 2020.
108. Institute, N.C. *Cancer Stat Facts: Melanoma of the Skin*. 2023 [cited 2023 12.01.2023]; Available from: <https://seer.cancer.gov/statfacts/html/melan.html>.
109. Conforti, C. and I. Zalaudek, *Epidemiology and Risk Factors of Melanoma: A Review*. *Dermatol Pract Concept*, 2021. **11**(Suppl 1): p. e2021161S.
110. Fitzpatrick, T.B., *The Validity and Practicality of Sun-Reactive Skin Types I Through VI*. *Archives of Dermatology*, 1988. **124**(6): p. 869-871.
111. Al Hashmi, M., et al., *Differential responsiveness to BRAF inhibitors of melanoma cell lines BRAF V600E-mutated*. *J Transl Med*, 2020. **18**(1): p. 192.
112. Arozarena, I. and C. Wellbrock, *Phenotype plasticity as enabler of melanoma progression and therapy resistance*. *Nature Reviews Cancer*, 2019. **19**(7): p. 377-391.
113. Ribeiro Moura Brasil Arnaut, J., et al., *Molecular landscape of Hereditary Melanoma*. *Crit Rev Oncol Hematol*, 2021. **164**: p. 103425.
114. Hodis, E., et al., *A landscape of driver mutations in melanoma*. *Cell*, 2012. **150**(2): p. 251-63.
115. Krauthammer, M., et al., *Exome sequencing identifies recurrent somatic RAC1 mutations in melanoma*. *Nat Genet*, 2012. **44**(9): p. 1006-14.
116. Davis, E.J., D.B. Johnson, J.A. Sosman, and S. Chandra, *Melanoma: What do all the mutations mean?* *Cancer*, 2018. **124**(17): p. 3490-3499.
117. Curtin, J.A., et al., *Distinct sets of genetic alterations in melanoma*. *N Engl J Med*, 2005. **353**(20): p. 2135-47.
118. Gosman, L.M., D.A. Țăpoi, and M. Costache, *Cutaneous Melanoma: A Review of Multifactorial Pathogenesis, Immunohistochemistry, and Emerging Biomarkers for Early Detection and Management*. *Int J Mol Sci*, 2023. **24**(21).
119. Tsao, H., et al., *Genetic interaction between NRAS and BRAF mutations and PTEN/MMAC1 inactivation in melanoma*. *J Invest Dermatol*, 2004. **122**(2): p. 337-41.
120. Huang, F.W., et al., *Highly recurrent TERT promoter mutations in human melanoma*. *Science*, 2013. **339**(6122): p. 957-9.
121. Pearlman, R.L., M.K. Montes de Oca, H.C. Pal, and F. Afaq, *Potential therapeutic targets of epithelial-mesenchymal transition in melanoma*. *Cancer Lett*, 2017. **391**: p. 125-140.
122. Damsky, W.E., N. Theodosakis, and M. Bosenberg, *Melanoma metastasis: new concepts and evolving paradigms*. *Oncogene*, 2014. **33**(19): p. 2413-2422.
123. Peinado, H., et al., *Pre-metastatic niches: organ-specific homes for metastases*. *Nature Reviews Cancer*, 2017. **17**(5): p. 302-317.
124. Suman, S. and S.N. Markovic, *Melanoma-derived mediators can foster the premetastatic niche: crossroad to lymphatic metastasis*. *Trends Immunol*, 2023. **44**(9): p. 724-743.
125. Miller, A.J. and M.C. Mihm, Jr., *Melanoma*. *N Engl J Med*, 2006. **355**(1): p. 51-65.
126. Hanahan, D., *Hallmarks of Cancer: New Dimensions*. *Cancer Discov*, 2022. **12**(1): p. 31-46.

127. Fares, J., et al., *Molecular principles of metastasis: a hallmark of cancer revisited*. Signal Transduction and Targeted Therapy, 2020. **5**(1).
128. Chiang, S.P., R.M. Cabrera, and J.E. Segall, *Tumor cell intravasation*. Am J Physiol Cell Physiol, 2016. **311**(1): p. C1-c14.
129. Valastyan, S. and R.A. Weinberg, *Tumor metastasis: molecular insights and evolving paradigms*. Cell, 2011. **147**(2): p. 275-92.
130. Huh, S.J., et al., *Transiently entrapped circulating tumor cells interact with neutrophils to facilitate lung metastasis development*. Cancer Res, 2010. **70**(14): p. 6071-82.
131. Trovato, R., et al., *The Engagement Between MDSCs and Metastases: Partners in Crime*. Front Oncol, 2020. **10**: p. 165.
132. Gershenwald, J.E., et al., *Melanoma staging: Evidence-based changes in the American Joint Committee on Cancer eighth edition cancer staging manual*. CA Cancer J Clin, 2017. **67**(6): p. 472-492.
133. Jenkins, R.W. and D.E. Fisher, *Treatment of Advanced Melanoma in 2020 and Beyond*. Journal of Investigative Dermatology, 2021. **141**(1): p. 23-31.
134. Curti, B.D. and M.B. Faries, *Recent Advances in the Treatment of Melanoma*. N Engl J Med, 2021. **384**(23): p. 2229-2240.
135. Amaria, R.N., et al., *Neoadjuvant systemic therapy in melanoma: recommendations of the International Neoadjuvant Melanoma Consortium*. Lancet Oncol, 2019. **20**(7): p. e378-e389.
136. Carlino, M.S., J. Larkin, and G.V. Long, *Immune checkpoint inhibitors in melanoma*. Lancet, 2021. **398**(10304): p. 1002-1014.
137. Johnson, D.B., C.A. Nebhan, J.J. Moslehi, and J.M. Balko, *Immune-checkpoint inhibitors: long-term implications of toxicity*. Nature Reviews Clinical Oncology, 2022. **19**(4): p. 254-267.
138. Shevtsov, M., et al., *Magnetic nanoparticles in theranostics of malignant melanoma*. EJNMMI Res, 2021. **11**(1): p. 127.
139. Martins, F., et al., *Adverse effects of immune-checkpoint inhibitors: epidemiology, management and surveillance*. Nat Rev Clin Oncol, 2019. **16**(9): p. 563-580.
140. Conroy, M. and J. Naidoo, *Immune-related adverse events and the balancing act of immunotherapy*. Nature Communications, 2022. **13**(1): p. 392.
141. Jin, M.-Z. and W.-L. Jin, *The updated landscape of tumor microenvironment and drug repurposing*. Signal Transduction and Targeted Therapy, 2020. **5**(1): p. 166.
142. Arner, E.N. and J.C. Rathmell, *Metabolic programming and immune suppression in the tumor microenvironment*. Cancer Cell, 2023. **41**(3): p. 421-433.
143. Elia, I. and M.C. Haigis, *Metabolites and the tumour microenvironment: from cellular mechanisms to systemic metabolism*. Nat Metab, 2021. **3**(1): p. 21-32.
144. Webb, B.A., M. Chimenti, M.P. Jacobson, and D.L. Barber, *Dysregulated pH: a perfect storm for cancer progression*. Nat Rev Cancer, 2011. **11**(9): p. 671-7.
145. Peppicelli, S., et al., *Metformin is also effective on lactic acidosis-exposed melanoma cells switched to oxidative phosphorylation*. Cell Cycle, 2016. **15**(14): p. 1908-18.
146. Zahalka, A.H. and P.S. Frenette, *Nerves in cancer*. Nat Rev Cancer, 2020. **20**(3): p. 143-157.

147. Mellman, I. and R.M. Steinman, *Dendritic cells: specialized and regulated antigen processing machines*. Cell, 2001. **106**(3): p. 255-8.
148. Cancel, J.C., K. Crozat, M. Dalod, and R. Mattiuz, *Are Conventional Type 1 Dendritic Cells Critical for Protective Antitumor Immunity and How?* Front Immunol, 2019. **10**: p. 9.
149. Dudziak, D., et al., *Differential antigen processing by dendritic cell subsets in vivo*. Science, 2007. **315**(5808): p. 107-11.
150. Ni, J., et al., *Sustained effector function of IL-12/15/18-preactivated NK cells against established tumors*. J Exp Med, 2012. **209**(13): p. 2351-65.
151. Cerwenka, A. and L.L. Lanier, *Natural killer cells, viruses and cancer*. Nat Rev Immunol, 2001. **1**(1): p. 41-9.
152. Messaoudene, M., et al., *Mature cytotoxic CD56(bright)/CD16(+) natural killer cells can infiltrate lymph nodes adjacent to metastatic melanoma*. Cancer Res, 2014. **74**(1): p. 81-92.
153. Kirchhammer, N., et al., *NK cells with tissue-resident traits shape response to immunotherapy by inducing adaptive antitumor immunity*. Sci Transl Med, 2022. **14**(653): p. eabm9043.
154. Böttcher, J.P., et al., *NK Cells Stimulate Recruitment of cDC1 into the Tumor Microenvironment Promoting Cancer Immune Control*. Cell, 2018. **172**(5): p. 1022-1037.e14.
155. Simiczyjew, A., et al., *The Influence of Tumor Microenvironment on Immune Escape of Melanoma*. Int J Mol Sci, 2020. **21**(21).
156. Cao, X., et al., *Granzyme B and perforin are important for regulatory T cell-mediated suppression of tumor clearance*. Immunity, 2007. **27**(4): p. 635-646.
157. Qiu, Y., et al., *FOXP3+ regulatory T cells and the immune escape in solid tumours*. Front Immunol, 2022. **13**: p. 982986.
158. Santoni, M., et al., *CXC and CC chemokines as angiogenic modulators in nonhaematological tumors*. BioMed research international, 2014. **2014**.
159. Sato, T., et al., *Interleukin 10 in the tumor microenvironment: a target for anticancer immunotherapy*. Immunologic research, 2011. **51**: p. 170-182.
160. Gao, S., J. Hu, X. Wu, and Z. Liang, *PMA treated THP-1-derived-IL-6 promotes EMT of SW48 through STAT3/ERK-dependent activation of Wnt/ $\beta$ -catenin signaling pathway*. Biomedicine & Pharmacotherapy, 2018. **108**: p. 618-624.
161. Veglia, F., E. Sanseviero, and D.I. Gabrilovich, *Myeloid-derived suppressor cells in the era of increasing myeloid cell diversity*. Nature Reviews Immunology, 2021. **21**(8): p. 485-498.
162. Wang, Y., Y. Ding, N. Guo, and S. Wang, *MDSCs: Key Criminals of Tumor Pre-metastatic Niche Formation*. Front Immunol, 2019. **10**: p. 172.
163. Olkhanud, P.B., et al., *Tumor-evoked regulatory b cells promote breast cancer metastasis by converting resting CD4+ T cells to T-regulatory cells* cancer-promoting role of B cells cancer-promoting role of B cells. Cancer research, 2011. **71**(10): p. 3505-3515.
164. Galon, J. and D. Bruni, *Approaches to treat immune hot, altered and cold tumours with combination immunotherapies*. Nat Rev Drug Discov, 2019. **18**(3): p. 197-218.

165. Hegde, P.S., V. Karanikas, and S. Evers, *The Where, the When, and the How of Immune Monitoring for Cancer Immunotherapies in the Era of Checkpoint Inhibition*. Clin Cancer Res, 2016. **22**(8): p. 1865-74.
166. Duan, Q., H. Zhang, J. Zheng, and L. Zhang, *Turning Cold into Hot: Firing up the Tumor Microenvironment*. Trends in cancer, 2020. **6**(7): p. 605-618.
167. Grimbaldston, M.A., et al., *Mast cell-deficient W-sash c-kit mutant Kit W-sh/W-sh mice as a model for investigating mast cell biology in vivo*. Am J Pathol, 2005. **167**(3): p. 835-48.
168. Sunderkötter, C., et al., *Subpopulations of mouse blood monocytes differ in maturation stage and inflammatory response*. J Immunol, 2004. **172**(7): p. 4410-7.
169. Iuliano, C., et al., *Fetal Tissue-Derived Mast Cells (MC) as Experimental Surrogate for In Vivo Connective Tissue MC*. Cells, 2022. **11**(6): p. 928.
170. Hallgren, J. and M.F. Gurish, *Mast cell progenitor trafficking and maturation*. Adv Exp Med Biol, 2011. **716**: p. 14-28.
171. Li, Z., et al., *Adult Connective Tissue-Resident Mast Cells Originate from Late Erythro-Myeloid Progenitors*. Immunity, 2018. **49**(4): p. 640-653.e5.
172. Subramanian, H., K. Gupta, and H. Ali, *Roles of Mas-related G protein-coupled receptor X2 on mast cell-mediated host defense, pseudoallergic drug reactions, and chronic inflammatory diseases*. J Allergy Clin Immunol, 2016. **138**(3): p. 700-710.
173. Netea, M.G., et al., *Trained immunity: A program of innate immune memory in health and disease*. Science, 2016. **352**(6284): p. aaf1098.
174. De Zuani, M., et al., *LPS Guides Distinct Patterns of Training and Tolerance in Mast Cells*. Front Immunol, 2022. **13**: p. 835348.
175. Yang, D., Z. Han, and J.J. Oppenheim, *Alarmins and immunity*. Immunol Rev, 2017. **280**(1): p. 41-56.
176. Leyva-Castillo, J.M., et al., *Mast cell-derived IL-13 downregulates IL-12 production by skin dendritic cells to inhibit the T(H)1 cell response to cutaneous antigen exposure*. J Allergy Clin Immunol, 2021. **147**(6): p. 2305-2315.e3.
177. Cayrol, C. and J.P. Girard, *IL-33: an alarmin cytokine with crucial roles in innate immunity, inflammation and allergy*. Curr Opin Immunol, 2014. **31**: p. 31-7.
178. Cayrol, C. and J.P. Girard, *Interleukin-33 (IL-33): A nuclear cytokine from the IL-1 family*. Immunol Rev, 2018. **281**(1): p. 154-168.
179. Tang, Z., et al., *GEPIA: a web server for cancer and normal gene expression profiling and interactive analyses*. Nucleic acids research, 2017. **45**(W1): p. W98-W102.
180. Hanahan, D. and R.A. Weinberg, *Hallmarks of cancer: the next generation*. Cell, 2011. **144**(5): p. 646-74.
181. Wernersson, S. and G. Pejler, *Mast cell secretory granules: armed for battle*. Nat Rev Immunol, 2014. **14**(7): p. 478-94.
182. Saito, R., et al., *Downregulation of Ral GTPase-activating protein promotes tumor invasion and metastasis of bladder cancer*. Oncogene, 2013. **32**(7): p. 894-902.
183. Humphries, B., Z. Wang, and C. Yang, *Rho GTPases: Big Players in Breast Cancer Initiation, Metastasis and Therapeutic Responses*. Cells, 2020. **9**(10).
184. Jin, J., et al., *CCL2: An Important Mediator Between Tumor Cells and Host Cells in Tumor Microenvironment*. Front Oncol, 2021. **11**: p. 722916.

185. Liu, Y., et al., *Crucial biological functions of CCL7 in cancer*. PeerJ, 2018. **6**: p. e4928.
186. Dolton, G., et al., *Targeting of multiple tumor-associated antigens by individual T cell receptors during successful cancer immunotherapy*. Cell, 2023. **186**(16): p. 3333-3349.e27.
187. Kawai, S., et al., *Interferon-alpha enhances CD317 expression and the antitumor activity of anti-CD317 monoclonal antibody in renal cell carcinoma xenograft models*. Cancer Sci, 2008. **99**(12): p. 2461-6.
188. Soler, A., et al., *CXCL5 Facilitates Melanoma Cell-Neutrophil Interaction and Lymph Node Metastasis*. Journal of Investigative Dermatology, 2018. **138**.
189. Legler, D.F., E. Uetz-von Allmen, and M.A. Hauser, *CCR7: roles in cancer cell dissemination, migration and metastasis formation*. Int J Biochem Cell Biol, 2014. **54**: p. 78-82.
190. Chatterjee, S., B. Behnam Azad, and S. Nimmagadda, *The intricate role of CXCR4 in cancer*. Adv Cancer Res, 2014. **124**: p. 31-82.
191. Amersi, F.F., et al., *Activation of CCR9/CCL25 in cutaneous melanoma mediates preferential metastasis to the small intestine*. Clin Cancer Res, 2008. **14**(3): p. 638-45.
192. Saito, Y., et al., *The Role of Type-2 Conventional Dendritic Cells in the Regulation of Tumor Immunity*. Cancers (Basel), 2022. **14**(8).
193. Zebley, C.C. and B. Youngblood, *Mechanisms of T cell exhaustion guiding next-generation immunotherapy*. Trends Cancer, 2022. **8**(9): p. 726-734.
194. Ramos-Casals, M., et al., *Immune-related adverse events of checkpoint inhibitors*. Nature Reviews Disease Primers, 2020. **6**(1): p. 38.
195. de Jesús-Gil, C., et al., *The Translational Relevance of Human Circulating Memory Cutaneous Lymphocyte-Associated Antigen Positive T Cells in Inflammatory Skin Disorders*. Front Immunol, 2021. **12**: p. 652613.
196. Gaffen, S.L., R. Jain, A.V. Garg, and D.J. Cua, *The IL-23–IL-17 immune axis: from mechanisms to therapeutic testing*. Nature Reviews Immunology, 2014. **14**(9): p. 585-600.
197. Lee, J.H., D.H. Cho, and H.J. Park, *IL-18 and Cutaneous Inflammatory Diseases*. Int J Mol Sci, 2015. **16**(12): p. 29357-69.
198. Helmby, H. and R.K. Grencis, *IL-18 regulates intestinal mastocytosis and Th2 cytokine production independently of IFN-gamma during Trichinella spiralis infection*. J Immunol, 2002. **169**(5): p. 2553-60.
199. He, S.H., *Key role of mast cells and their major secretory products in inflammatory bowel disease*. World J Gastroenterol, 2004. **10**(3): p. 309-18.
200. Hsu, P., et al., *IL-10 Potentiates Differentiation of Human Induced Regulatory T Cells via STAT3 and Foxo1*. J Immunol, 2015. **195**(8): p. 3665-74.
201. Gray, C.P., A.V. Franco, P. Arosio, and P. Hersey, *Immunosuppressive effects of melanoma-derived heavy-chain ferritin are dependent on stimulation of IL-10 production*. International Journal of Cancer, 2001. **92**(6): p. 843-850.
202. Kneilling, M., et al., *Targeted mast cell silencing protects against joint destruction and angiogenesis in experimental arthritis in mice*. Arthritis Rheum, 2007. **56**(6): p. 1806-16.

203. Eissmann, M.F., et al., *IL-33-mediated mast cell activation promotes gastric cancer through macrophage mobilization*. Nature communications, 2019. **10**(1): p. 2735.
204. Meurer, S.K., et al., *Isolation of Mature (Peritoneum-Derived) Mast Cells and Immature (Bone Marrow-Derived) Mast Cell Precursors from Mice*. PLoS One, 2016. **11**(6): p. e0158104.
205. Swindle, E.J., *Generation of Mast Cells from Murine Stem Cell Progenitors*. Methods Mol Biol, 2020. **2163**: p. 85-89.
206. Ohnmacht, C. and D. Voehringer, *Basophil effector function and homeostasis during helminth infection*. Blood, The Journal of the American Society of Hematology, 2009. **113**(12): p. 2816-2825.
207. Tsai, M., et al., *Using mast cell knock-in mice to analyze the roles of mast cells in allergic responses in vivo*. Mast Cells in Allergic Diseases, 2005. **87**: p. 179-197.
208. Roy, S., et al., *Multifaceted MRGPRX2: New insight into the role of mast cells in health and disease*. J Allergy Clin Immunol, 2021. **148**(2): p. 293-308.
209. Enoksson, M., et al., *Human cord blood-derived mast cells are activated by the Nod1 agonist M-TriDAP to release pro-inflammatory cytokines and chemokines*. J Innate Immun, 2011. **3**(2): p. 142-9.
210. Tancowny, B.P., V. Karpov, R.P. Schleimer, and M. Kulka, *Substance P primes lipoteichoic acid- and Pam3CysSerLys4-mediated activation of human mast cells by up-regulating Toll-like receptor 2*. Immunology, 2010. **131**(2): p. 220-30.
211. Nakajima, T., et al., *Marked increase in CC chemokine gene expression in both human and mouse mast cell transcriptomes following Fcepsilon receptor I cross-linking: an interspecies comparison*. Blood, 2002. **100**(12): p. 3861-8.
212. Zhao, J., et al., *S100A8 modulates mast cell function and suppresses eosinophil migration in acute asthma*. Antioxidants & redox signaling, 2011. **14**(9): p. 1589-1600.
213. Xing, W., K.F. Austen, M.F. Gurish, and T.G. Jones, *Protease phenotype of constitutive connective tissue and of induced mucosal mast cells in mice is regulated by the tissue*. Proceedings of the National Academy of Sciences, 2011. **108**(34): p. 14210-14215.
214. Saito, H., et al., *Gene expression profiling of human mast cell subtypes: an in silico study*. Allergy International, 2006. **55**(2): p. 173-179.
215. Ribatti, D. and E. Crivellato, *Mast cells, angiogenesis, and tumour growth*. Biochim Biophys Acta, 2012. **1822**(1): p. 2-8.
216. He, Z., et al., *Epithelial-derived IL-33 promotes intestinal tumorigenesis in ApcMin/+ mice*. Scientific Reports, 2017. **7**(1): p. 5520.
217. Nian, J.B., et al., *Epithelial cells expressed IL-33 to promote degranulation of mast cells through inhibition on ST2/PI3K/mTOR-mediated autophagy in allergic rhinitis*. Cell Cycle, 2020. **19**(10): p. 1132-1142.
218. Griesenauer, B. and S. Paczesny, *The ST2/IL-33 Axis in Immune Cells during Inflammatory Diseases*. Frontiers in Immunology, 2017. **8**.
219. Gao, K., et al., *Transgenic expression of IL-33 activates CD8(+) T cells and NK cells and inhibits tumor growth and metastasis in mice*. Cancer Lett, 2013. **335**(2): p. 463-71.

220. Gao, X., et al., *Tumoral expression of IL-33 inhibits tumor growth and modifies the tumor microenvironment through CD8+ T and NK cells*. J Immunol, 2015. **194**(1): p. 438-45.
221. Lucarini, V., et al., *IL-33 restricts tumor growth and inhibits pulmonary metastasis in melanoma-bearing mice through eosinophils*. Oncoimmunology, 2017. **6**(6): p. e1317420.
222. Schuijs, M.J., et al., *ILC2-driven innate immune checkpoint mechanism antagonizes NK cell antimetastatic function in the lung*. Nat Immunol, 2020. **21**(9): p. 998-1009.
223. Brunner, S.M., et al., *Tumor-infiltrating, interleukin-33-producing effector-memory CD8(+) T cells in resected hepatocellular carcinoma prolong patient survival*. Hepatology, 2015. **61**(6): p. 1957-67.
224. Yang, M., et al., *Lower expression level of IL-33 is associated with poor prognosis of pulmonary adenocarcinoma*. PLoS One, 2018. **13**(3): p. e0193428.
225. Duault, C., et al., *TCRV $\gamma$ 9  $\gamma\delta$  T Cell Response to IL-33: A CD4 T Cell-Dependent Mechanism*. J Immunol, 2016. **196**(1): p. 493-502.
226. Tamma, R., et al., *Spatial distribution of mast cells and macrophages around tumor glands in human breast ductal carcinoma*. Exp Cell Res, 2017. **359**(1): p. 179-184.
227. Shime, H., et al., *Toll-like receptor 2 ligand and interferon- $\gamma$  suppress anti-tumor T cell responses by enhancing the immunosuppressive activity of monocytic myeloid-derived suppressor cells*. Oncoimmunology, 2017. **7**(1): p. e1373231.
228. Binnewies, M., et al., *Understanding the tumor immune microenvironment (TIME) for effective therapy*. Nature Medicine, 2018. **24**(5): p. 541-550.
229. Bindea, G., et al., *Spatiotemporal dynamics of intratumoral immune cells reveal the immune landscape in human cancer*. Immunity, 2013. **39**(4): p. 782-95.
230. Gajewski, T.F., *The Next Hurdle in Cancer Immunotherapy: Overcoming the Non-T-Cell-Inflamed Tumor Microenvironment*. Semin Oncol, 2015. **42**(4): p. 663-71.
231. Zemek, R.M., et al., *Sensitization to immune checkpoint blockade through activation of a STAT1/NK axis in the tumor microenvironment*. Sci Transl Med, 2019. **11**(501).
232. Liu, Z., C. Han, and Y.X. Fu, *Targeting innate sensing in the tumor microenvironment to improve immunotherapy*. Cell Mol Immunol, 2020. **17**(1): p. 13-26.
233. Xia, Y., et al., *Endogenous IL-33 exerts CD8(+) T cell antitumor responses overcoming pro-tumor effects by regulatory T cells in a colon carcinoma model*. Biochem Biophys Res Commun, 2019. **518**(2): p. 331-336.
234. Jin, Z., et al., *IL-33 Released in the Liver Inhibits Tumor Growth via Promotion of CD4(+) and CD8(+) T Cell Responses in Hepatocellular Carcinoma*. J Immunol, 2018. **201**(12): p. 3770-3779.
235. Villarreal, D.O., et al., *Alarmin IL-33 acts as an immunoadjuvant to enhance antigen-specific tumor immunity*. Cancer Res, 2014. **74**(6): p. 1789-800.
236. Geng, D., et al., *When Toll-like receptor and T-cell receptor signals collide: a mechanism for enhanced CD8 T-cell effector function*. Blood, 2010. **116**(18): p. 3494-504.
237. Cottalorda, A., et al., *TLR2 engagement on CD8 T cells lowers the threshold for optimal antigen-induced T cell activation*. Eur J Immunol, 2006. **36**(7): p. 1684-93.

238. Adams, S., *Toll-like receptor agonists in cancer therapy*. Immunotherapy, 2009. **1**(6): p. 949-64.
239. Huang, B., et al., *TLR signaling by tumor and immune cells: a double-edged sword*. Oncogene, 2008. **27**(2): p. 218-24.
240. Feng, Y., et al., *A toll-like receptor agonist mimicking microbial signal to generate tumor-suppressive macrophages*. Nat Commun, 2019. **10**(1): p. 2272.
241. Syn, N.L., M.W.L. Teng, T.S.K. Mok, and R.A. Soo, *De-novo and acquired resistance to immune checkpoint targeting*. Lancet Oncol, 2017. **18**(12): p. e731-e741.
242. Chen, J., et al., *Interleukin-33 Contributes to the Induction of Th9 Cells and Antitumor Efficacy by Dectin-1-Activated Dendritic Cells*. Front Immunol, 2018. **9**: p. 1787.
243. Meeth, K., et al., *The YUMM lines: a series of congenic mouse melanoma cell lines with defined genetic alterations*. Pigment Cell Melanoma Res, 2016. **29**(5): p. 590-7.
244. Sasaki, H., et al., *New inducible mast cell-deficient mouse model (Mcpt5/Cma1(DTR))*. Biochem Biophys Res Commun, 2021. **551**: p. 127-132.
245. Ciążyńska, M., et al., *The incidence and clinical analysis of non-melanoma skin cancer*. Scientific Reports, 2021. **11**(1): p. 4337.
246. Emmett, M.S., et al., *Prediction of melanoma metastasis by the Shields index based on lymphatic vessel density*. BMC Cancer, 2010. **10**: p. 208.
247. Wei, C., et al., *Delineating the early dissemination mechanisms of acral melanoma by integrating single-cell and spatial transcriptomic analyses*. Nat Commun, 2023. **14**(1): p. 8119.
248. Alve, S., et al., *DLL4-Notch3-WNT5B axis mediates bi-directional pro-metastatic crosstalk between melanoma and lymphatic endothelial cells*. JCI Insight, 2023.
249. Pastushenko, I., et al., *Identification of the tumour transition states occurring during EMT*. Nature, 2018. **556**(7702): p. 463-468.
250. Caramel, J., et al., *A switch in the expression of embryonic EMT-inducers drives the development of malignant melanoma*. Cancer Cell, 2013. **24**(4): p. 466-80.
251. Gupta, P.B., et al., *The melanocyte differentiation program predisposes to metastasis after neoplastic transformation*. Nat Genet, 2005. **37**(10): p. 1047-54.
252. Yin, G., et al., *Targeting small GTPases: emerging grasps on previously untamable targets, pioneered by KRAS*. Signal Transduction and Targeted Therapy, 2023. **8**(1): p. 212.
253. Zeisberg, M. and E.G. Neilson, *Biomarkers for epithelial-mesenchymal transitions*. J Clin Invest, 2009. **119**(6): p. 1429-37.
254. Kalluri, R. and R.A. Weinberg, *The basics of epithelial-mesenchymal transition*. J Clin Invest, 2009. **119**(6): p. 1420-8.
255. Bidwell, B.N., et al., *Silencing of Irf7 pathways in breast cancer cells promotes bone metastasis through immune escape*. Nat Med, 2012. **18**(8): p. 1224-31.
256. Qian, B.Z., et al., *CCL2 recruits inflammatory monocytes to facilitate breast-tumour metastasis*. Nature, 2011. **475**(7355): p. 222-5.
257. Wyler, L., et al., *Brain metastasis in renal cancer patients: metastatic pattern, tumour-associated macrophages and chemokine/chemoreceptor expression*. Br J Cancer, 2014. **110**(3): p. 686-94.

258. Ren, X., et al., *Inhibition of CCL7 derived from Mo-MDSCs prevents metastatic progression from latency in colorectal cancer*. *Cell Death Dis*, 2021. **12**(5): p. 484.
259. Roberts, E.W., et al., *Critical Role for CD103(+)/CD141(+) Dendritic Cells Bearing CCR7 for Tumor Antigen Trafficking and Priming of T Cell Immunity in Melanoma*. *Cancer Cell*, 2016. **30**(2): p. 324-336.
260. Zhao, J., et al., *Tumor-derived CXCL5 promotes human colorectal cancer metastasis through activation of the ERK/Elk-1/Snail and AKT/GSK3 $\beta$ / $\beta$ -catenin pathways*. *Mol Cancer*, 2017. **16**(1): p. 70.
261. Mao, Z., et al., *CXCL5 promotes gastric cancer metastasis by inducing epithelial-mesenchymal transition and activating neutrophils*. *Oncogenesis*, 2020. **9**(7): p. 63.
262. Soler-Cardona, A., et al., *CXCL5 Facilitates Melanoma Cell-Neutrophil Interaction and Lymph Node Metastasis*. *J Invest Dermatol*, 2018. **138**(7): p. 1627-1635.
263. Dudeck, A., et al., *Mast cells are key promoters of contact allergy that mediate the adjuvant effects of haptens*. *Immunity*, 2011. **34**(6): p. 973-84.
264. Shelburne, C.P., et al., *Mast cells augment adaptive immunity by orchestrating dendritic cell trafficking through infected tissues*. *Cell Host Microbe*, 2009. **6**(4): p. 331-42.
265. Dudeck, J., et al., *Engulfment of mast cell secretory granules on skin inflammation boosts dendritic cell migration and priming efficiency*. *J Allergy Clin Immunol*, 2019. **143**(5): p. 1849-1864.e4.
266. Spranger, S., D. Dai, B. Horton, and T.F. Gajewski, *Tumor-Residing Batf3 Dendritic Cells Are Required for Effector T Cell Trafficking and Adoptive T Cell Therapy*. *Cancer Cell*, 2017. **31**(5): p. 711-723.e4.
267. Clark, E.A., T.R. Golub, E.S. Lander, and R.O. Hynes, *Genomic analysis of metastasis reveals an essential role for RhoC*. *Nature*, 2000. **406**(6795): p. 532-5.
268. Elsheikh, S., et al., *Ran GTPase is an independent prognostic marker in malignant melanoma which promotes tumour cell migration and invasion*. *J Clin Pathol*, 2022. **75**(1): p. 24-29.
269. Quintana, E., et al., *Human melanoma metastasis in NSG mice correlates with clinical outcome in patients*. *Sci Transl Med*, 2012. **4**(159): p. 159ra149.
270. Khoja, L., et al., *Tumour- and class-specific patterns of immune-related adverse events of immune checkpoint inhibitors: a systematic review*. *Ann Oncol*, 2017. **28**(10): p. 2377-2385.
271. Lozano, A.X., et al., *T cell characteristics associated with toxicity to immune checkpoint blockade in patients with melanoma*. *Nature Medicine*, 2022. **28**(2): p. 353-362.
272. Satya, D. and B.J. Douglas, *Immune-related adverse events and anti-tumor efficacy of immune checkpoint inhibitors*. *Journal for ImmunoTherapy of Cancer*, 2019. **7**(1): p. 306.
273. Lim, S.Y., et al., *Circulating Cytokines Predict Immune-Related Toxicity in Melanoma Patients Receiving Anti-PD-1-Based Immunotherapy*. *Clin Cancer Res*, 2019. **25**(5): p. 1557-1563.
274. Nuñez, N.G., et al., *Immune signatures predict development of autoimmune toxicity in patients with cancer treated with immune checkpoint inhibitors*. *Med*, 2023. **4**(2): p. 113-129.e7.

275. Akdis, M., et al., *TH17 and TH22 cells: a confusion of antimicrobial response with tissue inflammation versus protection*. Journal of Allergy and Clinical Immunology, 2012. **129**(6): p. 1438-1449.
276. von Euw, E., et al., *CTLA4 blockade increases Th17 cells in patients with metastatic melanoma*. J Transl Med, 2009. **7**: p. 35.
277. Tarhini, A.A., et al., *Baseline circulating IL-17 predicts toxicity while TGF- $\beta$ 1 and IL-10 are prognostic of relapse in ipilimumab neoadjuvant therapy of melanoma*. Journal for immunotherapy of cancer, 2015. **3**: p. 1-6.
278. Dudakov, J.A., A.M. Hanash, and M.R. van den Brink, *Interleukin-22: immunobiology and pathology*. Annu Rev Immunol, 2015. **33**: p. 747-85.
279. Liang, S.C., et al., *Interleukin (IL)-22 and IL-17 are coexpressed by Th17 cells and cooperatively enhance expression of antimicrobial peptides*. J Exp Med, 2006. **203**(10): p. 2271-9.
280. He, Y., et al., *IL22 drives cutaneous melanoma cell proliferation, migration and invasion through activation of miR-181/STAT3/AKT axis*. J Cancer, 2020. **11**(9): p. 2679-2687.
281. Ciccicarese, C., et al., *New toxicity profile for novel immunotherapy agents: focus on immune-checkpoint inhibitors*. Expert Opin Drug Metab Toxicol, 2016. **12**(1): p. 57-75.
282. Kanjanapan, Y., et al., *Delayed immune-related adverse events in assessment for dose-limiting toxicity in early phase immunotherapy trials*. Eur J Cancer, 2019. **107**: p. 1-7.
283. Sanlorenzo, M., et al., *Pembrolizumab Cutaneous Adverse Events and Their Association With Disease Progression*. JAMA Dermatol, 2015. **151**(11): p. 1206-1212.
284. Coleman, E., et al., *Inflammatory eruptions associated with immune checkpoint inhibitor therapy: A single-institution retrospective analysis with stratification of reactions by toxicity and implications for management*. J Am Acad Dermatol, 2019. **80**(4): p. 990-997.
285. Nakamura, Y., et al., *Critical Role for Mast Cells in Interleukin-1 $\beta$ -Driven Skin Inflammation Associated with an Activating Mutation in the Nlrp3 Protein*. Immunity, 2012. **37**(1): p. 85-95.
286. Nemunaitis, J., et al., *Comparison of serum interleukin-10 (IL-10) levels between normal volunteers and patients with advanced melanoma*. Cancer Invest, 2001. **19**(3): p. 239-47.

## List of Publications

### Published:

**Iuliano C\***, Absmaier-Kijak M\*, Sinnberg T, Hoffard N, Hils M, Köberle M, Wölbing F, Shumilina E, Heise N, Fehrenbacher B, Schaller M, Lang F, Kaesler S, Biedermann T. Fetal Tissue-Derived Mast Cells (MC) as Experimental Surrogate for In Vivo Connective Tissue MC. *Cells*. 2022 Mar 8;11(6):928. doi: 10.3390/cells11060928. PMID: 35326379; PMCID: PMC8946182.

\*equally contributed

Hils M, Hoffard N, **Iuliano C**, Kreft L, Chakrapani N, Swiontek K, Fischer K, Eberlein B, Köberle M, Fischer J, Hilger C, Ohnmacht C, Kaesler S, Wölbing F, Biedermann T. IgE and anaphylaxis specific to the carbohydrate alpha-gal depend on interleukin-4. *J Allergy Clin Immunol*. 2023 Dec 20:S0091-6749(23)02453-3. doi: 10.1016/j.jaci.2023.12.003. Epub ahead of print. PMID: 38135009.

Absmaier-Kijak M\*, **Iuliano C\***, Kaesler S, Biedermann T, Posch C, Brockow K. T-Cell Subtypes and Immune Signatures in Cutaneous Immune-Related Adverse Events in Melanoma Patients under Immune Checkpoint Inhibitor Therapy. *Cancers (Basel)*. 2024 Mar 20;16(6):1226. doi: 10.3390/cancers16061226. PMID: 38539560; PMCID: PMC10969757.

\*equally contributed